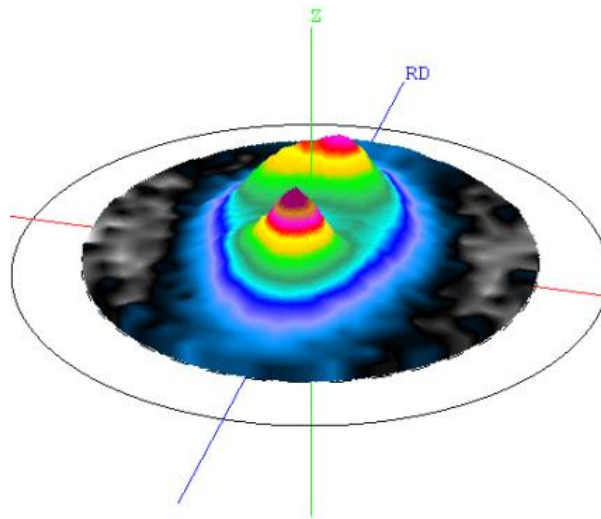


**L
A
B
S
O
F
T**

LaboTex

Version 3.0

Texture Analysis Software for Windows



Introduction to LaboTex

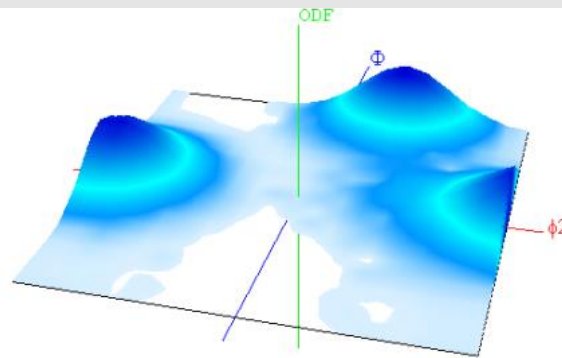
LaboSoft s.c.
Phone: +48 502 311 838
Fax: +48 12 395 3891
E-mail: office@labosoft.com.pl
© LaboSoft 1997-2019
V-3/55

Contents

1. Introduction	4
1.1. Main Program Features.....	4
1.2. LaboTex - Range of Applicability	5
1.3. Representation of Orientations by Euler Angles.	5
1.4. Crystal and sample coordinate systems: LaboTex Axis and Angles Convention.	6
1.5. ODF definition.....	7
1.6. Basic ranges of ODF. LaboTex structure code.....	7
1.7. Pole Figures	8
1.8. The ODF Calculation.....	9
1.9. Definitions of fit error in ODF calculation	9
1.10. Qualitative Texture Analysis	10
1.11. Modelling of ODF, pole figures and inverse pole figures	10
1.12. Quantitative Texture Analysis. I - Volume fraction of texture components by integration methods (IM).	10
The overlapping problem.....	11
1.13. Quantitative Texture Analysis. II - Volume fraction of texture components by Model Function Methods (MFM).....	12
1.17. 2D and 3D Graphics	13
1.18. Detailed Manuals (www.labosoft.com.pl and www.labotex.com).....	14
1.19. ADC method: Opinions and Applications	15
2. Getting started	16
2.1. System Requirements	16
2.1.1 Minimal requirements:.....	Błąd! Nie zdefiniowano zakładki.
2.1.2 Recommended system configuration:.....	Błąd! Nie zdefiniowano zakładki.
2.2. Installation	16
2.3. Configuration.....	17
3. LaboTex Objects and Object Containers.....	18
3.1 Introduction.....	18
3.2 LaboTex Objects Types.....	20
3.2.1 CPF - Corrected Pole Figures	20
3.2.2 NPF - Normalized Pole Figures.....	20
3.2.3. RPF - Recalculated Pole Figures	21
3.2.4. APF - Additional Pole Figures	21
3.2.5. INV - INVerse pole figures	21
3.2.6.ODF - Orientation Distribution Function	22
3.3. Example CPF, NPF, RPF objects	22
3.4. LaboTex Jobs.....	23
4. LaboTex Formats	24
4.1. EPF file format.....	24
4.2. EPF Example	25
4.3. PPF file format.....	26
4.4. SOR file format.....	26

4.5. POW format.....	26
4.6. COR format	27
4.7. Other data formats	27
4.8. How make given format accessible for LaboTex	33
5. LaboTex - Frequently Asked Questions (FAQ).....	38
6. References.....	47
6.1 The LaboTex Reference:	47
6.2 ADC Method - Main References:	47
6.3 Other selected references on LaboTex and ADC:	47
6.4 ODF Transformation references	71
6.5 Calculation of the Volume Fraction of Texture Component and the ODF Modeling references ...	71
6.6 Measurement of Pole Figures references.....	72
6.7 Texture and Quantitative Phase Analysis references.....	72
6.8 Texture and ODF references.....	72
7. LaboTex: Technical specifications.....	72

1. Introduction



1.1. Main Program Features

LaboTex software is a Windows 2000/XP/2003 tool for complex and detailed analysis of crystallographic textures. This user-friendly program enables you to conduct a variety different calculations and graphic analyses of Orientation Distribution Function (ODF), Pole Figures (PFs) and Inverse Pole Figures (IPFs). The main LaboTex features include:

- ODF calculation by ADC method with the ghost correction;
- ODF free from truncation errors of the series;
- ODF calculation using both types of experimental data: pole figures and sets of individual orientations;
- ODF, PF and IPF data measured, calculated and presented in a wide range of grid cells from radial angle 1.0 to 10 degrees with a background and defocusing correction;
- texture analysis of all types of sample symmetry;
- a fiber texture analysis;
- a texture analysis for materials of all types of the crystal lattice symmetry;
- 2D and 3D graphic presentation of ODFs , PFs and IPFs;
- simple on-line identification of the orientations, giving its parameters in Euler angles and Miller indices;
- creation of additional pole figures and inverse pole figures;
- creation of misorientation histograms;
- creation of model ODF on the base of model functions (Gauss, Lorentz);
- comparisons of ODFs and PFs (up to 12);
- diagrams for the skeleton lines (alpha fiber, beta fiber etc.);
- an on-line qualitative texture analysis;
- a texture database;
- a quantitative texture analysis: the volume fraction of texture components by a model function and integration in the Euler space;
- ODF transformations (frame rotations, crystallites rotation models);
- ODFs logical functions (sum, union etc.);
- transformations of ODF to a set of single orientations;
- input data in more than 30 data formats;
- rotations and symmetrizations of experimental pole figures;
- plotting graphics on mono and colour printers;

- passing graphical objects to other Windows applications via the clipboard or creating image files in the *.BMP or *.TIF format;
- exporting ODF and pole figures to the ASCII format;
- easy management of the data and results by collecting in symmetries, projects, samples and jobs.

1.2. LaboTex - Range of Applicability

LaboTex is a versatile piece of software which can be used to handle: crystallographic textures of materials such as metals and alloys, ceramics and composites, semiconductors and superconductors, polymers and rocks.

All these materials can be:

- of all types of the sample symmetry :
 - 1) orthorhombic,
 - 2) monoclinic,
 - 3) triclinic,
 - 4) axial,
- of all types of the crystal lattice symmetry :
 - 1) triclinic (symmetries after Schoenflies: C_1),
 - 2) monoclinic, (C_2),
 - 3) orthorhombic (D_2),
 - 4) trigonal (D_3, C_3),
 - 5) tetragonal (D_4, C_4),
 - 6) hexagonal (D_6, C_6),
 - 7) cubic (O, T).

1.3. Representation of Orientations by Euler Angles.

Crystal orientation is commonly described by three Euler angles. The three Euler angles ($\varphi_1, \Phi, \varphi_2$) are defined in the space of $0 - 2\pi$ for φ_1 , $0 - \pi$ for Φ and $0 - 2\pi$ for φ_2 . The orientation is described by the rotation that transforms a sample fixed coordinate system into a crystal-fixed coordinate system of a crystallite. The orientation can be described by three counter clockwise partial rotations:

- (a) the crystal coordinate system is rotated by φ_1 angle around Z axis of the sample coordinate system,
- (b) then it is rotated by Φ angle around X axis (in a new position) of the crystal coordinate system,
- (c) Finally it is rotated by φ_2 angle around Z axis of the crystal coordinate system.

1.4. Crystal and sample coordinate systems: LaboTex Axis and Angles Convention.

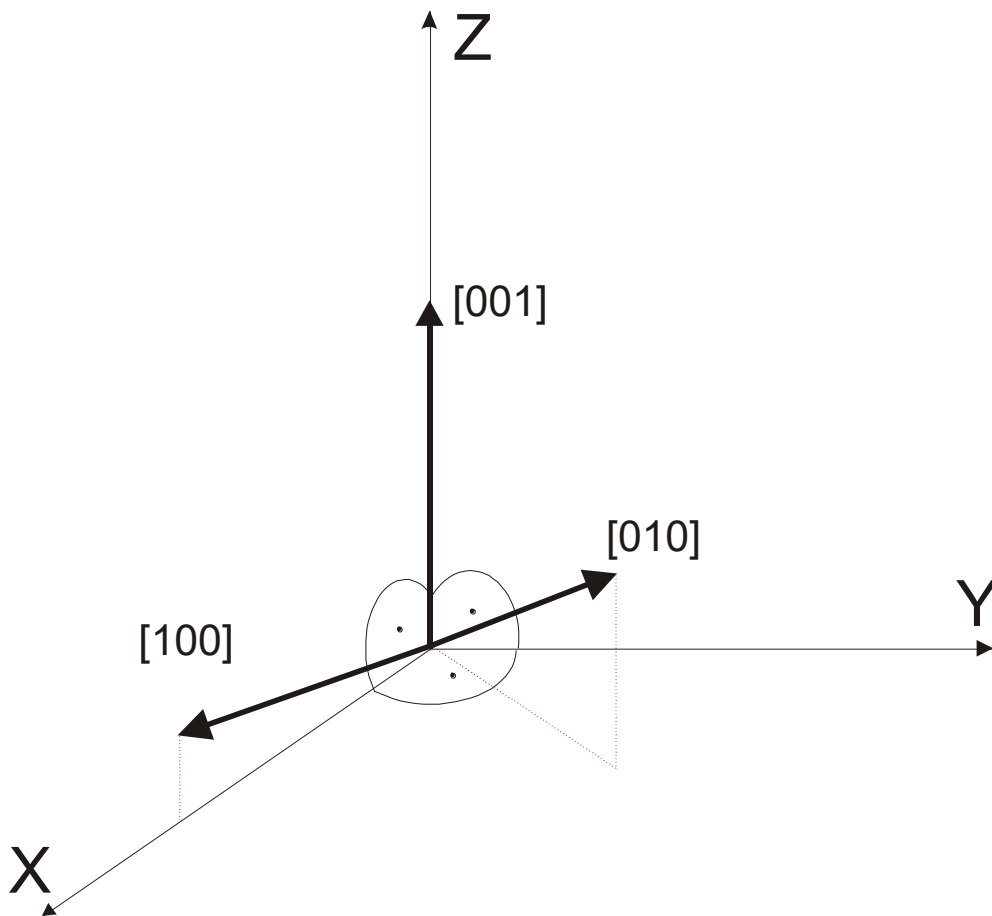


Figure 1

LaboTex uses the following convention of the axis for fixing the crystal and sample coordinate system (Figure 1) :

1. X,Y,Z axis are perpendicular to each other.
2. [100] axis is in XZ plane.
3. Z axis is parallel to the [001] crystallographic axis.
4. The crystal coordinate system and the sample coordinate system should be at the same order i.e. both right-handed or both left-handed.
5. Bunge definition of Euler angles:

where X,Y,Z - the axis of the crystal coordinate system,
[100], [010],[001] - the crystallographic axis.

The exception is the hexagonal system for which user may to choose axis convention A or B (Figure 2) :

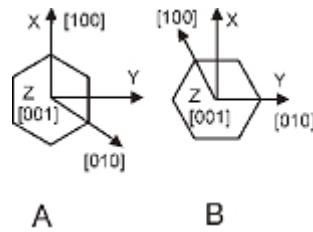


Figure 2

1.5. ODF definition

The Orientation Distribution Function (ODF) is defined as:

$$\frac{dV}{V} = f(g)dg$$

where :

$f(g)$ - values of ODF;

$g(\phi_1, \Phi, \phi_2)$ - orientation;

dV - the volume of crystallites with the orientation g in the element of the orientation space

$dg = \sin\Phi d\Phi d\phi_1 d\phi_2$ where ϕ_1, Φ, ϕ_2 are Euler angles;

V - the sample volume.

1.6. Basic ranges of ODF. LaboTex structure code.

LaboTex shows ODF in a reduced basic range. The Euler angle space can be reduced due to the crystal and sample symmetries. The boundaries of the basic range of ODF in the Euler space and symmetry structure code used in LaboTex are collected in table below:

Symmetry		Cubic**		Hexagonal		Tetragonal		Trigonal		Ortho- rhombic	Mono- clinic	Triclinic
		O	T	D ₆	C ₆	D ₄	C ₄	D ₃	C ₃	D ₂	C ₂	C ₁
LaboTex structure code		7	6	11	10	5	4	9	8	3	2	1
ϕ_1	triclinic* (C ₁)	360°	360°	360°	360°	360°	360°	360°	360°	360°	360°	360°
	monoclinic* (C ₂)	180°	180°	180°	180°	180°	180°	180°	180°	180°	180°	180°
	orthorhombic*(D ₂)	90°	90°	90°	90°	90°	90°	90°	90°	90°	90°	90°
	axial*	-***	-	-	-	-	-	-	-	-	-	-
Φ		90°	90°	90°	180°	90°	180°	90°	180°	90°	180°	180°
ϕ_2		90°	180°	60°	60°	90°	90°	120°	120°	180°	180°	360°

* - sample symmetry

** - there are three non-linear basic regions inside the described region

*** - for any ϕ_1 angle

The structure code is introduced to experimental data files (EPF,POW,PPF...).

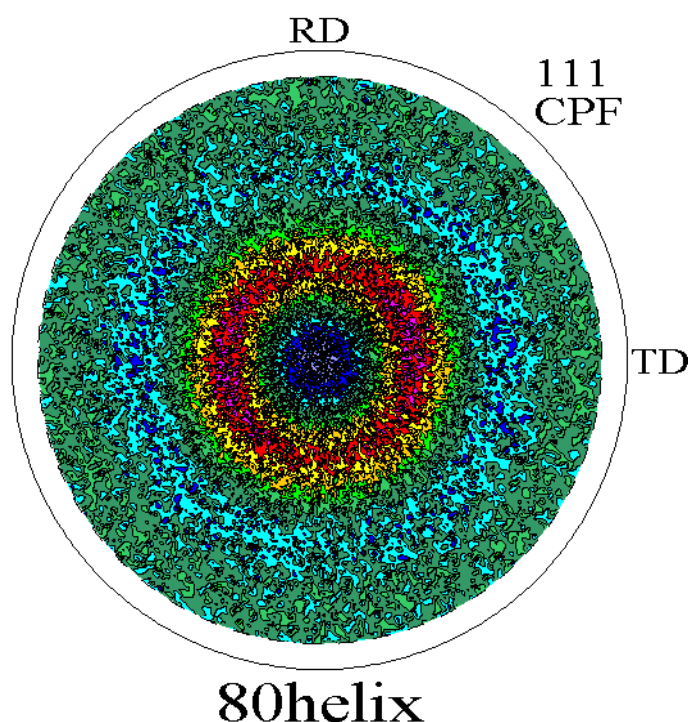
1.7. Pole Figures

The experimental pole figures are obtained via X-ray and neutron measurements. LaboTex pole figures processing comprises of the correction of the pole figures on account of their defocusing and background, as well as the preliminary normalization and the possibility of different kinds of symmetrization. ODF calculation from the pole figures is one of the main areas of applications of LaboTex. Experimental pole figures are unnormalised i.e. the measured intensities depend on the type of X-ray or neutron source, on the type of a counter, the collimating system, the absorption properties of measured material and so on. Therefore experimental pole figures cannot be compared with each other. Pole figures can be correctly normalized only in the ODF calculation process. There are three types of pole figures, from point of view of normalization, used in LaboTex:

- i - unnormalized
- ii - approximately normalised
- iii - precisely normalised.

Pole figures (also max. intensities) from the experimental pole figures (i and ii) usually have different intensities than type iii pole figures. All comparisons between pole figures should be conducted inside type iii pole figures. Quantitative analysis can be done using **only normalised** pole figures.

You can find more details in the LaboTex manual:
“Pole Figures: Registration and Plot Conventions” available from our websites:
www.labosoft.com.pl or www.labotex.com



1.8. The ODF Calculation

The orientation distribution functions determined using LaboTex are ghost corrected. In comparison with the method of the ODF reproduction based on Fourier series, the results obtained using LaboTex are free from truncation errors of the series. Obtaining these error-free results is of great importance when very sharp textures are analyzed. LaboTex calculates the ODF using both types of experimental data:

- ODF calculation from Pole Figures using the ADC method [1-10]. The algorithm of the ADC method used in the program has been verified using a large number of models and experimental data. The results were published in many papers and proceedings (see *ADC Method* on www.labosoft.com.pl/adcmethod). LaboTex reproduces the orientation distribution function with a great precision in a wide range of texture sharpness (from textures close to the random distribution to those of deformed single crystals). ODF can be calculated from complete and incomplete pole figures (measured in an arbitrary range of a radial angle).
- ODF calculation from a set of individual orientations. The number of individual orientations may be arbitrary. Individual orientations may be weighted or not. Individual orientations should be given in Euler angles (degrees or radians are valid).

1.9. Definitions of fit error in ODF calculation

The texture index and definitions of fit error RP (controlling the iteration procedure of ODF calculation) are defined as:

$$f^2 = \frac{1}{8\pi^2} \int_G f^2(g) dg$$

where :

f^2 – texture index,

$f(g)$ – value of ODF,

g – orientation,

G - orientation space.

$$RP_{\{hkl\}} = \frac{1}{N} \sum_{i=1}^N \left| \frac{\{PF_{exp.}\}_i - \{PF_{calc.}\}_i}{\{PF_{exp.}\}_i} \right| \cdot 100\%$$

where :

$RP_{\{hkl\}}$ - relative error for $\{hkl\}$ pole figure,

$\{PF_{exp.}\}_i$ - intensity of experimental (corrected and normalized) pole figure in point i ,

$\{PF_{calc.}\}_i$ - intensity of calculated pole figure in point i ,

N - number of measured points on pole figure.

$$RP = \frac{1}{M} \sum_{j=1}^M RP_{\{hkl\}_j}$$

dRP – absolute change of RP between successive iterations.

1.10. Qualitative Texture Analysis

The Identification of the orientation using cursors, giving their parameters in Euler angles and Miller indices, can be done on the PF and ODF. The identification of the orientation on the different types of objects (PF and ODF) is possible simultaneously in the *Compare* mode. The *Compare* mode is very important for education (the interdependence of orientations on PF and ODF). The values of PFs and ODFs are shown in the points chosen by the cursor. The orientations are optionally collected by users from the orientation data base. Users can add, edit and delete the orientations from the database. The orientations can be entered in a form of Miller indices (HKL UVW) or Euler angles (ϕ_1, Φ, ϕ_2). There is an option to write the angles or indices of the orientation directly into the text box visible in the toolbar. Users can see the value of the intensity for the selected orientation. The values of ODF or/and PF are displayed on the status bar (the sums PF value(s) or/and ODF value).

Qualitative analysis is easy and straightforward to conduct. Users select the appropriate objects and then click 'SORT'. A window with assorted orientations from database by PF or ODF will appear. Users can also analyse the near (HKL)[UVW] orientations by clicking in the selected points on the pole figure or the ODF projection. "Near orientations" can be sorted by PF or ODF values, Miller indices or distance.

1.11. Modelling of ODF, pole figures and inverse pole figures

An ODF model can be easily created using LaboTex.

In order to do that, user should select only:

- Crystal Symmetry;
- Sample Symmetry;
- Grid cells for output ODF.

Then one or more components (up to 10) should be selected. For each texture component users can choose:

- volume fraction;
- FWHM for each Euler angle (ϕ_1, ϕ_2 and ϕ);
- distribution (Gauss or Lorentz).

You can find more details in the LaboTex manual:
“**LaboTex: Modelling of ODF, Pole Figures and Inverse Pole Figure**” available
from our website www.labosoft.com.pl or www.labotex.com

1.12. Quantitative Texture Analysis. I - Volume fraction of texture components by integration methods (IM).

LaboTex includes on-line quantitative analysis of a volume fraction of texture components. The volume fraction of each component, g , can be calculated by integrating over the appropriate subvolume in the orientation space [11] according to:

$$\frac{dv}{V} = \frac{1}{8\pi^2} \iiint f(g) dg$$

where

- dv/V is the volume fraction of grains with orientation $g(\phi_1, \Phi, \phi_2)$,
- $f(g)$ is the value of orientation distribution function, and $dg = \sin\Phi d\Phi d\phi_1 d\phi_2$
- ϕ_1, Φ, ϕ_2 are Euler angles that parameterize the orientation space.

The fundamentals for calculating a volume fraction of texture components are:

- LaboTex makes the integration around the orientation in the ranges delta chosen by the user for each Euler angle:
 - $(\phi_1 - \Delta\phi_1)$ to $(\phi_1 + \Delta\phi_1)$,
 - $(\Phi - \Delta\Phi)$ to $(\Phi + \Delta\Phi)$,
 - $(\phi_2 - \Delta\phi_2)$ to $(\phi_2 + \Delta\phi_2)$,
- In the case of exceeding the basic region of ODF space (Euler angles space) LaboTex continues the integration in the equivalent area of the basic region.

The overlapping problem

The overlapping problem appears when the integration ranges (delta) are too wide or when the orientations are closely situated in the Euler angles space. The integration area of texture components can be overlapped in two ways:

- i) by overlapping of the integration ranges between symmetrically equivalent positions of the component;
- ii) by overlapping of the integration ranges between the different components.

LaboTex offers three different abilities (strategies) to solve the problem of overlapping of the integration ranges between symmetrically equivalent positions of component (case i):

- "Simple Integration" – the overlapping region is multiple integrated. The integration around any single component in the full range of basic region gives $(100\% \text{ minus background}) \times \text{number of a symmetrically equivalent position}$.
- "Single Counts in Overlapping Area" - the overlapping region is only single integrated for the component. The integration around any single component in a full range of the basic region gives 100% minus background.
- "Divide by Number of Symmetrically Equivalent Position" - LaboTex integrates for all symmetrically equivalent positions of the components with proper weight equal to $1/\text{number of symmetrically equivalent positions}$. Integration around any single components in a full range of the basic region gives 100% minus background.

To solve the problem of overlapping of integration ranges between different components in LaboTex (case ii) users can:

- Adjust the total percent of overlapping (overlapping volume fraction) which is displayed in the *Orientations Overlap* window. Overlapping volume fraction can be limited by diminishing integration ranges of texture components.

1. In "Simple Integration" the overlapping volume fraction refers to the sum of overlapping between different components and between symmetrically equivalent positions of all overlapped components.

2. In "Single Counts in Overlapping Area" the overlapping volume fraction refers to the sum overlapping between different components.

3. In "Divide by Number of Symmetrically Equivalent Position" the overlapping volume fraction refers to the excessive orientation overlap. The excessive orientation overlap area is defined in the points where the sum of weights is greater than 1. The weight is equal to $1/\text{number of the symmetrically equivalent positions}$. The excessive ODF value in given point is equal to the product of the ODF value and sum of weights minus 1. The volume fraction of the excessive orientation overlap is the integral of excessive ODF values in the mentioned area.

- An overlapping volume fraction can be divided among overlapping orientations. This option causes the division of ODF values from overlap areas among overlapping orientations:
 1. In "Simple Integration" and "Singlely Counts in Overlapping Area" the ODF values in the overlapping areas are divided proportionally to the number of the symmetrically equivalent overlap orientations.
 2. In "Divide by Number of Symmetrically Equivalent Position" the excessive ODF values in the overlapping areas are divided among components proportionally to the weights and to the number of symmetrically equivalent overlapping orientations.

You can find more details in the LaboTex manual:
**“Determination of Volume Fraction of Texture Components
 Using LaboTex - Integration Method”**
 Available from our websites: www.labosoft.com.pl or www.labotex.com

1.13. Quantitative Texture Analysis. II - Volume fraction of texture components by Model Function Methods (MFM)

LaboTex program includes a second method for determination of the volume fraction of texture components. Users can fit a model ODF (described in point 1.11.) to a real ODF and they select only the components (up to 10 components) and the distribution (Gauss or Lorentz).

LaboTex fits:

- volume fraction;
- FWHM for each Euler angle (ϕ_1 , ϕ_2 and ϕ);

Users can also change the initial volume fraction and the FWHM parameters.

Crystal symmetry, sample symmetry and grid cells for an output ODF are the same as for a real ODF.

You can find more details in the LaboTex manual:
**“Determination of Volume Fraction of Texture Components
 Using LaboTex - Model Functions Method”**
 Available from our websites: www.labosoft.com.pl or www.labotex.com

1.14. ODFs Comparison

LaboTex offers three methods for comparison of ODFs:

- **ODF line sections (cuts)** - users define two points in Euler Space. LaboTex shows ODF intensity along the section defined on the basis of these points. Users can also choose the initial points from the orientations database (by clicking the 'Start Point' or 'End Point' button). It is possible to compare up to 12 ODFs.
- **Skeleton lines** - users can create a number of diagrams such as alpha-fiber, beta-fiber, gamma fiber etc. Users can choose the skeleton lines on the basis of the Euler angle (Φ_1 , Φ or Φ_2) and:
 - **maximal intensity;**
 - **integral intensity.**

Users can change the range in which LaboTex will look for the maximal ODF value or will conduct the integration (from ± 2 to ± 20 deg). Users can make comparisons of up to 12 skeleton lines.

- **Misorientation histograms.** Users define the starting point in Euler Space from which LaboTex will show the misorientation diagrams. Misorientations diagrams are calculated on the basis of ODFs within the range from 0 to 80 degrees counting from the starting point

(the starting orientation). LaboTex shows the intensity which is the relative intensity, that is the intensity which relates to the intensity of a random sample ($I=I(\text{sample})/I(\text{random sample})$) for the same range of the misorientation angle. Users can make comparisons of up to 12 misorientations histograms. Users can change the histogram step within the range from 1 to 10 degrees.

1.15. ODF Transformation

LaboTex calculates a new ODF which is a result of transformation of the initial ODF. The new ODF is created in a new job for sample of initial ODF. There are two kinds of transformations:

- **Frame rotations** - users can rotate a sample frame along any Euler angle. This option is very important to see the ODF for other (different) sample position (for example, to see the ODF for the perpendicular surface with relation to the surface which was measured, you should transform the initial ODF by $\Phi=90\text{deg}$). Users can create a changed sample symmetry for a new ODF.
- **Model rotations builder** - (crystalites/planes rotations) firstly, users should build a rotation model and save it. Secondly, you can choose up to 10 orientations of the rotation model for which you set:
 - the ranges of Euler angle around the center of the orientation (and for the symmetrically equivalent positions);
 - the vector "hkl" around which crystalites/planes will be rotated (only these crystalites/planes which are included in the chosen ranges);
 - the rotation angle;
 - the percent of the rotated crystalites/planes (from 0 to 100%).

Finally, users choose the rotation model and conduct the ODF transformation.

1.16. ODFs - logical operations

Logical operations are conducted on the basis of two ODFs. LaboTex creates a new ODF which is one of:

- an intersection of ODF A and ODF B,
- a difference of ODF A and ODF B (or B-A),
- a union of ODF A and ODF B,
- a sum of ODF A and ODF B,
- an ODF difference : A or B - an intersection A and B,
- an inverted ODF (only for A).

1.17. 2D and 3D Graphics

The program includes an on-screen graphic presentation of calculated ODFs, PFs and INVs in a form of contour levels (isolines) shown in 2D and 3D spaces. 3D objects plotted on the screen can be increased, decreased, shifted, rotated and animated. Up to 100 PFs or INVs can be presented in one window. In Compare Mode the objects of the same kind (PFs vs PFs, or INVs vs INV, or ODFs vs ODFs) or of different kinds (PFs vs ODFs, PFs vs INV, INV vs ODFs) can be shown in two separated windows. Users can use pole figures cuts.

In order to do that, define the starting and end points on the pole figure and Labotex will show you the intensity along the selected section. The following cuts are available:

- 'Arc' (in the range from 0 to 360 degrees);
- 'Radial' (in the range from 0 to 90 degrees);
- 'Radial (full)' (in the range 90 - 0 - 90 degrees).

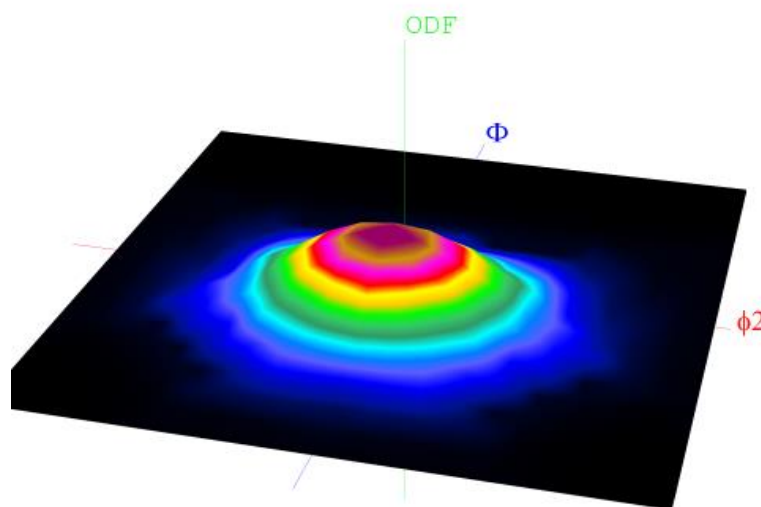
Users can define a grid for the alpha angle and/or a grid for the beta angle of the PF.

1.18. Detailed Manuals (www.labosoft.com.pl and www.labotex.com)

You can find more details about LaboTex in our manuals:

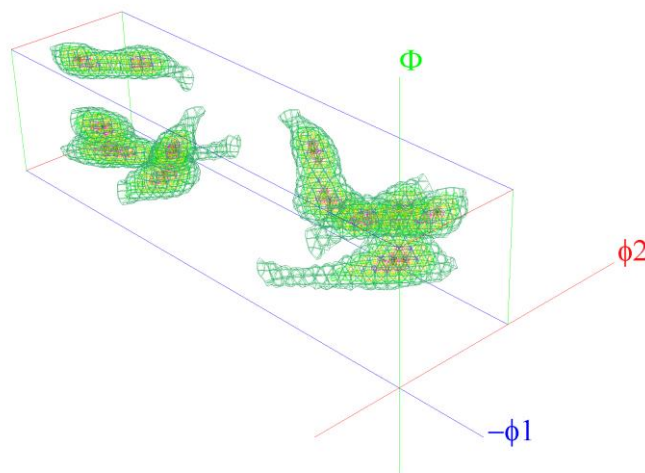
- 1) Introduction to LaboTex 3.0
- 2) Menu Guide to LaboTex
- 3) Determination of Volume Fraction of Texture Components Using LaboTex - Integration Method
- 4) Determination of Volume Fraction of Texture Components Using LaboTex - Model Functions Method
- 5) Nomenclature of Inverse Pole Figures Use in LaboTex
- 6) Pole Figures: Registration and Plot Conventions
- 7) LaboTex: Modeling of ODF, Pole Figures and Inverse Pole Figure
- 8) Texture Analysis on the Base of the EBSD Data
- 9) "Device-independent" pole figures for quantitative texture analysis (Techniques: PIM and IM)
- 10) Fundamentals of 3-D Texture Analysis. Symmetry aspects of 3-D texture analysis
- 11) Hexagonal Axes: Conventions & Conversions
- 12) LaboTex – The Texture Analysis Software - Getting Started
- 13) LaboTex: Modelling of ODF, Pole Figures and Inverse Pole Figure
- 14) LaboTex: Skeleton Lines and Misorientation Diagrams

All manuals are available on our websites www.labosoft.com.pl and www.labotex.com



1.19. ADC method: Opinions and Applications

- "... The strong and weak points of each method are examined showing that the iterative discrete methods (ADC and WIMV) are better suited for the reproduction of the texture function in the present case. In comparing these two discrete methods, it is evidenced that the ADC method reproduces more accurately both the experimental and synthetic texture functions over the entire range of texture sharpness considered ..." F.Caleyo, T.Baudin, M.H.Mathon and R.Penelle - Comparison of several methods for the reproduction of the orientation distribution function from pole figures in medium to strong textured materials - Eur. Phys. J. AP 15 (2001), p85-96.
- "... A discrete method (called as the Arbitrarily Defined Cells method) was applied to calculate the ODF. The 3-D distribution of orientations of the cellulose crystalline areas was reconstructed in the space of the Euler angles. Additionally, the complete pole figures as well as the inverse ones were recalculated. The presented analysis of the cellulose texture provides more extensive information on the space organisation of microfibrils than the standard methods...", Olek W., Pawlik K., Bonarski J. (2000): Space orientation of the crystalline areas of cellulose. Proceedings of the International Conference on Wood and Wood Fiber Composites, 13-15 April 2000, Stuttgart, Germany: 37-46.
- "... Direct Methods (WIMV, ADC) With 1 Degree Resolution Are Preferred...", K.J.Kozaczek,D.S.Kurtz, Quantitative texture analysis of blanket films and interconnects, Workshop on Texture in Electronic Applications NIST, Gaithersburg, MD, October 10-11, 2000.



2. Getting started

2.1. System Requirements

LaboTex runs on MS Windows OS 7,8 or 10 platforms.

1.2 Minimal hardware requirements

Computer PC, Processor PENTIUM IV (or compatible) 2 GHz, 512 MB RAM, 1 GB HD space, graphic card - resolution 1024x768, USB port.

To use the full version of LaboTex, you need to install the protection key (you will need a USB port to do this).

1.3 Recommended hardware requirements

Processor Intel Core 2 Duo or Athlon 64 X2 or higher, 10 GB HD space, 4 GB RAM, graphic card resolution 1920x1080, USB port, color laser jet or inkjet printer.

If your data are measured in the grid less than 5x5 degrees, double free disk space (20 GB) is recommended.

2.2. Installation

To install LaboTex:

1. Switch off the computer.
2. Insert the USB Sentinel/HASP dongle (includes Protect Key & Electronic Media) to USB port.
3. Switch the computer on.

You have to have Administrator credentials to complete the installation procedure!

4. Select drive assigned to USB dongle drive (using Windows Explorer on My Computer icon).
Execute *Setup.exe* file and click *OK*.
5. You will see the 'Welcome' screen, click *Next*. The Software License Agreement will be displayed.
6. Read the Software License Agreement and click *Next* to accept it.
7. Specify a directory to install LaboTex (we strongly recommend that you install LaboTex in the
default directory to avoid further possible conflicts) and click *Next*.
8. Enter the data for the main user, institution and serial number. The serial number can be found on the dongle and in the License Agreement.
9. Double check if all settings are correct and click *Next*. If you need to change any of the settings, click the *Back* button.
10. Now LaboTex is installed and you are prompted whether or not you want to view the *README* file. To proceed further click *Yes*.
11. **In order to install protect key driver (Sentinel/HASP) from the LaboSoft folder run "HASP Protect Key Installation" (double click the "HASP Protect Key Installation" file).**

If you experience any problems during the installation process, please contact us via email office@labosoft.com.pl

2.3. Configuration

The first time you run LaboTex, you will need to configure a few options to your further optimize work:

- 1) From the main menu select '*Edit*' > '*LaboTex Options...*'
- 2) In the Tab *Miscellaneous* check if the following directories point to the right space on your hard drive:
 - A) Temporary Directory
 - B) Experimental Data Directory (EPF and other)
 - C) Correction Data Directory (COR)

You may change the default setup of the directories by clicking the '*New*' button.

3. LaboTex Objects and Object Containers

3.1 Introduction

Pole figures and orientations distribution functions (ODF) are LaboTex objects. Figure 3 shows a diagram for creating objects, calculation and analyses in LaboTex.

Labotex operates six types of objects:

No	Denotation	Object Types
1	CPF	Corrected Pole Figures
2	NPF	Normalized Pole Figures
3	RPF	Recalculated Pole Figures
4	APF	Additional Pole Figures
5	INV	INVerse Pole figures
6	ODF	Orientation Distribution Function

These six types of objects can be stored in three types of containers: Pole Figures Container, Inverse Pole Figures Container and Orientation Distribution Function container :

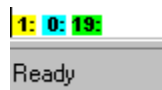
No	Container	Objects	Color
1	Pole Figures Container	CPF, NPF, RPF, APF	yellow color
2	Inverse Pole Figures Container	INV	blue color
3	Orientation Distribution Function container	ODF	green color

Objects from one container can be only shown in a single window at a time. Objects from two containers can be shown simultaneously only in the comparison mode (double windows - see: *Compare Window Mode*). To add or delete an object from a container click the relevant button on the object toolbar:

Button	Objects
HKL	CPF,NPF,RPF,APF
XYZ	INV
Projection	ODF

The number of objects in containers is shown in the left bottom corner of the window (yellow for the pole figures container, blue for the inverse pole figures and green for the orientation distribution function container). There can only be one projection in the container of the ODF objects at a given time. For the ODF container the number of objects indicates the number of 2-D ODF sections.

The figure below shows an example when the Pole Figures Container contains 1 pole figure, the Inverse Pole Figures Container is empty (0 INV object) and the Orientation Distribution Function container contains a ODF projection which has 19 2-D ODF sections



Objects Creations, Calculations and Analysis in LaboTex Program

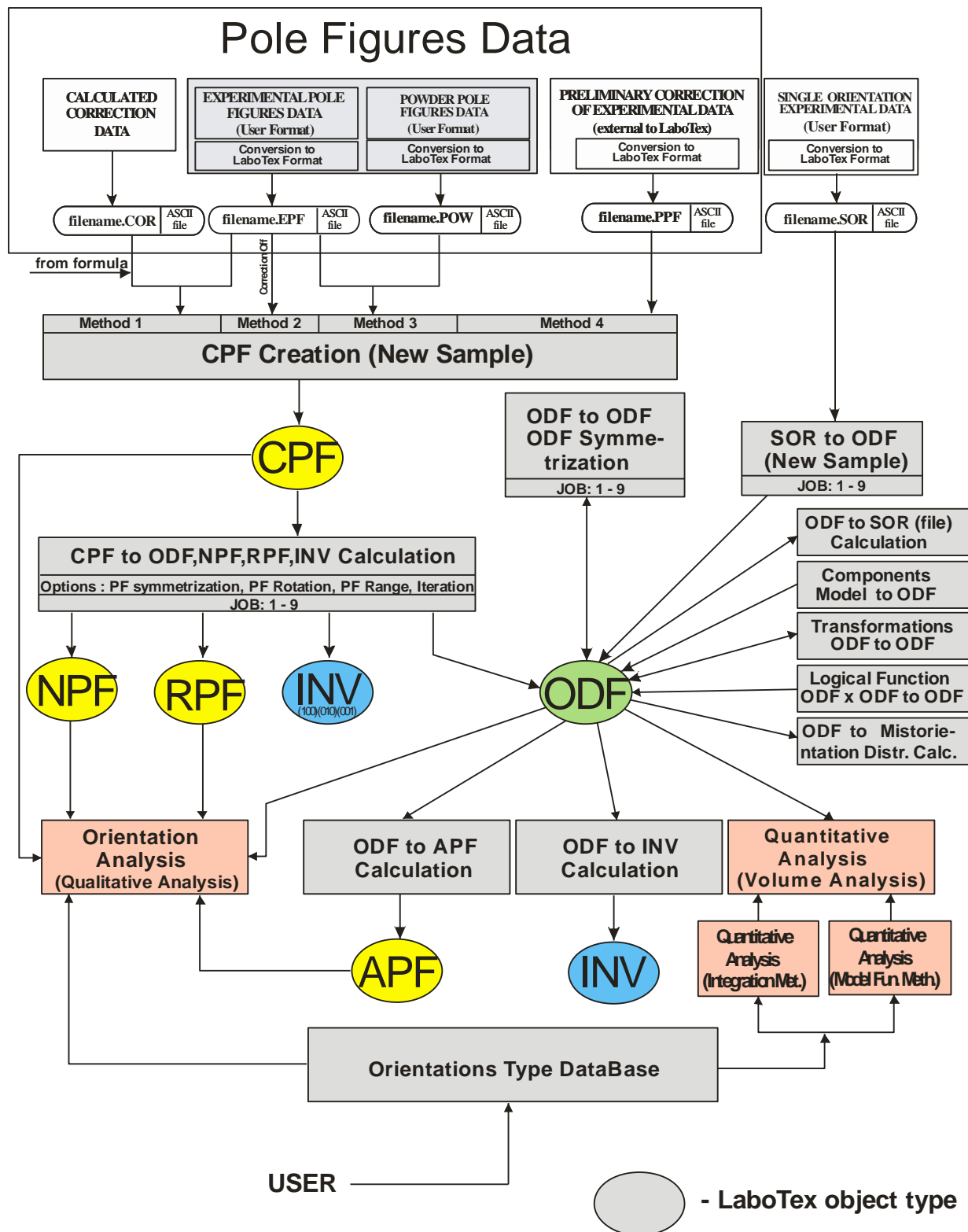


Figure 3

For the ODF objects only one projection ϕ_{11} or ϕ_{21} or ϕ_{Φ} can be stored in a container at a given time. To add or delete objects from the containers, click the relevant button on the object toolbar (for the pole figures container and the inverse pole figures container).

Container	Objects	Limitation
HKL	CPF,NPF,RPF,APF	maximum up to 100 objects
XYZ	INV	maximum up to 100 objects
Projection	ODF Projection	maximum up to 360 2D ODF sections

All objects in the container have to be in the same crystal symmetry. Objects arrangement on the screen can be changed as a new default (in *LaboTex Options* -> *Edit Menu*) or temporarily for the current session in *Edit Menu* -> *Arrangement*.

To delete all objects in containers use *Edit Menu* -> *Clear All* or select the toolbar button 

3.2 LaboTex Objects Types

Pole figures used in LaboTex are of three types from the point of view of normalization:

- i - unnormalised : EPF
- ii - approximately normalised : CPF
- iii - precisely normalised: NPF, RPF, and APF

Pole figures from the experiment EPF and CPF have usually different intensities from pole figures of type iii (NPF, RPF and APF).


All comparisons between pole figures should be done inside pole figures of type iii.

Quantitative analysis can be conducted using normalised pole figures.

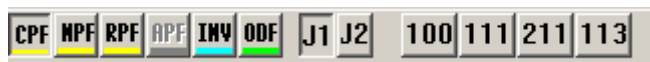
3.2.1 CPF - Corrected Pole Figures

Experimental pole figures obtained from X-ray or neutron diffraction are unnormalised i.e. measurement intensities depend on the type of the X-ray or neutron source, the type of the counter, the collimating system, the absorption properties of measured material and so on. Therefore experimental pole figures are not comparable between each other. Pole figures can be correctly normalized only during the ODF calculation process.

Corrected Pole Figures (CPF) can be corrected (according to background and de-focussing) and only **preliminary** normalized to experimental pole figures **prepared for the ODF calculation**. CPF object should not be used for analysis. CPF objects contain single pole figures of the hkl type.

To create CPF objects from your experimental files, select *File->New Sample* or click  on the toolbar. You can calculate ODFs after creating CPF objects and create other objects.

To display CPF objects click the CPF button on the object toolbar, then click one or more buttons with the hkl indices:

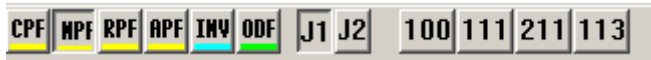


Note: CPF objects are the same for all jobs.

3.2.2 NPF - Normalized Pole Figures

Normalized Pole Figures are completely normalized (during the ODF calculation process) experimental pole figures. They are correctly normalized and they can be compared between

each other. They are created after the ODF calculation. To display an NPF object click the NPF button on the object toolbar and then click one or more buttons with the *hkl* indices:

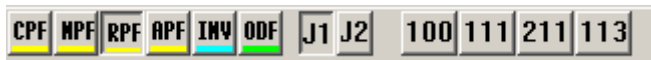


Note: If more than one job have been created, choose the relevant job using the job buttons (J1,J2 ..) on the object toolbar.

3.2.3. RPF - Recalculated Pole Figures


Recalculated Pole Figures are calculated from ODFs, equivalent to those PFs used as data to ODF reproduction. They are **complete** pole figures.

To display RPF objects click the RPF button object toolbar, then click one or more buttons with the hkl indices:



Note: If more than one job have been created, choose the relevant job using the job buttons (J1,J2 ..) on the object toolbar.

3.2.4. APF - Additional Pole Figures


Additional Pole Figures are calculated from the ODF pole figures of HKL types which were **not used for ODF determination**. APF objects contain a collection of single additional pole figures. To calculate additional pole figures (APF) select *Calculation menu -> ODF to APF* or click the button  from the toolbar.

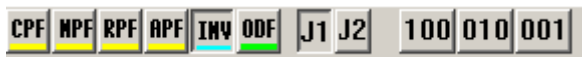
For displaying APF object click the APF button on the object toolbar, then click one or more buttons with the hkl indices:



Note: If more than one job have been created, choose the relevant job using the job buttons (J1,J2 ..) on the object toolbar.


3.2.5. INV - INVerse pole figures

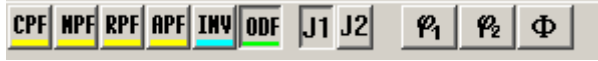
INVerse pole figures are calculated from ODFs. An inverse pole figures object (INV object) contains a collection of single inverse pole figures of XYZ types. INV objects: (100),(010) and (001) are always created after the ODF calculation. To calculate other inverse pole figures (INV) select *Calculation menu ->ODF to INV* or click the button  on the toolbar. To display an INV object click the INV button on the object toolbar, then click one or more buttons with the XYZ indices:



Note: If more than one job have been created, choose the relevant job using the job buttons (J1,J2 ..) on the object toolbar.

3.2.6.ODF - Orientation Distribution Function

Orientation Distribution Function is calculated from experimental pole figures (CPF objects) by the ADC method or from sets of single orientations. To calculate ODF and create ODF objects open the *Calculation menu ->CPF to ODF, NPF, RPF, INV*, *Calculation menu ->SOR to ODF* or click the button  from the toolbar. The ODF objects are 2-D ODF projections: ϕ_1 , ϕ_2 and Φ . To display an ODF object click ODF button on the object toolbar, then click the button with the ODF projection:



Note: If more than one job have been created, choose the relevant job using the job buttons (J1,J2 ..) on the object toolbar.

3.3. Example CPF, NPF, RPF objects

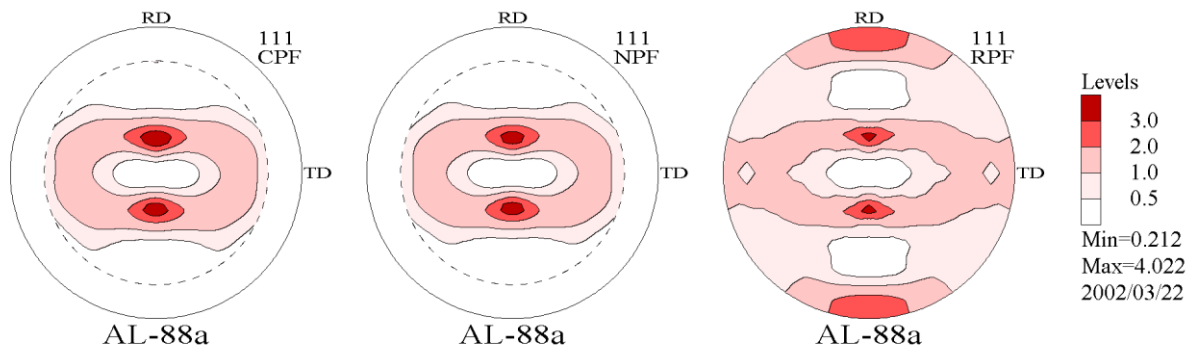
In the example below:

CPF – experimental $\{111\}$ pole figure (incomplete pole figure).

ODF - calculated for symmetrization : triclinic to orthorhombic.

NPF – normalized $\{111\}$ pole figure.

RPF - recalculated from ODF $\{111\}$ pole figure (complete pole figure).



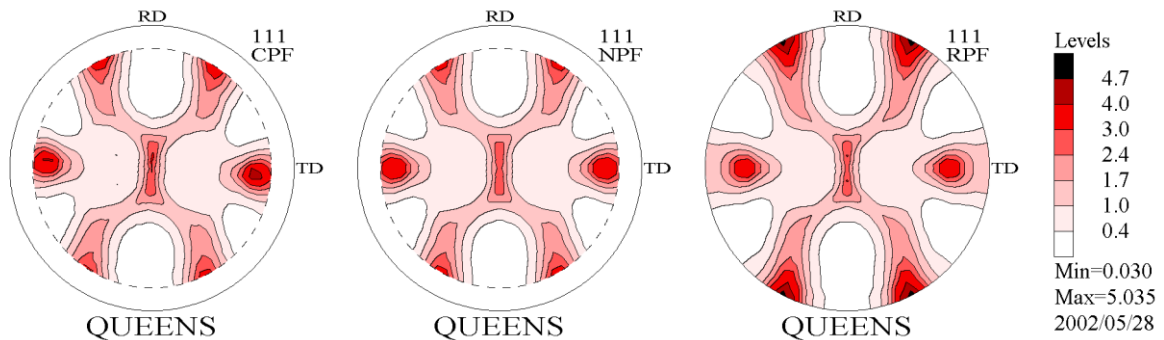
In the example below:

CPF – experimental $\{111\}$ pole figure (incomplete pole figure).

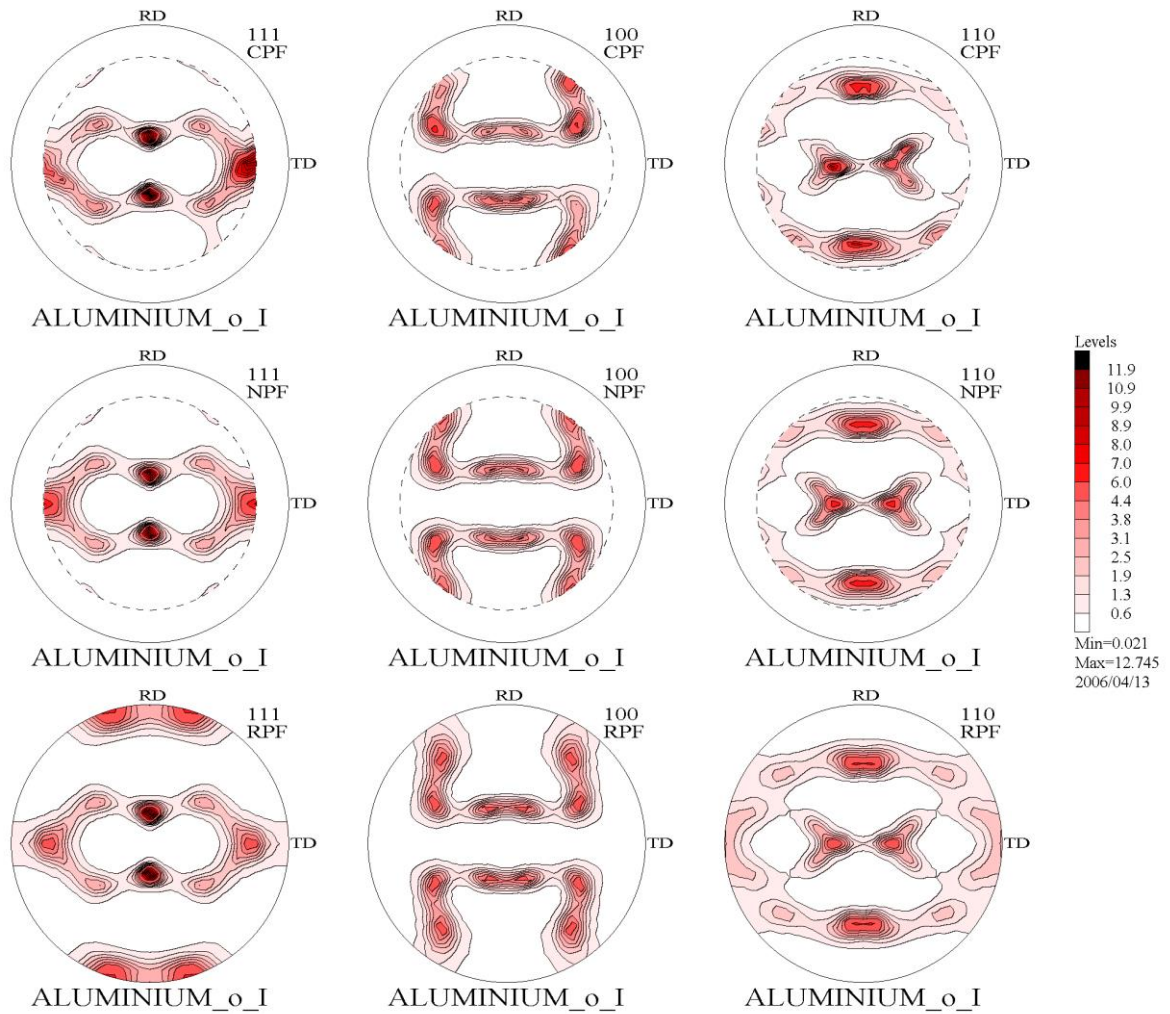
ODF - calculated for symmetrization : triclinic to orthorhombic and rotation of PF(s)= -2.5 deg.

NPF – normalized $\{111\}$ pole figure.

RPF - recalculated from ODF $\{111\}$ pole figure (complete pole figure).



Experimental pole figures - aluminium - pole figures: CPFs, NPFs, RPFs



3.4. LaboTex Jobs

When one calculation (job) is already running, selecting next calculations of ODFs from the same sample creates new jobs. If more than one job has been created, select the relevant job using the job buttons (J1,J2 ..) on the object toolbar. A new job is also created when the ODF symmetrisation is launched

Job buttons:



Note: The maximal number of jobs is 9

4. LaboTex Formats

4.1. EPF file format

*.EPF (Experimental Pole Figures) files refer to the raw experimental data and their background. **In order to use the EPF files you will need a correction file: *.COR or *.POW**

The table below provides a detailed description of the *.EPF data format:

Line	No of data in line	Description	Type
1 – 2		Arbitrary title	Character
3		Remarks for data in line 4	
4	1	Structure Code (symmetries after Schoenflies): 1 - C ₁ (triclinic) 2 - C ₂ (monoclinic) 3 - D ₂ (orthorhombic) 4 - C ₄ (tetragonal) 5 - D ₄ (tetragonal) 6 - T (cubic) 7 - O (cubic) 8 - C ₃ (trigonal) 9 - D ₃ (trigonal) 10 - C ₆ (hexagonal) 11 - D ₆ (hexagonal)	Integer
4	2	Lattice constant, a (absolute or relative)	Real
4	3	Lattice constant, b (absolute or relative)	Real
4	4	Lattice constant, c (absolute or relative)	Real
4	5	Lattice angle, α in degrees	Real
4	6	Lattice angle, β in degrees	Real
4	7	Lattice angle, γ in degrees	Real
5	1	Number of Pole Figures (including background PFs) (N)	Integer
6		Remarks for data in line 7	Character
7 to 7+N	1	2 θ Bragg angle in degrees	Real
7 to 7+N	2	α_s - beginning of polar angle in degrees	Real
7 to 7+N	3	α_e - ending of polar angle in degrees	Real
7 to 7+N	4	$\Delta\alpha$ - step of polar angle in degrees. Permissible value: 1.0, 1.2, 1.25, 1.5, 2.0, 2.5, 3.0, 3.75, 5.0, 6.0, 7.5, 10.0.*	Real
7 to 7+N	5	β_s - beginning of azimuthal angle in degrees (0 or 2.5)	Real Positive values for pole figures drawn clockwise or negative values for counter-clockwise
7 to 7+N	6	β_e - ending of azimuthal angle in degrees	Real Positive values for pole figures drawn clockwise or negative values for counter-clockwise
7 to 7+N	7	$\Delta\beta$ - step of azimuthal angle in degrees . Permissible values: 1.0, 1.2, 1.25, 1.5, 2.0, 2.5, 3.0, 3.75, 5.0, 6.0, 7.5, 10.0. for textured pole figures, and the same values or multiplicity of above-mentioned values for background PFs	Real Positive values for pole figures drawn clockwise or negative values for counter-clockwise
7 to 7+N	8	Index - must be 0	Real
7 to 7+N	9	Index <i>h</i> of <i>hkl</i> pole figure	Integer
7 to 7+N	10	Index <i>k</i> of <i>hkl</i> pole figure	Integer
7 to 7+N	11	Index <i>l</i> of <i>hkl</i> pole figure	Integer
7 to 7+N	12	Type of Data (1-Pole Figure, 0-Background)	Integer
7+N+1		Blank line	
7+N+2	1 to 8	Data 1 to 8 (1 st Pole Figure)	Real
7+N+3	1 to 8	Data 9 to 16 (1 st Pole Figure)	Real
7+N+4 to end of data for 1 st PF	1 to 8	Data for 1 st Pole Figure	Real
...		Blank line (separates block of data)	
...	1 to 8	Data for 2 nd pole figure	Real
...		Blank line (separates block of data)	
...	1 to 8	Data for the next PF (up to end followed by blank line)	Real

Please note: Real and integer input data must be separated by one or more space signs.

*LaboTex version 2.1.006 and higher allows new grid cell 1.8x1.8,2.25x2.5,3.6x3.6,4.5x4.5 (exceptions: trigonal,hexagonal and crystal lattice symmetry)

See the specifications below for: EPF Example, COR file format , POW file format , PPF file format , SOR file format.

4.2. EPF Example

Example of an experimental data file *.EPF - test.epf:

```
line 1: Test of LaboTex program - ADC method for ODF calculation.
line 2: Sample: FeSi, pole figures: 200 110 112
line 3: Structure Code a b c alfa beta gamma
line 4: 7 1 1 1 90 90 90
line 5: 6 number of Pole Figures
line 6: 2theta alf-s alf-e d-alf bet-s bet-e d-bet indx H K L P/B
line 7: 45.250 0.0 85.0 5.0 0.0 355.0 5.0 0 2 0 0 1
line 8: 52.050 0.0 85.0 5.0 0.0 355.0 5.0 0 1 1 0 1
line 9: 77.450 0.0 85.0 5.0 0.0 355.0 5.0 0 1 1 2 1
line 10: 48.500 0.0 85.0 5.0 0.0 270.0 90.0 0 2 0 0 0
line 11: 70.000 0.0 85.0 5.0 0.0 270.0 90.0 0 1 1 0 0
line 12: 80.000 0.0 85.0 5.0 0.0 270.0 90.0 0 1 1 2 0
line 13:
line 14: 172763. 172763. 172763. 172763. 172763. 172763. 172763. 172763.
line 15: 172763. 172763. 172763. 172763. 172763. 172763. 172763. 172763.
line 16: 172763. 172763. 172763. 172763. 172763. 172763. 172763. 172763.
... (line 17-172)
line 173: 12871. 15208. 15536. 13571. 10464. 7874. 6977. 7874.
line 174: 10464. 13571. 15536. 15208. 12871. 9947. 7753. 6885.
line 175: 7512. 9977. 15302. 23949. 32907. 36331. 32369. 25152.
line 176:
line 177: 12319. 12319. 12319. 12319. 12319. 12319. 12319. 12319.
line 178: 12319. 12319. 12319. 12319. 12319. 12319. 12319. 12319.
line 179: 12319. 12319. 12319. 12319. 12319. 12319. 12319. 12319.
... (line 180-335)
line 336: 11977. 13260. 15924. 19655. 23043. 23659. 22398. 23659.
line 337: 23043. 19655. 15924. 13260. 11977. 12233. 14581. 19084.
line 338: 24630. 30445. 36111. 40462. 38757. 30857. 21645. 15090.
line 339:
line 340: 142442. 142442. 142442. 142442. 142442. 142442. 142442. 142442.
line 341: 142442. 142442. 142442. 142442. 142442. 142442. 142442. 142442.
line 342: 142442. 142442. 142442. 142442. 142442. 142442. 142442. 142442.
... (line 343-498)
line 499: 19467. 17249. 16302. 15782. 15387. 15200. 15068. 15200.
line 500: 15387. 15782. 16302. 17249. 19467. 22203. 22229. 18484.
line 501: 13296. 9168. 7555. 7739. 8997. 11247. 13362. 14321.
line 502:
line 503: 830. 792. 679. 717. 830. 792. 679. 717.
line 504: 822. 784. 672. 710. 814. 777. 666. 703.
line 505: 806. 769. 659. 696. 798. 762. 653. 689.
... (line 506-508)
line 509: 519. 495. 424. 448. 441. 421. 361. 381.
line 510: 362. 346. 296. 313. 287. 274. 235. 248.
line 511: 220. 210. 180. 190. 164. 157. 134. 142.
line 512:
line 513: 2258. 2156. 1848. 1951. 2258. 2156. 1848. 1951.
line 514: 2258. 2156. 1848. 1951. 2236. 2134. 1830. 1931.
line 515: 2236. 2134. 1830. 1931. 2236. 2134. 1830. 1931.
... (line 516-518)
line 519: 1981. 1891. 1621. 1711. 1851. 1767. 1515. 1599.
line 520: 1637. 1562. 1339. 1413. 1329. 1268. 1087. 1147.
line 521: 922. 880. 754. 796. 330. 315. 270. 285.
line 522:
line 523: 9209. 8791. 7535. 7954. 9209. 8791. 7535. 7954.
line 524: 9118. 8704. 7460. 7875. 9118. 8704. 7460. 7875.
line 525: 9029. 8618. 7387. 7798. 8941. 8535. 7315. 7722.
... (line 526-528)
line 529: 7611. 7265. 6227. 6573. 6977. 6660. 5708. 6025.
line 530: 5903. 5635. 4830. 5098. 4723. 4508. 3864. 4079.
line 540: 3143. 3000. 2572. 2715. 1246. 1190. 1020. 1076.
```

See the specifications below for: EPF file format, COR file format, POW file format, PPF file format, SOR file format.

4.3. PPF file format

***PPF** (**P**reliminary **C**orrected **P**ole **F**igures^K) files refer to the experimental data after conducting the background and de-focussing effects corrections using external procedures (not conducted in LaboTex).

The structure of a ***PPF** file is identical to ***EPF** and ***POW** except for the data for the background of pole figures.

See the specifications below for: EPF file format, COR file format, POW file format , SOR file format .

4.4. SOR file format

***SOR** (**S**ingle **O**rientation) files refer to experimental, single orientation set in the LaboTex format

The table below provides a detailed description of ***SOR** data format:

Line	No of data in line	Description	Type
1 - 2		Arbitrary title	Character
3		Remarks for data in line 4	
4	1	Structure Code (symmetries after Schoenflies): 1 - C ₁ (triclinic) 2 - C ₂ (monoclinic) 3 - D ₂ (orthorhombic) 4 - C ₄ (tetragonal) 5 - D ₄ (tetragonal) 6 - T (cubic) 7 - O (cubic) 8 - C ₃ (trigonal) 9 - D ₃ (trigonal) 10 - C ₆ (hexagonal) 11 - D ₆ (hexagonal)	Integer
4	2	Lattice constant, a (absolute or relative)	Real
4	3	Lattice constant, b (absolute or relative)	Real
4	4	Lattice constant, c (absolute or relative)	Real
4	5	Lattice angle, α in degrees	Real
4	6	Lattice angle, β in degrees	Real
4	7	Lattice angle, γ in degrees	Real
4	8	Step for output ODF (grid cells). Permissible values (deg): 1.0, 1.2, 1.25, 1.5, 2.0, 2.5, 3.0, 3.75, 5.0, 6.0, 7.5, 10.0*	Real
4	9	Weight for data (1 – present, 0 – absent)	Integer
4	10	Angle Unit: 0 – deg, 1 – rad	Integer
4	11	Angle Convention: 0 – Bunge 1 – Roe	Integer
5 to the end	1	ϕ_1	Real
5 to the end	2	Φ	Real
5 to the end	3	ϕ_2	Real
5 to the end	[4]	Weight (optionally) (if parameter <i>weight</i> in line 4 is 1)	Real

Note: Real and integer input data must be separated in line by one or more spaces.

*LaboTex allows new grid cell from version 21.006: 1.8x1.8,2.25x2.5,3.6x3.6,4.5x4.5 (exceptions: trigonal,hexagonal crystal lattice symmetry

See the specifications below for: EPF file format, COR file format, POW file format , PPF file format.

4.5. POW format

***POW** (**P**OWder pole figures) files refer to the powder sample pole figures measured, if possible, for a specific sample.

You should measure the pole figures of the powder sample for defocusing correction from the same material as the "textured samples". The powder sample is treated as "non-texture" sample which helps to identify the absorption curve for defocusing correction.

The structure of ***POW** file is identical to ***EPF**.

See the specifications below for: EPF file format, COR file format, SOR file format , PPF file format.

4.6. COR format

*.**COR** (**COR**rection) files refer to coefficients for the de-focussing effect.

*.**COR** files contain a set of correction coefficients for the de-focussing effect.

The table below provides a detailed description of *.**COR** data format:

Line	No of data in line	Description	Type
1 – 2		Arbitrary title	Character
3	1 to n	α in degrees (polar angle)	Real
4	1	{hkl} of first pole figure (three digits number)	Real
4	2 to n+1	correction coefficients for de-focussing effect	Real
5	1	{hkl} of second pole figure (three digits number)	Real
5	2 to n+1	correction coefficients for de-focussing effect	Real
...		...	
3+N*2	1	{hkl} (three digits number) N - number of pole figure	Real
4+N*2	2 to n+1	correction coefficients for de-focussing effect	Real

Please note: Real and integer input data must be separated by one or more space signs.

See the specifications below for : EPF file format, PPF file format, SOR file format, POW file format.

4.7. Other data formats

List of the compatible LaboTex data formats.

All trademarks are the properties of their respective owners and are only used in a descriptive fashion without any intention to infringe.

(For the updates and the current list of LaboTex compatible file formats see: www.labosoft.com.pl)

- **'TSV'** Single Orientations Files,
 - Single orientations data files: *.tsv can be selected from *File->New Sample-> Choose Experimental Data*
- **'PLF'** Queens Univ. PF Format files (4*5deg) - (corrected pole figures),
 - Pole figures data files : *.plf can be selected from *File->New Sample-> Choose Experimental Data*
- **'PLF'** 5*5deg - (corrected pole figures),
 - Pole figures data files : *.plf can be selected from *File->New Sample-> Choose Experimental Data*
- **'CON'** McGill University PF Format files - (corrected pole figures),
 - Pole figures data files : *.con can be selected from *File->New Sample-> Choose Experimental Data*
- **'HKL'** HKL - Kawasaki KTEC Format files - (corrected pole figures),
 - Pole figures data files : *-hkl. can be selected from *File->New Sample-> Choose Experimental Data*
- **'hkl'** AGH main format,
 - Pole figures data files : *.hkl can be selected from *File->New Sample-> Choose Experimental Data*
 - Background pole figures data files: *-b.hkl can be selected from *File->New Sample-> Choose Experimental Data*

- Random(powder) pole figures data files: *-p.hkl can be selected from *File->New Sample-> Choose Experimental Data*
- Background random(powder) pole figures data files: *-t.hkl can be selected from *File->New Sample-> Choose Experimental Data*
- 'x**fb**' AGH second format (corrected pole figures),
 - Pole figures data files : *.xfb can be selected from *File->New Sample-> Choose Experimental Data*
- 'C**TF**' HKL Single Orientations Files,
 - Single orientations data files: *.CTF can be selected from *File->New Sample-> Choose Experimental Data*
- 'S**NG**' TSL Single Orientations Files,
 - Single orientations data files: *.sng can be selected from *File->New Sample-> Choose Experimental Data*
- 'T**XT**' HKL Single Orientations Files,
 - Single orientations data files: *.txt can be selected from *File->New Sample-> Choose Experimental Data*
- 'U**XD**' (file version 1) - SIEMENS/BRUKER (corrected pole figures, ASCII-files!,GADDS/D-8 Discover XRD). Use only one pole figure in one file. Parameter "_sample" has to contain Miller indices of PF (in triangle brackets) for example: "Ir<111>".
 - Pole figures data files: *.uxd can be selected from *File->New Sample-> Choose Experimental Data*
 - **Please note:** Convert the binary files from the GADDS/D-8 Discover XRD to the the ASCII UXD files using software from Siemens/Bruker (XCH or other).
- 'U**XD**' (file version 2) - BRUKER (corrected pole figures, ASCII-file!,GADDS/D-8 Discover XRD).
 - Pole figures data files: *.uxd can be selected from *File->New Sample-> Choose Experimental Data*
 - **Please note:** Convert the binary files from the GADDS/D-8 Discover XRD to the ASCII UXD files using the software from Bruker (XCH or other).Use only one pole figure in one file. The parameter "_sample" has to contain Miller indices of PF (in triangle brackets), for example: "Ir<111>".

LaboTex can read background files for the UXD format:

1) mark the data for background with 'B' letter in indices of pole figure (for example, the filename should be '<111B>cu brut').

```

-----
_FILEVERSION=2
_SAMPLE="<111B> cu brut"
_SITE='UNIV ...'
_USER='LAMBDA'
...
-----

```

2) LaboTex requires one pole figure in one UXD file.

Each pole figure and background file has to be in a separate file with the extension *.UXD.

For example: sample_100.UXD, sample_100BL.UXD, sample_100BR.UXD, ...

(the filenames which terminate with 'BL' or 'BR' include the background from the 'left' and 'right' side of PF. LaboTex average BL and BR values.)

3) You may use only BL or BR file.

4) Background files in the UXD format can have only one background value for one alpha value!

For example, if you have one pole figure, Cu-brut_111.UXD, you should make 3 files in XRD software:

a) Cu-brut_111.UXD (pole figure data+ parameter sample: _SAMPLE="<111> cu brut")

b) Cu-brut_111BL.UXD (left background data + parameter sample: _SAMPLE="<111B> cu brut")

c) Cu-brut_111BR.UXD (right background data+ parameter sample: _SAMPLE="<111B> cu brut")

o Many pole figures in a file (2 cases). Please convert XCH (or any other format) to UXD with options: 2Theta-Intensity and with one column of intensity values. You can input data for azimuthal (KHI) angle in ranges: 0.0-360.0,0.0-180.0,0.0-90.0 or 0.0-X degrees (where 0.0<X<=50.0)

- enter manually the hkl indices in triangle brackets to the UXD file in places where the pole figure data starts (available from version 3.0.004)::

```
-----  
... (header)  
_ANODE='Cu'  
<111>  
; (Data for Range number 1) <--- start (data for first pole figure)  
_DRIVE='PHI'  
_STEPTIME=5.000000  
...  
<110>  
; (Data for Range number 17) <--- start (data for second pole figure)  
_DRIVE='PHI'  
_STEPTIME=5.000000  
...  
-----
```

For the background data add 'B' letter to the hkl indices (for example: <111B>). The background data in UXD format can have only one background value for one alpha/PHI value!

You can also enter defocussing correction data (from version 3.0.004).

Random (powder) pole figures data files: *.UXD can be selected "Choose Defocussing Correction" list.

- (available from version 3.0.006):

enter manually the hkl indices in triangle brackets to the UXD file from the second line in the file. For the background data please add 'B' letter to the hkl indices (for example: <111B>).

```
-----  
;remarks line (first line)  
<111>  
<111B>  
<111B>  
<200>  
<200B>  
<200B>  
<311>  
<311B>  
<311B>  
_FILEVERSION=2  
_SAMPLE='Copper'  
...  
-----
```

Background data in UXD format can have only one background value for one alpha/PHI value! If your file contains background data with a label "_RATE_BKG=", LaboTex will automatically correct your pole figure. In such case do not enter the hkl indices for the background into your file. You can enter the defocussing correction data in the same way. Random (powder) pole figures data files: *. can be selected from *File->New Sample-> Choose Defocussing Correction*.

- 'UXD' As 'UXD' formats above (SIEMENS/BRUKER file version 1 and 2) - only with reversed radial direction! Corrected pole figures (ASCII-files).
- 'HKL' Chalk River Neutron Diffraction Data (corrected pole figures)
 - Pole figures data files: *.* can be selected from *File->New Sample-> Choose Experimental Data*
- 'ANA' - EMSE Format files (corrected pole figures)
 - Pole figures data files: *.ana can be selected from *File->New Sample-> Choose Experimental Data*
- 'epf' - popLA PF Format files (corrected pole figures).

Please note: Files in popLA format have the same extension as LaboTex files: "EPF". Select "epf" (**small capitals!**) data format in LaboTex Options for files in popLA format.

- Pole figures data files: *.epf can be selected from *File->New Sample-> Choose Experimental Data*
- 'RAW' - popLA Format files
 - Pole figures data files: *.raw can be selected from *File->New Sample-> Choose Experimental Data*
 - Defocussing correction data files: *.dfb can be selected from *File->New Sample-> Choose Defocussing Correction*
- 'ASC' - Rigaku ASC format (1PF/file)
 - Pole figures data files: *.asc can be selected from *File->New Sample-> Choose Experimental Data*
 - Random(powder) pole figures data files: *.asc can be selected from *File->New Sample-> Choose Defocussing Correction*
- 'XPF' - BEARTEX data format (corrected pole figures)
 - Pole figures data files: *.xpf can be selected from *File->New Sample-> Choose Experimental Data*
- 'PFG' - RIST data format from RIGAKU (ASCII)
 - Pole figures data files: *.pfg can be selected from *File->New Sample-> Choose Experimental Data*
 - Random pole figures data files: *.pfg can be selected from *File->New Sample-> Choose Defocussing Correction*
- 'TXT' - RIST data format from PHILIPS (ASCII- corrected pole figures)
 - Pole figures data files: *.txt can be selected from *File->New Sample-> Choose Experimental Data*

- **'RW1'** - PHILIPS X'Pert binary data format (Binary)
 - Pole figures data files: *.rw1 can be selected from *File->New Sample-> Choose Experimental Data*
 - Background pole figures data files: *.bgr can be selected from *File->New Sample-> Choose Experimental Data*
 - Defocussing correction data files: *.cor can be selected from *File->New Sample-> Choose Defocussing Correction*

Please note: Background pole figures data files may have the same extension as defocussing correction data files ('COR'). Please change 'COR' extension for the background files to 'BGR'!

- **'NJA'** - Seifert ASCII data format (compatible also with data from PSD)
 - Pole figures data files: *.NJA can be selected from *File->New Sample-> Choose Experimental Data*
 - Random pole figures data files: *.NJA can be selected from *File->New Sample-> Choose Defocussing Correction*
- **'NJC'** - Seifert binary data format (compatible also with data from PSD)
 - Pole figures data files: *.NJC can be selected from *File->New Sample-> Choose Experimental Data*
 - Random pole figures data files: *.NJC can be selected from *File->New Sample-> Choose Defocussing Correction*
- **'DAT'** - Seifert ISO-DEBYFLEX 3003 - ASCII data format. Use only one pole figure in one file. Pole figure indices are 3 last characters before the period in the filename (example: PC_200.DAT for 200 pole figure). Optionally you may add the parameter "2THETA" before label "XDATA" in the file (for example 2THETA=33.45). Values of 2THETA are essential for defocussing correction from Schultz equation. You may also use non equal angle step: 5deg for inclination angle (chi or alpha) and 10 deg for the azimuthal angle (phi or betha) - data are approximated to 5x5 grid. Background data (one data for each value of inclination angle) are first after the label "XDATA".
 - Pole figures data files: *.DAT can be selected from *File->New Sample-> Choose Experimental Data*
 - Random pole figures data files: *.DAT can be selected from *File->New Sample-> Choose Defocussing Correction*
- **'COA'** COA data format (corrected pole figures).
- **'POL'** - The University of Birmingham/HiltonBrooks Texture Data.
 - Pole figures data files: *.POL can be selected from *File->New Sample-> Choose Experimental Data*
 - Random pole figures data files: *.POL can be selected from *File->New Sample-> Choose Defocussing Correction*
- **'DAT'** - TU Berlin data format (1PF/file)
 - Pole figures data files: *.DAT can be selected from *File->New Sample-> Choose Experimental Data*

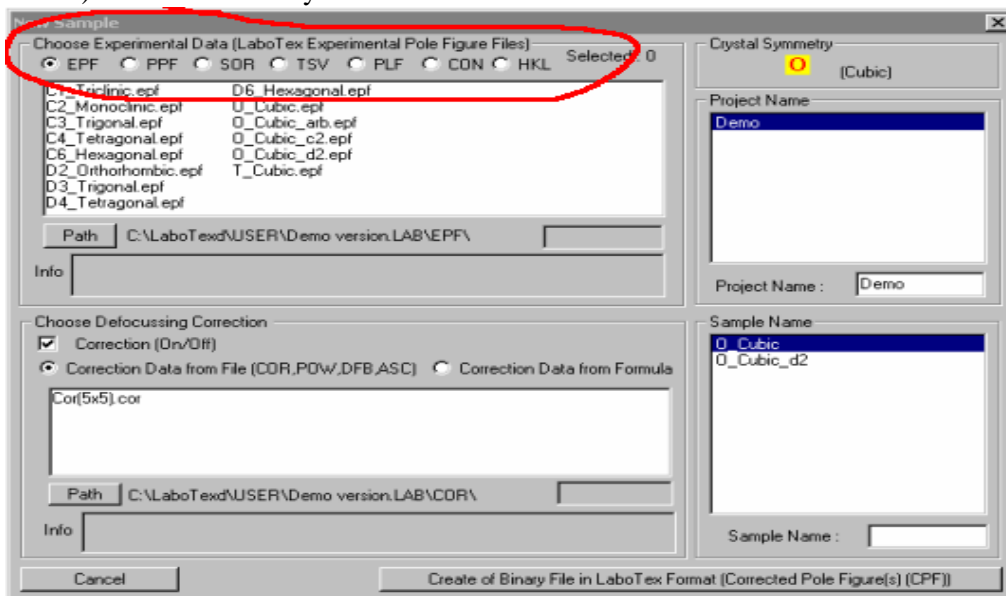
- **'POL'** - The University of Birmingham with background (add '_b' to filename for background data).
 - Pole figures data files: *.POL can be selected from *File->New Sample-> Choose Experimental Data*
 - Background data for pole figures (filename_b.pol): *.POL can be selected from *File->New Sample-> Choose Experimental Data*
 - Random pole figures data files: *.POL can be selected from *File->New Sample-> Choose Defocussing Correction*
 - Background data for random pole figures (filename_b.pol): *.POL can be selected from *File->New Sample-> Choose Defocussing Correction*
- **'000'** - U.Paris-Sud (Neutron Diffr.Data) (1PF/file) (add '_b' to filename for background data)
 - Pole figures data files: *.DAT can be selected from *File->New Sample-> Choose Experimental Data*
 - Background data for pole figures (filename_b.000): *.DAT can be selected from *File->New Sample-> Choose Experimental Data*
- **'RWA'** - Philips ATC3 (add '_b' to filename for background data)
 - Pole figures data files: *.RWA can be selected from *File->New Sample-> Choose Experimental Data*
 - Background data for pole figures (filename_b.RWA): *.RWA can be selected from *File->New Sample-> Choose Experimental Data*
 - Random pole figures data files: *.RWA can be selected from *File->New Sample-> Choose Defocussing Correction*
 - Background data for random pole figures (filename_b.RWA): *.RWA can be selected from *File->New Sample-> Choose Defocussing Correction*
- **'M'** - University of Northeastern (Shenyang) (add '_b' to filename for background data)
 - Pole figures data files: *.M can be selected from *File->New Sample-> Choose Experimental Data*
 - Background data for pole figures (filename_b.M): *.M can be selected from *File->New Sample-> Choose Experimental Data*
 - Random pole figures data files: *.M can be selected from *File->New Sample-> Choose Defocussing Correction*
 - Background data for random pole figures (filename_b.M): *.M can be selected from *File->New Sample-> Choose Defocussing Correction*
- **'EXP'** (also **'CAL'** and **'COR'**) (add '_b' to filename for background data) - Experimental data - RWTH Aachen ('CAL' - recalculated pole figures and 'COR' - corrected pole figures can be also used.)
 - Pole figures data files: *.EXP (or *CAL or *COR) can be selected from *File->New Sample-> Choose Experimental Data*;

- Background data for pole figures (filename_b.EXP,) can be selected from *File->New Sample-> Choose Experimental Data* ;
- Random pole figures data files: *.EXP can be selected from *File->New Sample-> Choose Defocussing Correction*
- Background data for random pole figures (filename_b.EXP) can be selected from *File->New Sample-> Choose Defocussing Correction*
- 'HPF' (add '_b' to filename for background data) - Experimental data - pole figures
 - Pole figures data files: *.HPF can be selected from *File->New Sample-> Choose Experimental Data*;
 - Background data for pole figures (filename_b.HPF) can be selected from *File->New Sample-> Choose Experimental Data*;
 - Random pole figures data files: *.HPF can be selected from *File->New Sample-> Choose Defocussing Correction*
 - Background data for random pole figures (filename_b.HPF) can be selected from *File->New Sample-> Choose Defocussing Correction*

4.8. How make given format accessible for LaboTex

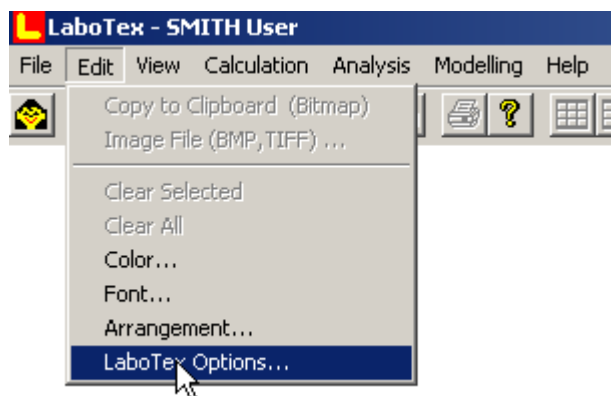
To enter experimental or modeling data to LaboTex select *File> New Sample*. You can change the data formats using the radio buttons in the top of the *New Sample* window (see below). If your data format is not listed (for example like on the screenshot below it is not “EPF”, “PPF”, “SOR”, “TSV”, “PLF”, “CON”, “HKL”), you can select your data format from *Edit>LaboTex Options>Data Formats* tab (see below for the detailed instructions).

LaboTex allows a maximum of 7 active data formats in the *New Sample* window. The formats EPF, PPF and SOR are the default fixed active formats. You can choose up to 4 more active data formats (non-LaboTex). LaboTex allows you to choose from **36 different** data formats.

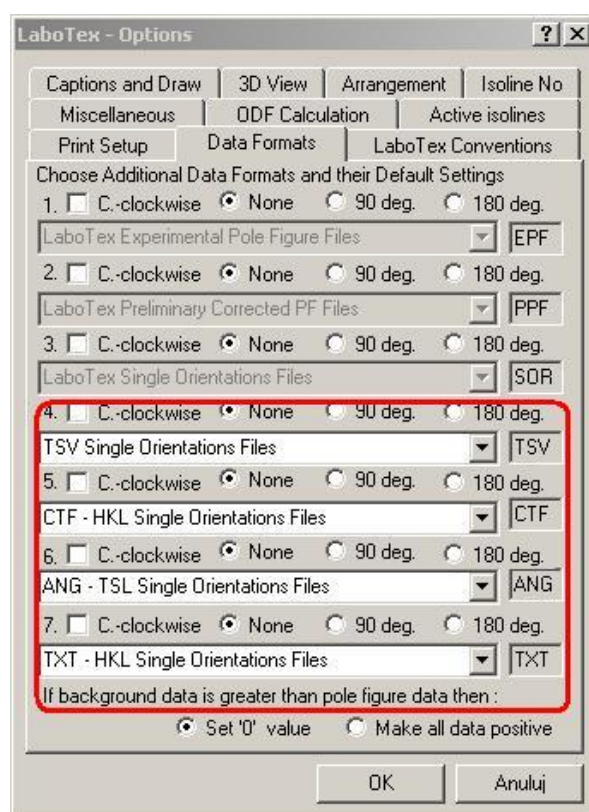


To select the active data formats for the window *New Sample* for creation of CPF files:

- a) from the main menu select *Edit>LaboTex Options*

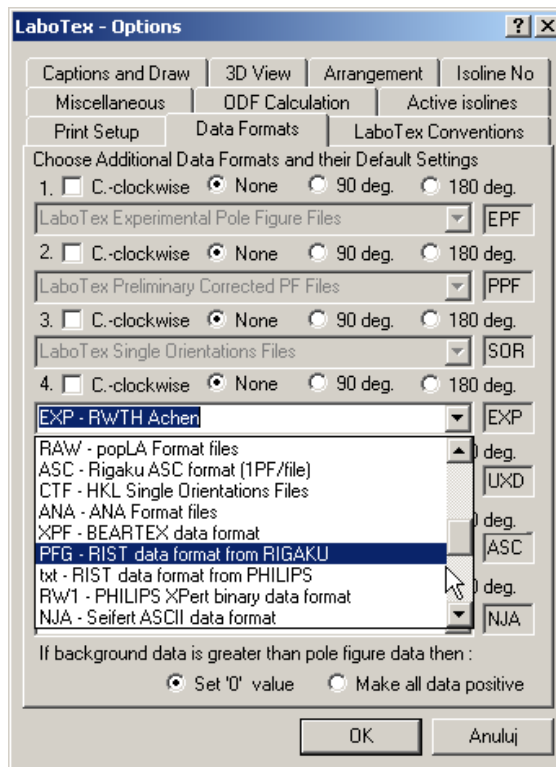


- b) in the window *LaboTex-Options* select the tab *Data Formats*
 c) the first three formats (EPF, PPF, SOR) are preselected and fixed out but you can change formats 4 to 7 using the drop down list (see the screenshot below).



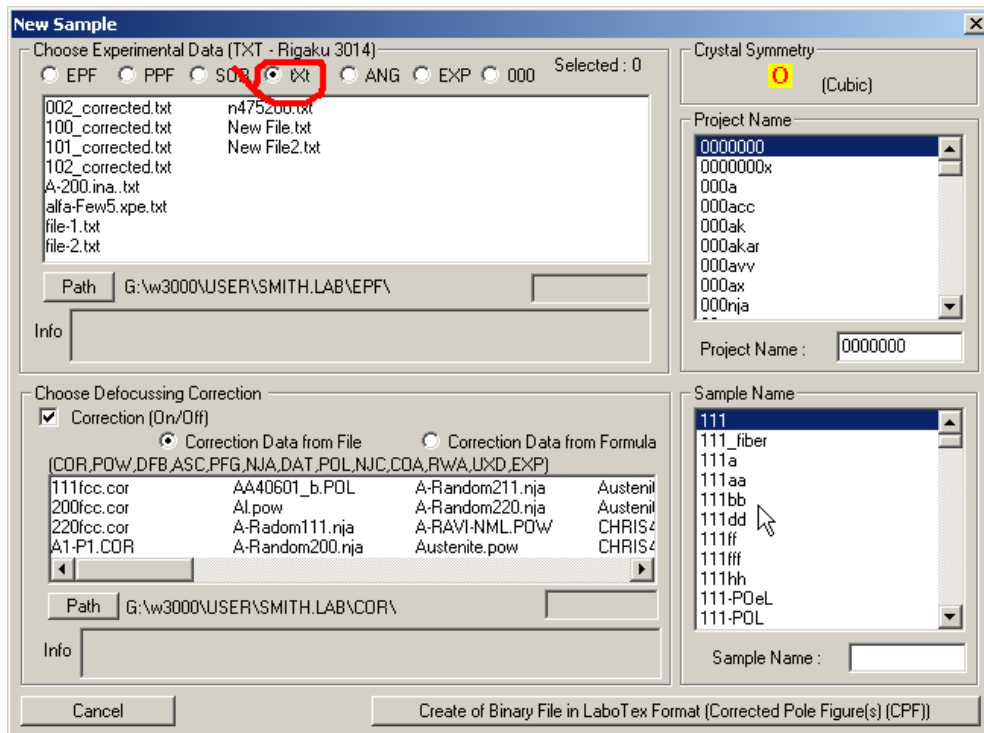
For example, to make format PFG (Rigaku ASCII or binary data format) accessible for creation of CPF:

- a) from the main menu select *Edit>LaboTex Options...*
 b) in the window *LaboTex-Options* select the tab *Data Formats*
 c) from one of the drop down lists (from 4 to 7) select '**PFG**' - RIST data format 3014 (see the following screenshot).



You can change the default parameters for data format using relevant the checkboxes or radio buttons.

Now when you open the *New Sample* window (*File>New Sample*), you will see the “PFG” file format listed.



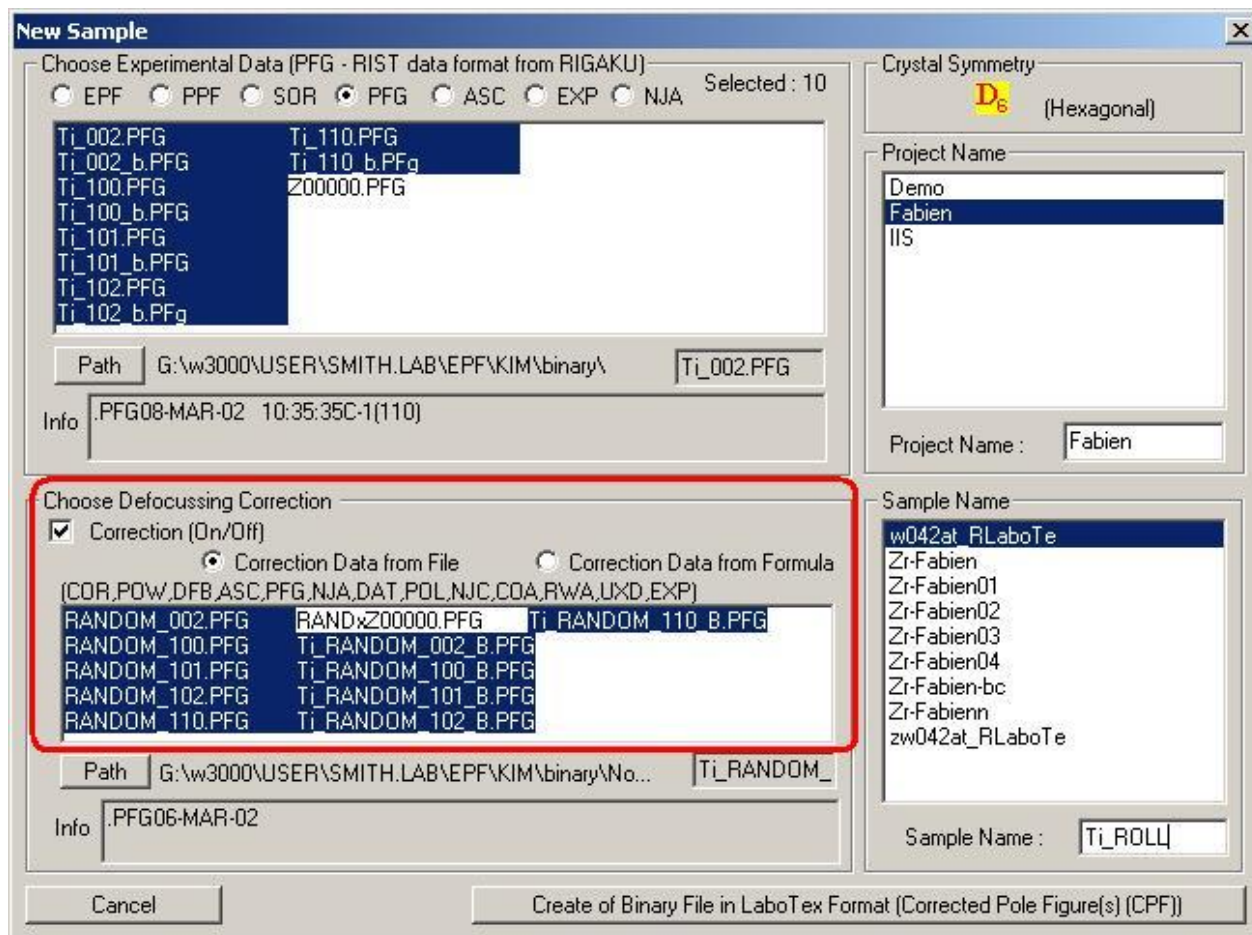
To **simultaneously** use **several files** with **the data from the same sample** :

select the relevant files in the files selection box by holding the Ctrl key on your keyboard and left-clicking the filenames with your mouse. The selected files will be highlighted in blue (see the screenshot below).

If you have files with corrected pole figures, select these files from the file list in the *New Sample* window ("Choose Experimental Data").

If you have files with non-corrected pole figures and files with data for defocussing and background correction, set the extension for all these files to PFG (*.pfg). The files with the background correction data should also have “_B” in their filename before file extension “.PFG” (for example: *ferrite_B.PFG*). Once you adjusted all file extensions, you can select the data from the lists in the 'New Sample' window:

- Pole figures - data files: *.pfg (from the "Choose Experimental Data" list)
- Background of pole figures - data files: *_B.pfg (from the "Choose Experimental Data" list)
- Defocussing correction data files (files with pole figures from a 'random' (powder) sample): *.pfg (from the "Choose Defocussing Correction" list)
- Background of pole figures with defocussing correction data - files: *_B.pfg (from the "Choose Defocussing Correction" list)



For more details see 'Pole Figures: Plot and Registration Conventions' PDF file on www.labosoft.com.pl or www.latotex.com

Please note:

LaboTex can input data for different azimuthal and radial steps (azimuthal step is adjusted to radial step by linear interpolation).

Azimuthal step has to be within the range 1-10 deg., one of radial steps from: 1., 2., 1.2, 1.25, 1.5, 2., 2.5, 3., 3.75, 5., 6., 7.5, 10. degrees and extra: 1.8 ,2.25 ,3.6 ,4.5 except from trigonal and hexagonal crystal lattice symmetry.

The radial step for defocussing correction data has to be the same as for the pole figures(!).

To make format accessible for creation of CPF files:

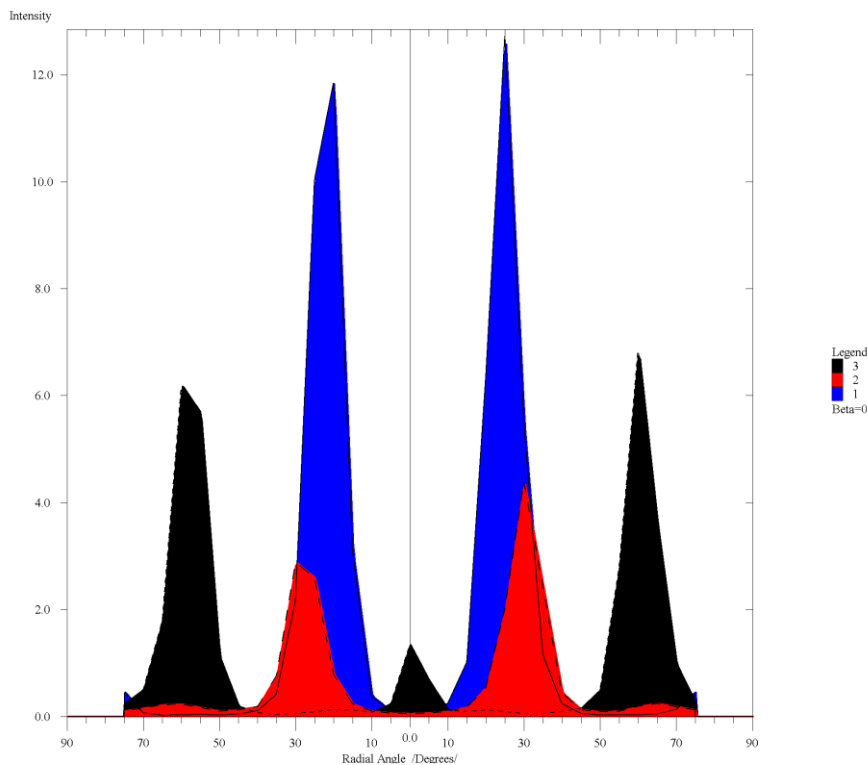
- a) select *Edit->LaboTex Options*;
- b) select the *Data Formats* tab;
- c) select the names of desired format from the drop down menus 4 -7.

To **simultaneously** use **several files** with **the data from the same sample** :

select the relevant files in the files selection box by holding the Ctrl key on your keyboard and left-clicking the filenames with your mouse. The selected files will be highlighted in blue (see the screenshot below).

If the extensions of your data files differ from those available, please to change them: for example, (in RW1 format) background pole figures data files have the *.COR extension by default. This extension is the same as for defocussing correction data files. Change the extension of the background pole figures data files to *.BGR before entering them to LaboTex.

All trademarks are the properties of their respective owners and are only used in a descriptive fashion without any intention to infringe.



5. LaboTex - Frequently Asked Questions (FAQ)

Q: In the LaboTex demo version the raw data for the pole figure contains the data from 0 to 90 deg alpha angle tilt. In our pole figure the data obtained by the reflection method ranges from 0 to 75 deg as at the higher angles the beam is parallel to the sample surface leading to defocussing. Is the incomplete pole figure data obtained by us using the back reflection method enough to conduct analysis?

A: Yes, you can use incomplete pole figures for analysis. LaboTex accepts pole distances smaller than 90 deg. It can be 85, 80, 75 deg. and so on. You can cut off the pole figure in the center as well and start the pole distance not from 0 deg. but from 5, 10, 15.... deg. (for the transmission technique).

Q: At each alpha tilt angle we get the background values. There is no information in the software how to do the background correction by using these values. Also the raw data does not give the background values.

A: In the demo version we have not used the background values. However, if you check the structure of an EPF file (see *HELP* menu), you will see that LaboTex accepts the background data.

Q: We need to do the ODF for the HCP metals like Titanium, Zirconium and some cubic metals like steel. We may not need the other crystal geometry.

A: LaboTex calculates ODF for all crystal symmetries. You can use whichever you wish.

Q: The maximum intensity value of PF data which is obtained by X-ray machine is different from the one appearing on the computer screen of LABOTEX PF analysis. Any reason?

A: Experimental pole figures obtained from X-ray diffraction are unnormalized. The measured intensities depend on the type of the X-ray source, the type of a counter, the colimating system, the absorption properties of measured material and so on. Therefore the pole figures from an X-ray machine are not comparable between each other. Pole figures can be normalised in the ODF calculation process.

Pole figures used in LaboTex program are of two types:

I - approximately normalised : .CPF

II - precisely normalised: .NPF, .RPF, and .APF

Pole figures and the maximum intensities from X-ray and .EPF and .CPF usually have different intensities than pole figures of type II (.NPF, .RPF, and .APF). All comparisons between pole figures should be done inside the pole figures of type II! Quantitative analysis can be made using only normalized pole figures!

Q: Does the accuracy or the reliability of PF-to-ODF conversion depend on the type of the feature of the textures concerned? For example, is there any difference in the accuracy between Goss and cube oriented textures?

A: No, the accuracy of different texture components does not depend on the type of texture component in calculation by the ADC method in LaboTex.

Q: Is the algorithm for calculation of ODF's different from the 'WIMV' algorithm in the POPLA package?

A: The algorithm used in LaboTex is different from the WIMV method. LaboTex implements the original ADC algorithm.

There are some similarities between WIMV and ADC methods:

- 1) both methods belong to the same group of so called direct methods (or discrete methods) in opposition to Fourier series methods;
- 2) both methods use iteration procedures.

The main differences between ADC and WIMV methods:

- 1) different principles of the iteration procedure;
- 2) different principles of "ghosts" correction.

For more details see:

H.-R. Wenk, K. Pawlik, J. Pospiech and J.S. Kallend (1994) *Deconvolution of superposed pole figures by discrete ODF methods: Comparison of ADC and WIMV for quartz and calcite with trigonal crystal and triclinic specimen symmetry*. Textures and Microstructures 22, 233-260.

U. F. Kocks, C. N. Tomi, H. R. Wenk, "Texture and Anisotropy", Cambridge University Press

F.Caleyo, T.Baudin, M.H.Mathon and R.Penelle, *Comparison of several methods for the reproduction of the orientation distribution function from pole figures in medium to strong textured materials* - Eur. Phys. J. AP 15 (2001), p85-96

("... The strong and weak points of each method are examined showing that the iterative discrete methods (ADC and WIMV) are better suited for the reproduction of the texture function in the present case. In comparing these two discrete methods, it is evidenced that the ADC method reproduces more accurately both the experimental and synthetic texture functions over the entire range of texture sharpness considered ...")

There are more papers describing the principles of the ADC method. For the references see the *ADC Method* section on our website www.labosoft.com.pl

Q: I am looking for a better reference or way to index ODF patterns. Mostly, I use figures from Bunge's book which show low index orientations. Working with steel, I come across many higher order reflections like {554}<225> and I can calculate these angles if I know what to look for, but it's very tedious to index some higher order reflections by guessing what they might be and then calculating the angles- checking, guessing again, calculating... I would like a program which takes Euler angles from the input and lists the closest {hkl}<uvw> indices. I guess I'll program something like this unless anyone can suggest a better method or point me towards something that has already been written.

A: Your problem of indexing ODF patterns can be solved using LaboTex. LaboTex is performing texture analysis using pole figures and ODF. LaboTex can do it simultaneously!

Q: What indices I should use for hexagonal symmetry?

A: In case of hexagonal symmetry you should transform {hkil} -> {hkl} by excluding {i} indices. For example: {01-11} to {011};

For pole figures, if the first or second index is negative, please rearrange it so that the first two indices are positive and exclude the third index (which is the negative sum of the first two). The last index remains the same.

For example: {-2110} to {11-20} and final {110};

For crystal directions <uvw> ==> <UVW> please calculate:

$$U=u-t$$

$$V=v-t$$

$$W=w$$

For example: <11-20> to <330> and final <110>;

Please, check this for calculate orientation {0,1,-1,1} <2,-1,-1,0>:

$$\{0,1,-1,1\} \langle 2,-1,-1,0 \rangle \implies \{0,1,1\} \langle 1,0,0 \rangle$$

Q: The format of the raw data as we get it is different than the one used by you. How do you propose to change the data structure so that it can be suitable for the software?

A: If format your data is not available in LaboTex (see: *Edit -> LaboTex Options -> Data Formats*), we have two suggestions:

1) Take a look at the description of data file structure in the *LaboTex Demo HELP* menu. Check the "*LaboTex Format of Experimental Data*" option and the examples of *.EPF, *.COR and *.POW. Then you can transform your data to EPF and COR type format.

2) You can send us examples of your data files and the LaboSoft team will prepare the LaboTex input to accept your data format, free of charge for our customers.

Q: Can I create a CPF file myself? We would like to calculate an ODF with pole figures which have been multiplied by corrected factors and which were not re-normalised after this multiplication.

A: .CPF files are binary files with a complicated structure. We can suggest two solutions:

1) You can save your special data as a 'PPF' file (for more details how to see *Help* section). This file does not include background data and you do not need to use .COR file.

2) You can save your special pole figures as 'EPF' file including the proper number of "0" values for the background for each pole figure at the end of the file. Remember to add the lines describing your data (at the beginning of the file) for each pole figure background. In such cases, you need to make a 'COR' file which includes correction coefficients equal to "1".

Q: What should I do to read Rigaku data?

A: For Rigaku data files, remember to use only one pole figure per file and to set the extension of your files to *.ASC (for example: 53110.ASC, 53200.ASC, 53211.ASC).

To make the *.ASC files accessible in LaboTex for creation of CPF files:

- a) select *Edit->LaboTex Options*;
- b) select the *Data Formats* tab;
- c) select "*ASC - Rigaku ASC format (1PF/file)*" one of the from the drop down lists 4 -7;
- d) select *File -> New sample* then select "*ASC*" data format. If you do not use defocusing correction, select "*off*" for "*Correction*";
- e) select *ASC pole figures* files;
- f) select the proper crystal symmetry for your sample.

Q: Could you please tell me whether LaboTex for Windows could be used for files generated with Bruker equipment?

A: Yes. UXD file version 1 and 2 and the UXD data format with reversed radial angle direction are all compatible with LaboTex. For more details see www.labotex.com/format.htm

Q: When using ASC format only one PF file can be included and other APF can be calculated by the software. Does that mean that it is not necessary to measure other PFs experimentally? Can I include other PFs such as 200 and 112 apart from 110 in the BCC structure? On the other hand, in the EPF format several PFs can be input simultaneously. How about the difference in the EPF and ASC cases?

A: It is possible use more PFs (files). You may use 110, 200 and 112 PFs simultaneously. In *File->New Sample* window select (by a mouse click) several ASC files simultaneously by holding the CTRL (control) key. Calculating the ODF from one PF is not always enough. In such cases, you should use more PFs.

Q: Is there any simple way to transfer ASC format into EPF format with 8 columns?

A: When you create a CPF file from an ASC file, LaboTex will convert ASC files to the EPF/POW or PPF files. You can then find these files in the LaboTex temporary directory (for example: C:\Labotex2\user\username.LAB\tmp...).

Q: As for the background data, I cannot find a way to input that to the file when an ASC has been included. Can the background data only be used in the EPF format?

A: Usually the measured pole figures must be corrected according to the background and the defocusing absorption. You should measure these values for your samples. These both corrections of the raw pole figures data are sometimes done by the software used with the experimental X-ray device (especially if you use PSD-Position Sensitive Detector). You should check whether this can be done with your x-ray device (i.e. whether it is a type of a PSD detector). Inside the ASC file format you can find two places in which the background values can be included. Find the lines with words: **LOW*, **HIGH*. Your files will have zero values in these places. You should decide whether this is the correct value. If it is not, consult the manual for your X-ray device to find how to measure and include the background values to your ASC files in positions **LOW* and **HIGH* inside the files.

Q: I am studying the texture in steel. Which correction file and the symmetry type should I choose when including the data?

A: In order to defocus the correction, measure the pole figures of the powder sample (from the same material as the "textured samples", which in your case is steel). The powder sample is treated as a "non-texture" sample. This helps to find the absorption curve for the defocusing correction. The files related to the powder sample should have the extension *.POW (LaboTex format), *.ASC (Rigaku format) or other (for details see www.labotex.com/format.htm). The files should be in the COR LaboTex directory (for the current user). In your case (the steel samples), you should choose the O-cubic symmetry. All symmetries are indicated according to the Schoenflies symbols (International Tables for Crystallography - ed.T.Hahn - 1983, D.Reidel publishing company. Dordrecht/Boston).

Q: As for the powder sample should I measure it in the same condition with the ordinary ones?

A: Yes.

Q: Can I choose a Corr file also in the ASC format?

A: Yes.

Q: How can I have the same numerical values of the odf as in the file .pod which we had before? We need these values for our calculations to determine the stored energy.

A: This option is available from the version 2.1 onwards (menu *File-->ODF export*). If you use version 2.0, the upgrade to version 2.1 is free of charge. For more details, please contact us via e-mail: office@labosoft.com.pl

Q: When LaboTex reads my data file (sample.epf) I get a message "Error: Improper data. Check data file". Please check my input data file.

A: Your data file is in popLA format which has the same extension as LaboTex files (.EPF). To make popLA *.EPF files accessible for creation of CPF files you should:

- a) select *Edit->LaboTex Options*;
 - b) select the *Data Formats* tab;
 - c) select "*EPF - popLA EPF files format*" from the drop down lists 4 -7;
 - d) select *File -> New sample* then select "**epf**" (small capitals!) data format (in this format the data is after the correction);
 - e) select your data file;
 - f) select the proper crystal symmetry for your sample.
-

Q: How does LaboTex define the sample and coordinate system?

A: LaboTex convention (from the version 2.1.006 onwards) for defining the sample and coordinate system is:

- 1) X, Y, Z axis are perpendicular to each other,
- 2) X, Y axis are in the (001) crystallographic plane and Z axis is perpendicular to (001) crystallographic plane,
- 3) X axis is parallel to the [100] crystallographic plane,

4) Crystal coordinate system and sample coordinate system should be at the same order i.e. both right-handed or both left-handed,

5) Bunge definition of Euler angles.

Q: LaboTex shows bad Euler angles for orientation (01-12)<2-201>= (012)<2-21>={38.11,42.61,0.0}. From my diagram it should be :{38,43,30} (Zr Alloy - hexagonal system).

A: Your diagram is made in a different convention than the LaboTex one. In the hexagonal system (for the hexagonal division: $a=b, c(\text{non equal } a), \alpha=\beta=90, \gamma=120$) two conventions are used for the sample and coordinate system. This is the reason for the difference between the values of Phi2 angle of about 30.

In LaboTex version 2.1.008 and higher it is possible to choose the axial convention in the hexagonal system.

Q: I have cell parameters for the trigonal system: $a=b=c, \alpha=\beta=\gamma < 120$. In the example for the trigonal system LaboTex has the same cell parameters as for the hexagonal system. Is this an error?

A: No. Rhombohedral crystal can always be described in terms of hexagonal axes. In the trigonal division of the hexagonal system two conventions are used: (1) rhombohedral axes (like for your data) and (2) hexagonal axes. LaboTex uses hexagonal axes and cell parameters have to be the same as for the hexagonal division.

You can find more details about the convention of cell parameters used in our report: "[Pole Figures: Plot and Registration Conventions](#)" available in PDF from our website www.labosoft.com.pl and www.labotex.com

Q: The volume fraction calculated in the software does not agree with the ones I calculated. I calculated it by the C coefficient from the texture data. Can you tell me how you calculate it?

A: The results of the volume fraction calculation can be different due to the following reasons:

1) When you use C coefficients with $l=22$ or $l=34$, in the case of strong texture peaks you obtain the truncation error of the Fourier series. This causes the error in the volume fraction calculation

2) When you use C coefficients, in reality you calculate the volume of the ideal model components not your real experimental texture peaks. This is the second reason for the error.

3) In LaboTex we eliminated the truncation error of the peaks by not using the harmonic series (the ODF calculation is based on ADC method which calculates the real ODF peaks not the truncated ones).

4) In LaboTex calculates the volume fraction by integration of the real texture peaks on ODFs (LaboTex does not use Gauss models). Additionally users can independently decide about integration width of the peak in 3 Euler angles. In the case of C coefficients you are not able to change the different width of the Gauss model in the 3 Euler angles.

5) You can see the comparison of different ODF calculation methods (including ADC method which is the base of the LaboTex software) which are described in the reference papers: [The ADC Method References](#)

Q: I would like to use the same values of contour pole density in the analysis of ODF for several samples. Is it possible in your program?

A: You can plot contour lines by any scale in LaboTex program.

In order to do this:

1. Plot any PF, ODF, or INV object using "AUTOMATIC" contours.
2. Press the "i" icon on the program toolbar.
3. Change the "AUTOMATIC" option to "MANUAL" in "PF isolines mode/ Load PF isolines".
4. Edit all isolines values you want in the "isolines/values" windows.
5. Tick the box "Value" (or/and "Color", "State").
6. Press the "Save PF Isolines" and save the isolines to the file.
7. Now, you can load these isolines from the file at any time.

Q: How do you get the COR file? Where is it generated? Can we get it from LaboSoft? Can I use our dbf file instead of the cor file?

A: COR files are automatic generated when powder samples are processed (used as *.POW files in LaboTex - see *HELP*). You can create this file manual when you know the correction coefficients (see the manuals about LaboTex formats and pole figures conventions on our website www.labosoft.com.pl). *.DBF files can be used instead of *.COR files

Q: What is the meaning of rotation of the PF step, lower and upper ranges?

A: You can rotate pole figures around the normal axis before the ODF calculation. Sometimes it is useful to correct the sample coordinates. Lower and upper ranges mean the ability to cut off the pole distance range from both sides (in the centre and in the maximum distance).

Important! You can use simultaneously the rotation and cut off for all pole figures or separately for each one. Check the appropriate switch!

Q: It is so difficult to use the X-ray data for every two degree scan! The reason is that we do a lot of work on textured thin films and 1 or 2 degrees are what would be ideal for us!

A: There is no problem to do that. LaboTex is able to use data measured with 1 or 2 deg. step. The ODF calculation time will be longer of course. That is because the data set (the amount of data) is bigger in that case.

Q: There is a 90 deg. rotation between the PF plotted between my old texture software and LaboTex.

A: There are two issues here:

I) Different ways of pole figures plotting:

- (1) clockwise rotation from the NS direction
- (2) counterclockwise rotation from the NS direction
- (3) clockwise rotation from the WE direction
- (4) counterclockwise rotation from the WE direction

LaboTex uses the pole figures presentation as in point A.1.

If the ODF from LaboTex and the ODF from your old software are the same, then the difference is only in the pole figure presentation (a different pole figures plotting convention).

If ODF from LaboTex and ODF from your old texture software are different then pole figures measurements convention are different.

II) Different ways of registration of pole figures in the dependence from the motion of the texture goniometer are :

- (1) clockwise rotation from the RD direction
- (2) counterclockwise rotation from the RD direction
- (3) clockwise rotation from the TD direction
- (4) counterclockwise rotation from the TD direction

LaboTex uses the convention **B.1**.

You can find more details about the adjustment of LaboTex to different plot and registration conventions in our technical report: "[Pole Figures: Plot and Registration Conventions](#)" which is available on our website www.labosoft.com.pl and www.labotex.com

Q: I didn't find any information about how to use the delta Phi1, Phi, Phi2 range for the calculation of the quantitative texture analysis. If for example I choose a phi integration range of 20° for a phi angle of 45 °, does it mean that the calculation will integrate in phi between 25 and 65 ° or between 35 and 55 °?

A: In quantitative analysis DeltaPhi1, DeltaPhi and DeltaPhi2 denote the half width of the integration range around the chosen orientation. So, if orientation is PHI1, PHI, PHI2, then the volume fraction is integrating in the range:

[PHI1 - DeltaPhi1 , PHI1 + DeltaPhi1]

[PHI - DeltaPhi , PHI + DeltaPhi]

[PHI2 - DeltaPhi2 , PHI2 + DeltaPhi2]

Of course, you can choose different Delta for each Euler angle and for each selected orientation (using the view of the orientation profiles in each Euler angle cross section). The calculation will then integrate in Phi between 25 and 65 ° for your example.

Q: How can I make defocusing correction?

A: The best way for making the defocusing correction is by measurement of a "random" sample. Firstly, you should take the measurement of a "random" sample just like a normal sample. A "random" sample has to be made from the same or similar material as the material of your sample. Secondly, enter the files with pole figures of the sample and the files with pole figures of the "random" sample simultaneously into LaboTex. The files with pole figures of the "random" sample can be selected from a different list in the same dialog window. Preparation of a good quality "random" sample is difficult. We offer a set of "random" samples (texture and strain free). For more details see our website www.labosoft.com.pl section [Prices&Orders](#)

Q: How can I check the quality of my texture measurement?

A: The best way in this case is using the measurements of texture standards. LaboSoft offers texture standards of different sample symmetry which also contain a "random" sample. All results of measurements pole figures are provided by the Accredited Testing Laboratorie. For more details see our website www.labosoft.com.pl section [Prices&Orders](#)

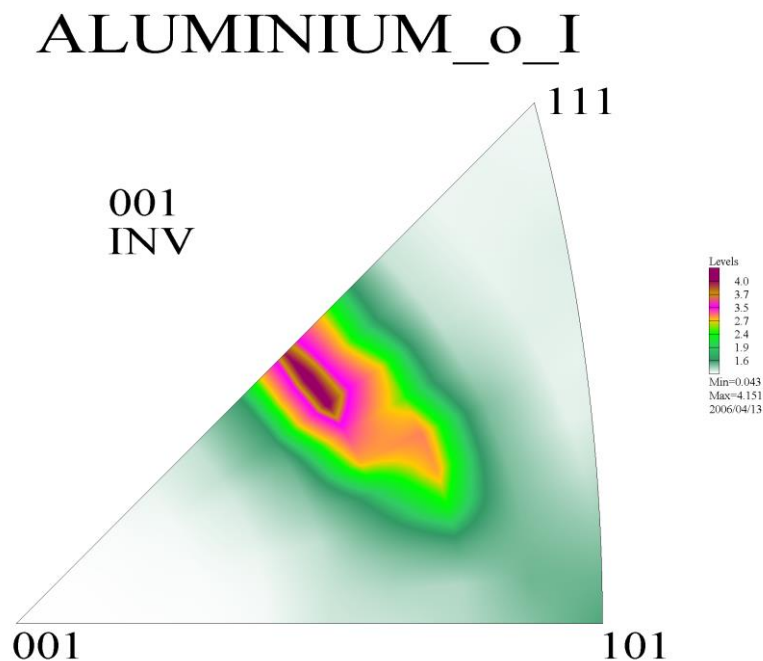
Q: Does LaboTex cooperate with VPSC texture modeling software packages?

A: Yes. You can input the data from a file with a set of single orientations. You can also generate a file which contains a set of single orientations on the base of ODFs.

Q: When I run the HASP Protect Key Installation on Windows, I get the following error message: "user has no access to the database registry 0x20 10000 0x0 0x0"and the installation is stopped.

A: In order to avoid this error when installing the HASP Protect Key on Windows NT/2000/XP, please follow the steps below:

- 1) Switch off your PC / laptop.
- 2) Plug in the HASP Protect Key into the USB slot (for earlier versions and older HASP Keys use the parallel printer slot).
- 3) Switch your PC/ laptop on.
- 4) Login to the Windows NT/2000/XP **with the Windows Administrator credentials** (otherwise you will not be able to carry out the installation!).
- 5) Install the HASP device driver. Remember to reboot the computer after the installation is complete.
- 6) To use LaboTex you do not need the Windows Administrator credentials. These are only needed during the installation.



6. References

6.1 The LaboTex Reference:

1. K.Pawlik, P.Ozga: "LaboTex: The Texture Analysis Software", 'Göttinger Arbeiten zur Geologie und Paläontologie', SB4, 1999.

6.2 ADC Method - Main References:

2. K.Pawlik - phys.stat.sol.(b) 134 (1986), p.477, "**Determination of the Orientation Distribution Function from Pole Figures in Arbitrarily Defined Cells**",
3. K.Pawlik, J.Pospiech - Proc. of Int. Workshop, Clausthal-Zellerfeld, Germany, (1986), p127
4. K.Pawlik, J.Pospiech, K.Lucke - Proc. of ICOTOM-8, Santa Fe, USA, (1987), p105, "The Development of a New Direct Method of ODF Reproduction From Pole Figures and its Testing with the Help of Model Functions"
5. K.Pawlik, W.Truszkowski, J.Pospiech, T.Pawlik - Proc. of ICOTOM-8, Santa Fe, USA (1987), p531
6. K.Pawlik, J.Pospiech, K.Lucke - Proc. of ICOTOM-9, Avignon, France, (1990), p25, "The ODF approximation from pole figures with the aid of the ADC-method".
7. K.Pawlik - Proc. of EPDIC-2, Enschede, The Netherlands, (1992), p151
8. K.Pawlik - Proc. of ICOTOM-10, Clausthal-Zellerfeld, Germany, (1993), p401
9. H.R.Wenk, K.Pawlik, J.Pospiech and J.S.Kallend - Deconvolution of superposed pole figures by discrete ODF methods: Comparison of ADC and WIMV for quartz and calcite with trigonal crystal and triclinic specimen symmetry - Textures and Microstructures 22 (1994), p233-260.
10. U.F.Kocks, C.N.Tome, H.R.Wenk, "Texture and Anisotropy", Cambridge University Press. (2000);

6.3 Other selected references on LaboTex and ADC:

11. "... The strong and weak points of each method are examined showing that the iterative discrete methods (ADC and WIMV) are better suited for the reproduction of the texture function in the present case. In comparing these two discrete methods, it is evidenced that the ADC method reproduces more accurately both the experimental and synthetic texture functions over the entire range of texture sharpness considered ..." F.Caleyo, T.Baudin, M.H.Mathon and R.Penelle - Comparison of several methods for the reproduction of the orientation distribution function from pole figures in medium to strong textured materials - Eur. Phys. J. AP 15 (2001), p85-96 [Abstract](#)
12. "... A discrete method (called as the Arbitrarily Defined Cells method) was applied to calculate the ODF. The 3-D distribution of orientations of the cellulose crystalline areas was reconstructed in the space of the Euler angles. Additionally, the complete pole figures as well as the inverse ones were recalculated. The presented analysis of the cellulose texture provides more extensive information on the space organisation of microfibrils than the standard methods...", Olek W., Pawlik K., Bonarski J. (2000): Space orientation of the crystalline areas of cellulose. Proceedings of the International Conference on Wood and Wood Fiber Composites, 13-15 April 2000, Stuttgart, Germany: 37-46.

13. "... Direct Methods (WIMV, ADC) With 1 Degree Resolution Are Preferred...", K.J.Kozaczek, D.S.Kurtz, Quantitative texture analysis of blanket films and interconnects, Workshop on Texture in Electronic Applications NIST, Gaithersburg, MD, October 10-11, 2000.
14. L. Tarkowski a, J. Bonarski, I. Alexandrov, Planar irregularities of texture and stress field in Ti detected by X-ray diffraction technique, Nuclear Instruments and Methods in Physics Research B 268 (2010) 352–355.
15. G. Dirras, H. Couque, J. Gubicza, A. Ouarem, T. Chauveau, P. Jenei, Fine-grained nickel deformed by direct impact at different velocities, Microstructure and mechanical properties, Materials Science and Engineering A 527 (2010) 4128–4135.
16. S.K. Sahoo, V.D. Hiwarkar, L. Jain, I. Samajdar, P. Pant, G.K. Dey, D. Srivastav R. Tewari, S. Banerjee, Deformed microstructures of two-phase Zr–2.5Nb alloy: Effects of the second phase hardness, Journal of Nuclear Materials 404 (2010) 222–230.
17. R. Chulist, W. Skrotzki, C.-G. Oertel, A. Bohm, T. Lippmann, E. Rybacki, Microstructure and texture in Ni₅₀Mn₂₉Ga₂₁ deformed by high-pressure torsion, Scripta Materialia 62 (2010) 650–653.
18. J. Arout Chelvane, S. Banumathy, Mithun Palit, Himalay Basumatary, A.K. Singh, S. Pandian, Texture and magnetostriction studies in Bridgman solidified Ho_{0.85}Tb_{0.15}Fe_{1.95} alloys, Journal of Alloys and Compounds 507 (2010) 162–166.
19. Li Li, Xinming Zhang, Changping Tang, Yunlai Deng, Nan Zhou, Mechanical properties and deep drawability of Mg–Gd–Y–Zr alloy rolling sheet at elevated temperatures, Materials Science and Engineering A 527 (2010) 1266–1274.
20. R. Chulist, W. Skrotzki, C.-G. Oertel, A. Bohmb, M. Potschke, Change in microstructure during training of a Ni₅₀Mn₂₉Ga₂₁ bicrystal, Scripta Materialia 63 (2010) 548–551.
21. R. Dakhlaoui, V. Klosek, M.H. Mathon, B. Marini, Orientation stress field analysis in polycrystalline bcc steel using neutron diffraction, Acta Materialia 58 (2010) 499–509.
22. Akinobu Shibata, Homuro Noda, Masato Sone, Yakichi Higo, Thin Solid Films 518 (2010) 5153–5158.
23. W.J. Kim, S.J. Yoo, H.T. Jeong, D.M. Kim, B.H. Choe and J.B. Lee, Effect of the speed ratio on grain refinement and texture development in pure Ti during differential speed rolling, Scripta Materialia 64 (2011) 49–52.
24. A. Chakraborty, M. Dutta, R. Pais, R.K. Ray, Analysis of an uncommon coating defect on industrial galvanized high strength interstitial free steel, Surface & Coatings Technology 204 (2010) 3481–3489.
25. B. Ravi Kumar, S.K. Das, Sailaja Sharma, J.K. Sahu, Effect of thermal cycles on heavily cold deformed AISI 304L austenitic stainless steel, Materials Science and Engineering A 527 (2010) 875–882.
26. Karen Pantleon, Marcel A.J. Somers, Interpretation of microstructure evolution during self-annealing and thermal annealing of nanocrystalline electrodeposits—A comparative study, Materials Science and Engineering A 528 (2010) 65–71.
27. Nicole Stanford, Dale Atwell, Matthew R. Barnett, The effect of Gd on the recrystallisation, texture and deformation behaviour of magnesium-based alloys, Acta Materialia 58 (2010) 6773–6783.

28. M. Lederer V. Gröger, G. Khatibi, B. Weiss, Size dependency of mechanical properties of high purity aluminium foils, *Materials Science and Engineering A* 527 (2010) 590–599.
29. M.J.N.V. Prasad , A.H. Chokshi, Superplasticity in electrodeposited nanocrystalline nickel, *Acta Materialia* 58 (2010) 5724–5736.
30. Raghavendra R. Adharapurapu, Fengchun Jiang, John F. Bingert, Kenneth S. Vecchio, Influence of cold work and texture on the high-strain-rate response of Nitinol, *Materials Science and Engineering A* 527 (2010) 5255–5267.
31. Mario Birkholz, "Thin Film Analysis by X-Ray Scattering", Wiley VCH, ISBN:3527607048, 227,236.
32. Panicker, R.; Chokshi, A.H.; Mishra, R.K.; Verma, R.; Krajewski, P.E. "Microstructural evolution and grain boundary sliding in a superplastic magnesium AZ31 alloy"; *Acta Materialia* Volume: 57, Issue: 13 (2009) 3683-3693
33. Chakraborty, A.; Ray, R.K. "Influence of microstructure and texture on the formability character of industrially produced galvanized coatings on three interstitial free steels"; *Surface & Coatings Technology* Volume: 203, Issue: 13 (2009) 1756-1764
34. Prasad, M.J.N.V.; Suwas, S.; Chokshi, A.H. "Microstructural evolution and mechanical characteristics in nanocrystalline nickel with a bimodal grain-size distribution" *Materials Science & Engineering A* Volume: 503, Issue: 1-2, (2009) 86-91.
35. Kim, W.J.; Yoo, S.J.; Chen, Z.H.; Jeong, H.T. "Grain size and texture control of Mg–3Al–1Zn alloy sheet using a combination of equal-channel angular rolling and high-speed-ratio differential speed-rolling processes"; *Scripta Materialia* Volume: 60, Issue: 10, (2009) 897-900
36. Gurao, Nilesh P.; Ali A, Ashkar; Suwas, Satyam, "Study of texture evolution in metastable β -Ti alloy as a function of strain path and its effect on α transformation texture"; *Materials Science & Engineering A* Volume: 504, Issue: 1-2, (2009) 24-35
37. Sahoo, S.K.; Hiwarkar, V.D.; Majumdar, A.; Samajdar, I.; Pant, P.; Dey, G.K.; Srivastav, D.; Tiwari, R.; et. al. "Presence and absence of significant twinning: Effects on cold deformed microstructures of single phase Zircaloy 2"; *Materials Science & Engineering A* Volume: 518, Issue: 1-2 (2009) 47-55.
38. Hiwarkar, V.D.; Sahoo, S.K.; Samajdar, I.; Narasimhan, K.; Mani Krishna, K.V.; Dey, G.K.; Srivastava, D.; et. al. "Annealing of cold worked two-phase Zr-2.5 Nb—Associated microstructural developments", *Journal of Nuclear Materials* Volume: 384, Issue: 1, (2009) 30-37.
39. Niranjani, V.L.; Hari Kumar, K.C.; Subramanya Sarma, V. "Development of high strength Al–Mg–Si AA6061 alloy through cold rolling and ageing" *Materials Science & Engineering A* Volume: 515, Issue: 1-2, (2009) 169-174.
40. W. Skrotzki, B. Kloden, A. Lankau, R. Chulist, V. Kopylov, H.-G. Brokmeier, "Texture Inhomogeneity in Titanium Deformed by ECAP", *ARCHIVES OF METALLURGY*, 53 (2008) 29-32.
41. Gravier, J.; Vignal, V.; Bissey-Breton, S.; Farre, J. "The use of linear regression methods and Pearson's correlation matrix to identify mechanical–physical–chemical parameters controlling the micro-electrochemical behaviour of machined copper" *Corrosion Science* Volume: 50, Issue: 10, (2008) 2885-2894

42. B. J. Bonarski, B. Mikułowski, E. Schafler, Ch. Holzleithner, M. J. Zehetbauer, "Crystallographic Textures of Single and Polycrystalline pure Mg and Cu Subjected to HPT Deformation", ARCHIVES OF METALLURGY, 53 (2008) 117-123.
43. Li, H.; Yin, F.; Sawaguchi, T.; Ogawa, K.; Zhao, X.; Tsuzaki, K. "Texture evolution analysis of warm-rolled Fe–28Mn–6Si–5Cr shape memory alloy"; Materials Science & Engineering A Volume: 494, Issue: 1-2, (2008) 217-226
44. A. Góral, J. Jura, H. Paul, "On the Orientation Characteristics in Directionally Crystallized Al-CuAl₂ Eutectic Alloy", ARCHIVES OF METALLURGY, 53 (2008) 139-143.
45. Yu, Z.M.; Odier, P.; Ortega, L.; Zhang, P.X.; Li, C.S.; Liu, X.H.; Zhou, L. "LZO covered Cu-based substrates"; Journal of Alloys and Compounds Volume: 460, Issue: 1-2 (2008) 519-523.
46. W. Olek, J. Bonarski, "Texture Changes in Thermally Modified Wood" ARCHIVES OF METALLURGY, 53 (2008) 207-211.
47. Souza, C.M.; Abreu, H.F.G.; Tavares, S.S.M.; Rebello, J.M.A. "The γ phase formation in annealed UNS S31803 duplex stainless steel: Texture aspects" Materials Characterization Volume: 59, Issue: 9, (2008), 1301-1306.
48. V. Klosek, M.H. Mathon, M.H. Aouni, R. Chiron, V. Ji, "In situ analysis of deformation mechanisms of Cu-based fcc materials under uniaxial loading", Materials Science Forum, 571-572 (2008) 89-94.
49. Jiang, Z.Z.; Yu, S.H.; Chun, Y.B.; Shin, D.H.; Hwang, S.K., "Grain refinement of pure vanadium by equal channel angular pressing", Materials Science & Engineering A, 479, 1-2 (2008) 285-292.
50. Jia, N.; Lin Peng, R.; Wang, Y.D.; Johansson, S.; Liaw, P.K. "Micromechanical behavior and texture evolution of duplex stainless steel studied by neutron diffraction and self-consistent modeling ", Acta Materialia Volume: 56, 4, (2008) 782-793.
51. Chun, Y.B.; Hwang, S.K., "Static recrystallization of warm-rolled pure Ti influenced by microstructural inhomogeneity", Acta Materialia 56, 3 (2008) 369-379.
52. Chakraborty, A.; Bhattacharjee, D.; Pais, R.; Ray, R.K., "Effect of galvannealing power on the texture and powdering resistance of industrially produced galvannealed coating on interstitial free steel", Scripta Materialia, 57, 8 (2007) 715-718.
53. Song, Jin-Hwa; Hong, Ki-Jung; Ha, Tae Kwon; Jeong, Hyo Tae, "The effect of hot rolling condition on the anisotropy of mechanical properties in Ti–6Al–4V alloy", Materials Science & Engineering A, 449-451, 25 (2007) 144-148.
54. Gabriel L. Converse, Weimin Yue, Ryan K. Roeder, "Processing and tensile properties of hydroxyapatite-whisker-reinforced polyetheretherketone", Biomaterials 28 (2007) 927-935. [Abstract](#)
55. S.B. Sadale, S.R. Barman, P.S. Patil, "Synthesis of type-II textured tungsten disulfide thin films with bismuth interfacial layer as a texture promoter", Thin Solid Films 515 (2007) 2935-2942.
56. Chowdhury SG, Datta S, Kumar BR, De PK, Ghosh RN, "Randomization of texture during recrystallization of austenite in a cold rolled metastable austenitic stainless steel", MATERIALS SCIENCE AND ENGINEERING A-STRUCTURAL MATERIALS PROPERTIES MICROSTRUCTURE AND PROCESSING 15 (2007) 114-119.

57. Jean-Marie Welter (Ed.), "Copper: Better Properties for Innovative Products", Wiley-VCH 2007. p.102.
58. Patro PK, Khatirkar R, Samajdar I, Kulkarni AR, Harendranath CS, "Strontium barium niobate-relating structural developments and dielectric constant", JOURNAL OF THE EUROPEAN CERAMIC SOCIETY 27 (5): (2007) 2255-2263.
59. Tom Walde, Hermann Riedel, "Simulation of earing during deep drawing of magnesium alloy AZ31", Acta Materialia 55 (2007) 867-874
60. S.B. Sadale, S.R. Barman, P.S. Patil, "Formation of α texture of tungsten disulfide thin films with nickel", Applied Surface Science 253 (2007) 3489-3495.
61. W.J. Kim, J.B. Lee, W.Y. Kim, H.T. Jeong and H.G. Jeong, "Microstructure and mechanical properties of Mg-Al-Zn alloy sheets severely deformed by asymmetrical rolling", Scripta Materialia 56 (2007) 309-312.
62. B. Ravi Kumar, Mainak Ghosh "Surface and mid-plane texture evolution in austenite phase of cold rolled austenitic stainless steels", Materials Science and Engineering A 457 (2007) 236-245.
63. Cedric Chauvya, Pierre Barberis, Frank Montheillet, "Microstructure transformation during warm working of beta-treated lamellar Zircaloy-4 within the upper alpha-range", Materials Science and Engineering A 431 (2006) 59-67.
64. Chun, Y.B.; Semiatin, S.L.; Hwang, S.K. "Monte Carlo modeling of microstructure evolution during the static recrystallization of cold-rolled, commercial-purity titanium", Acta Materialia Volume: 54, Issue: 14, August, pp. 3673-3689, 2006.
65. Kouadri, A.; Barrallier, L. "Texture characterisation of hexagonal metals: Magnesium AZ91 alloy, welded by laser processing", Materials Science & Engineering A Volume: 429, Issue: 1-2, August 15, pp. 11-17, 2006.
66. Sadale, S.B.; Patil, P.S. "Synthesis and characterization of type-II textured tungsten disulfide thin films by vdWR process with Pb interfacial layer as texture promoter", Journal of Crystal Growth Volume: 290, Issue: 2, May 1, 2006, pp. 363-368.
67. Mani K.K.V.; Sain A.; Samajdar I.; Dey, G.K.; Srivastava, D.; Neogy, S.; Tewari, R.; Banerjee, S. "Resistance to hydride formation in zirconium: An emerging possibility", Acta Materialia Volume: 54, Issue: 18, October, pp. 4665-4675, 2006.
68. Souza J.C.; Abreu, H.F.G.; Teodósio, J.R., "Comparação entre Diferentes Métodos de Cálculo da Função de Distribuição de Orientação Cristalográfica quando Aplicados em Aços Inoxidáveis Duplex", III Workshop sobre Textura, Sao Paulo, 176-184, 2006, ([Online Access](#))
69. I.V. Alexandrov, M.V. Zhilina, J.T. Bonarski, "Formation of texture inhomogeneity in severely plastically deformed copper", Bulletin of the Polish Academy of Sciences, Technical Sciences, Vol. 54, No 2, 2006 ([Online Access](#))
70. S.G. Chowdhury, E.V. Pereloma, D.B. Santos, "Evolution of Texture at the Initial Stages of Continuous Annealing of Cold Rolled Dual-Phase Steel, independent of Heating Rate", ([Online Access](#))
71. Chauvy C.; Barberis P.; Montheillet F., "Microstructure transformation during warm working of beta-treated lamellar Zircaloy-4 within the upper alpha-range", Materials Science & Engineering A Volume: 431, Issue: 1-2, September 15, pp. 59-67, 2006.

72. Kumar, B. R.; Singh, A.K.; Mahato, B.; De, P.K.; Bandyopadhyay, N.R.; Bhattacharya, D.K. "Deformation-induced transformation textures in metastable austenitic stainless steel", *Materials Science & Engineering A* Volume: 429, Issue: 1-2, August 15, pp. 205-211, 2006.
73. Chowdhury SG, Das S, Ravikumar B, "Twinning-induced sluggish evolution of texture during recrystallization in AISI 316L stainless steel after cold rolling", *METALL MATER TRANS A* 37A (8): pp. 2349-2359 AUG 2006.
74. Chowdhury SG, Dutta A, Ravikumar B. Kumar A, "Textural evolution during accumulative roll bonding of an Al-Li alloy", *MATERIALS SCIENCE AND ENGINEERING A-STRUCTURAL MATERIALS PROPERTIES MICROSTRUCTURE AND PROCESSING* 428 (1-2): 351-357 JUL 25 2006.
75. Pantleon K.; Somers M.A.J., "X-ray diffraction investigation of self-annealing in nanocrystalline copper electrodeposits", *SCRIPTA MATERIALIA*, 55 (4): pp. 283-286, 2006.
76. Etter AL, Baudin T, Mathon MH, Swiatnicki W, Penelle R, "Stored energy evolution in both phases of a duplex steel as a function of cold rolling reduction", *SCRIPTA MATERIALIA*, 54 (4): 683-688 FEB 2006.
77. Etter AL, Baudin T, Mathon MH, Swiatnicki W, Penelle R, "Stored energy evolution in both phases of a duplex steel as a function of cold rolling reduction", *SCRIPTA MATERIALIA*, 54 (4): 683-688 FEB 2006,
78. Etter AL, Baudin T, Rey C, Penelle R, "Microstructural and textural characterization of copper processed by ECAE", *MATERIALS CHARACTERIZATION* 56 (1): 19-25 JAN 2006,
79. Chowdhury, Sandip Ghosh; Srivastava, V.C.; Ravikumar, B.; Soren, S. "Evolution of texture during accumulative roll bonding (ARB) and its comparison with normal cold rolled aluminium–manganese alloy", *Scripta Materialia* Vol: 54, Issue: 9, May, 2006, pp. 1691-1696,
80. Bonarski J, Olek W, "Texture function application for wood ultrastructure description. Part 1: Theory", *WOOD SCI TECHNOL* 40 (2): 159-171 FEB 2006
81. Bonarski, Jan T., "X-ray texture tomography of near-surface areas", *Progress in Materials Science* Volume: 51, Issue: 1, January, 2006, pp. 61-149
82. E.Zschech, M.A.Meyer, I.Zienert, E.Langer, H.Geisler, A.Preusse, P.Huebler, "Electromigration-induced copper interconnect degradation and failure: the role of microstructure", *Physical and Failure Analysis of Integrated Circuits, 2005. IPFA 2005. Proceedings of the 12th International Symposium on the Physical & Failure Analysis of Integrated Circuits*, pp 85- 91.
83. Yu SH, Chun YB, Cao WQ, Kim MH, Chae SW, Kwun SI, Shin DH, Hwang SK, "Comparison of equal channel angular pressing and cold rolling in the evolution of microstructure and texture in zirconium", *METALS AND MATERIALS INTERNATIONAL* 11 (2): 101-111 APR 2005,
84. Chun YB, Yu SH, Semiatin SL, Hwang SK, "Effect of deformation twinning on microstructure and texture evolution during cold rolling of CP-titanium", *MATERIALS SCIENCE AND ENGINEERING A*. 398 (1-2): 209-219 MAY 25 2005,

85. Yu SH, Chun YB, Hwang SK, Shin DH, "Texture development and Monte-Carlo simulation of microstructure evolution in pure Zr grain-refined by equal channel angular pressing", *PHILOSOPHICAL MAGAZINE*, 85 (2-3): 345-371 Sp. Iss. SI JAN 11 2005,
86. Kim SH, You BS, Yim CD, Seo YM, "Texture and microstructure changes in asymmetrically hot rolled AZ31 magnesium alloy sheets", *MATERIALS LETTERS*, 59 (29-30), (2005),3876-3880.
87. Blicharski M, Jura J, Baudin T, Penelle R, Bonarski J, Kowalski M, "Development of the orientation relationship between ferritic and austenitic phases during long time annealing of duplex stainless steel" *ARCHIVES OF METALLURGY AND MATERIALS*, 50 (2): 495-502, SI 2005
88. R.Kumar, B.Mahato, N.R.Bandyopadhyay, D.K.Bhattacharya, "Comparison of rolling texture in low and medium stacking fault energy austenitic stainless steels", *Materials Science & Engineering A*, Vol: 394, Issue: 1-2, March 15, 2005.
89. Y.B.Chun,S.H.Yu, S.L.Semiatin, S.K.Hwang, "Effect of deformation twinning on microstructure and texture evolution during cold rolling of CP-titanium", *Materials Science & Engineering A* Vol: 398, Issue: 1-2, May 25, 2005.
90. Alexandrov IV, Zhilina MV, Scherbakov AV, Korshunov AI, Nizovtsev PN, Smolyakov AA, Solovyev VP, Beyerlein IJ, "Texture formation during severe plastic deformation", *MATERIALS SCIENCE FORUM*,495-497: 785-790 Part 1&2 2005,
91. M.V.Z. Zhilina, I.V. Alexandrov, J.T. Bonarski, A.V. Scherbakov, "Analysis of homogeneity of texture formation processes under high pressure torsion", *E-MRS Fall Meeting 2005, Symposium I*.
92. Kusnierz J, Bogucka J., "Evolution of texture during ARB processing of Al 99.8%", *MATERIALS SCIENCE FORUM*, 495-497: 797-802 Part 1&2 2005,
93. S.H. Yu, Y.B.Chun, S.K.Hwang, D.H.Shin, "Texture development and Monte-Carlo simulation of microstructure evolution in pure Zr grain-refined by equal channel angular pressing", *Philosophical Magazine*, Volume 85, Numbers 2-3, 11 January-21 January 2005.
94. Vogel SC, Hartig C, Von Dreele RB, Wenk HR, Williams DJ, "Quantitative texture measurements using neutron time-of-flight diffraction", *MATERIALS SCIENCE FORUM*, 495-497: 107-112 Part 1&2 2005,
95. Tarkowski L., Bonarski J., W.Dąbrowski "Application of the Si-strip detector in X-ray crystallographic texture measurements", *Nuclear Inst. and Methods in Physics Research, A* Volume: 551, Issue: 1, October 1, 2005, pp. 178-182.
96. Zhilina MV, Bonarski J, Scherbakov AV, Alexandrov IV, Makarychev K, "Analysis of texture formation homogeneity processes during equal-channel angular pressing", *ARCHIVES OF METALLURGY AND MATERIALS* 50 (2), 479-485 SI 2005.
97. Mizera J, Pakielna Z, Kurzydowski KJ, "Texture and residual stresses in Ti-Al and Ti-Al-Nb alloy subjected to severe plastic deformation", *ARCHIVES OF METALLURGY AND MATERIALS*, 50 (2), 395-402, SI 2005.
98. Espinoza Orias A.A., "THE RELATIONSHIP BETWEEN THE MECHANICAL ANISOTROPY OF HUMAN CORTICAL BONE TISSUE AND ITS MICROSTRUCTURE", Thesis, University of Notre Dame, 2005.

99. Kusnierz J, "Rolling texture of ECAP processed Al and Cu", TEXTURE AND ANISOTROPY OF POLYCRYSTALS II, SOLID STATE PHENOMENA, 105: 339-344 2005,
100. Kusnierz J, Bogucka J., "Accumulative roll-bonding (ARB) of A199.8%", ARCHIVES OF METALLURGY AND MATERIALS", 50 (1): 219-230 2005,
101. Ischia G, Wenk HR, Lutterotti L, Berberich F, "Quantitative Rietveld texture analysis of zirconium from single synchrotron diffraction images", JOURNAL OF APPLIED CRYSTALLOGRAPHY, 38: 377-380 (2) 2005.
102. Chateigner D, "Reliability criteria in quantitative texture analysis with experimental and simulated orientation distributions", JOURNAL OF APPLIED CRYSTALLOGRAPHY, 38: 603-611 Part 4 AUG 2005
103. Kapoor K., Lahiri D., Rao S.V.R., Sanyal T., Saibaba N., Kashyap B.P., "Texture evolution in two phase Zr – 2.5 wt-%Nb through modified route", Materials Science and Technology, October 2004, vol. 20, no. 10, pp. 1281-1289(9).
104. Sarma, V. Subramanya; Eickemeyer, J.; Mickel, C.; Schultz, L.; Holzapfel, B., "On the cold rolling textures in some fcc Ni-W alloys" MATERIALS SCIENCE AND ENGINEERING: A Volume: 380, Issue: 1-2, August 25, 2004, pp. 30-33
105. J.L.Jones, S.C.Vogel, E.B.Slamovich, K.J.Bowman, "Quantifying texture in ferroelectric bismuth titanate ceramics", Scripta Materialia, Vol: 51, Issue: 12, December, 2004
106. Jones JL, Slamovich EB, Bowman KJ, "Critical evaluation of the Lotgering degree of orientation texture indicator", JOURNAL OF MATERIALS RESEARCH, 19 (11): 3414-3422 NOV 2004,
107. Wenk HR, Lonardelli I, Williams D, "Texture changes in the hcp -> bcc -> hcp transformation of zirconium studied in situ by neutron diffraction", ACTA MATERIALIA, 52 (7): 1899-1907, 2004
108. Jones JL, Vogel SC, Slamovich EB, Bowman KJ, "Quantifying texture in ferroelectric bismuth titanate ceramics", SCRIPTA MATERIALIA, 51 (12): 1123-1127 DEC 2004,
109. Liu JT, Morris JG, "Recrystallization microstructures and textures in AA 5052 continuous cast and direct chill cast aluminum alloy", MATERIALS SCIENCE AND ENGINEERING A-STRUCTURAL MATERIALS PROPERTIES MICROSTRUCTURE AND PROCESSING, 385 (1-2): 342-351, 2004
110. Wenk HR, "The Textures of Rocks in the Earth's Deep Interior: Part I. Understanding Anisotropy and Textures in Earth Materials", Encyclopedia of Materials: Science and Technology, Elsevier (2004);
111. Li HL, Glavicic MG, Szpunar JA, "A model of texture formation in ZrO₂ films", MATERIALS SCIENCE AND ENGINEERING A, 366 (1): 164-174 FEB 5 2004,
112. Wenk HR, Lutterotti L, Vogel S, "Texture analysis with the new HIPPO TOF diffractometer", NUCLEAR INSTRUMENTS & METHODS IN PHYSICS RESEARCH SECTION A-ACCELERATORS SPECTROMETERS DETECTORS AND ASSOCIATED EQUIPMENT 515 (2003) 575-588;
113. Anderson PM, Bingert JF, Misra A, Hirth JP, "Rolling textures in nanoscale Cu/Nb multilayers", ACTA MATERIALIA 51 (2003) 6059-6075;

114. Hayakawa Y, Kurosawa M., "Orientation relationship between primary and secondary recrystallized texture in electrical steel", ACTA MATERIALIA 50 (18): 4527-4534 OCT 28 2002
115. Liu JT, Morris JG, "Macro-, micro- and mesotexture evolutions of continuous cast and direct chill cast AA 3105 aluminum alloy during cold rolling", MATERIALS SCIENCE AND ENGINEERING A-STRUCTURAL MATERIALS PROPERTIES MICROSTRUCTURE AND PROCESSING 357 (2003) 277-296;
116. Liu JT, Morris JG, "Texture and grain-boundary evolutions and direct chill cast AA 5052 aluminum alloy during cold rolling", METALLURGICAL AND MATERIALS TRANSACTIONS A-PHYSICAL METALLURGY AND MATERIALS SCIENCE 34A (2003) 951-966;
117. Liu JT, Morris JG, "Recrystallization textures of continuous cast AA 3015 alloy: Development of the P orientation $\{011\} \langle 566 \rangle$ ", METALLURGICAL AND MATERIALS TRANSACTIONS A-PHYSICAL METALLURGY AND MATERIALS SCIENCE 34A (2003) 2029-2032;
118. Kusnierz J, Bogucka J., "Effect of ECAP processing on the properties of cold rolled copper", ARCHIVES OF METALLURGY, 48 (2): 173-182 2003,
119. Kusnierz J, Baudin T, Jasienski Z, Penelle R., "Neutron and X-ray diffraction study of Al and Cu during ECA processing C and subsequent recrystallization", REVUE DE METALLURGIE-CAHIERS D INFORMATIONS TECHNIQUES, 100 (9): 825-833 SEP 2003,
120. Etter AL, Mathon MH, Baudin T, Penelle R., "Stored energy evolution as a function of cold rolling reduction for a Fe-53%Ni alloy and an austenitic-ferritic steel", REVUE DE METALLURGIE-CAHIERS D INFORMATIONS TECHNIQUES, 100 (9): 851-858 SEP 2003,
121. Bechade JL, Mathon MH, Branger V, Regle H, Alamo A., "Texture analysis of oxide dispersion strengthened (ODS) Fe alloys by X-ray and neutron diffraction", JOURNAL DE PHYSIQUE IV 12 (PR6): 155-163 JUL 2002,
122. Kusnierz J, Kurowski M., "Strain softening effects in texture and microstructure of torsioned pre-deformed Al rods", ZEITSCHRIFT FUR METALLKUNDE, 93 (12): 1233-1236 DEC 2002,
123. Etter AL, Mathon MH, Baudin T, Penelle R., "A method of determination of stored energy in single and dual phase cold rolled materials", TEXTURES OF MATERIALS, PTS 1 AND 2, MATERIALS SCIENCE FORUM, 408-4: 583-588 2002
124. Kusnierz J, Kurowski M, Mathon MH, Baudin T, Jasienski Z, Penelle R., "Effect of deformation path on torsion texture and stored energy of copper rods", TEXTURES OF MATERIALS, PTS 1 AND 2 MATERIALS SCIENCE FORUM, 408-4: 625-630 2002,
125. Kusnierz J, Mathon MH, Baudin T, Jasienski Z, Penelle R., "Neutron diffraction study of texture and stored energy in ECA pressed copper", TEXTURES OF MATERIALS, PTS 1 AND 2, MATERIALS SCIENCE FORUM, 408-4: 703-708 2002,
126. Kim BK, Szpunar JA, Varano R., "Texture evolution in grain growth of nanocrystalline Ni", TEXTURES OF MATERIALS, PTS 1 AND 2, MATERIALS SCIENCE FORUM, 408-4: 937-942 2002

127. Kim BK, Szpunar JA, Zhilyaev AP., "Annealing texture in thermal stability of ultrafine-grained Ni",TEXTURES OF MATERIALS, PTS 1 AND 2, MATERIALS SCIENCE FORUM, 408-4: 943-948 2002,
128. Jura J, Baudin T, Mathon MH, Swiatnicki W, Penelle R., "Microstructure and texture analysis in a cold-rolled austenitic-ferritic steel with duplex structure",TEXTURES OF MATERIALS, PTS 1 AND 2, MATERIALS SCIENCE FORUM, 408-4: 1359-1364 2002
129. Caleyó F, Baudin T, Penelle R, "Study of the development of the cube texture in Fe-50%Ni during recrystallization and normal grain growth", EUROPEAN PHYSICAL JOURNAL-APPLIED PHYSICS 20 (2002) 77-89;
130. Park JY, Szpunar JA, "Influence of the primary recrystallization texture on abnormal grain growth of goss grains in grain oriented electrical steels",TEXTURES OF MATERIALS, PTS 1 AND 2, MATERIALS SCIENCE FORUM, 408-4: 821-826 2002,
131. Park JY, Han KS, Woo JS, Chang SK, Rajmohan N, Szpunar JA,"Influence of primary annealing condition on texture development in grain oriented electrical steels",ACTA MATERIALIA, 50 (7): 1825-1834 APR 19 2002,
132. Etter AL, Mathon MH, Baudin T, Branger V, Penelle R.,"Influence of the cold rolled reduction on the stored energy and the recrystallization texture in a Fe-53%Ni alloy", SCRIPTA MATERIALIA, 46 (4): 311-317 FEB 28 2002,
133. Kusnierz J., "Microstructure and texture evolving under Equal Channel Angular (ECA) processing",ARCHIVES OF METALLURGY, 46 (4): 375-384 2001.
134. Starczewski L, Bonarski JT; "Stress-textural indicators of tribological wear"; MATERIALS SCIENCE AND ENGINEERING A-STRUCTURAL MATERIALS PROPERTIES MICROSTRUCTURE AND PROCESSING 288 (2000) 284-287;
135. Bonarski JT, Wrobel M, Pawlik K,"Quantitative phase analysis of duplex stainless steel using incomplete pole figures", MATERIALS SCIENCE AND TECHNOLOGY, 16 (2000) 657-662;
136. Okuda K, Sakata K, Eloit K, Furukimi O, Obara T, "Mechanism of strong formation of {111} recrystallization texture of cold rolled IF steel sheet with {111} hot band texture", TETSU TO HAGANE-JOURNAL OF THE IRON AND STEEL INSTITUTE OF JAPAN 85 (8): 633-638 AUG 1999,
137. Pawlowski A, Bonarski J,"Plastic deformation in Ti-46at.%Al alloy of cellular-lamellar structure",44 (1999) 267-278;
138. Nowak R, Yoshida F, Morgiel J, Major B,"Postdeposition relaxation of internal stress in sputter-grown thin films caused by ion bombardment",JOURNAL OF APPLIED PHYSICS, 85 (1999) 841-852;
139. Bonarski J, Pawlik K,"Development of texture determination method for the near-surface-layers",ARCHIVES OF METALLURGY, 43 (1998) 141-148;
140. Komatsubara M, Hayakawa Y, Takamiya T, Muraki M, Maeda C, Ishida M, Morito N,"Newly developed grain-oriented Si-steel with thinner gauges", JOURNAL DE PHYSIQUE IV, 8 (1998) 467-474;
141. Eloit K, Okuda K, Sakata K, Obara T,"Texture evolution during cold rolling and recrystallisation of IF steel with a strong {111} hot band texture";ISIJ INTERNATIONAL, 38 (1998) 602-609;

142. Tarasiuk J, Wierzbanowski K, Baczmanski A, "New algorithm for the ODF calculation from pole figures", *TEXTURE AND ANISOTROPY OF POLYCRYSTALS MATERIALS SCIENCE FORUM*, 273-2 (1998) 133-138;
143. Dutkiewicz J, Bonarski J, "Structure, texture and mechanical properties of AlZnMgCuZr alloy rolled after heat treatments", *MATERIALS & DESIGN*, 8 (4-6) (1997) 247-252;
144. Hayakawa Y, Szipunar JA, "A comprehensive model of recrystallization for interstitial free steel", *ACTA MATERIALIA* 45 (1997) 3721-3730;
145. Hayakawa Y, Szipunar JA, "Modeling of texture development during recrystallization of interstitial free steel", *ACTA MATERIALIA* 45 (1997) 2425-2434;
146. Rajmohan N, Hayakawa Y, Szipunar JA, Root JH, "Neutron diffraction method for stored energy measurement in interstitial free steel", *ACTA MATERIALIA* 45 (1997) 2485-2494;
147. Hayakawa Y, Szipunar JA, "The role of grain boundary character distribution in secondary recrystallization of electrical steels", *ACTA MATERIALIA* 45 (1997) 1285-1295;
148. Matthies S, Lutterotti L, Wenk HR, "Advances in texture analysis from diffraction spectra", *JOURNAL OF APPLIED CRYSTALLOGRAPHY*, 30: 31-42 Part 1 (1997);
149. Akdut N, Foct J, Gottstein G, "Cold rolling texture development of alpha/gamma duplex stainless steels", *STEEL RESEARCH* 67 (10) (1996) 450-455.
150. N.Akdut, J.Foct, "Phase Boundaries and Deformation in High Nitrogen Duplex Stainless Steels I. - Rolling Texture Development", *Scripta Metallurgica et Materiala*, Vol: 32, Issue: 1, January 1, 1995
151. N.Akdut, J.Foct, "Phase Boundaries and Deformation in High Nitrogen Duplex Stainless Steels II. - Analysis of Deformation Mechanisms by Texture Measurements in X2 CrNiMo 22 5 (1.4462) *Scripta Metallurgica et Materiala*, Vol: 32, Issue: 1, January 1, 1995.
152. Texture Modelling: Co-operation of LaboTex with VPSC, M.Zylina, A.Schrbakov, I.V.Alexandrov, "Computer Modelling of Processes of Texture Development in Pure Copper During Equal Channel Angular Pressing"
153. Bahl, S., Nithilaksh, P. L., Suwas, S., Kailas, S. V., & Chatterjee, K. (2017). Processing – Microstructure – Crystallographic Texture – Surface Property Relationships in Friction Stir Processing of Titanium. *Journal of Materials Engineering and Performance*, 26(9), 4206–4216. doi:View 10.1007/s11665-017-2865-6
154. Bishoyi, B. D., Sabat, R. K., & Sahoo, S. K. (2018). Materials Science & Engineering A Effect of temperature on microstructure and texture evolutions during uniaxial compression of commercially pure titanium. *Materials Science & Engineering A*, 718(October 2017), 398–411. doi:View 10.1016/j.msea.2018.01.128
155. Bishoyi, B. D., Sabat, R. K., Sahu, J., & Sahoo, S. K. (2017). Materials Science & Engineering A Effect of temperature on microstructure and texture evolution during uniaxial tension of commercially pure titanium. *Materials Science & Engineering A*, 703(July), 399–412. doi:View 10.1016/j.msea.2017.07.081
156. Bisht, A., Jagadeesh, G., & Suwas, S. (2017). Investigation on Shock Wave-Assisted Deformation of Nano Nickel. doi:View 10.1007/978-3-319-44866-4
157. Chatterjee, S., Ghosh, A., & Mallick, A. B. (2018). ScienceDirect Understanding the evolution of microstructural features in the in- situ intermetallic phase reinforced Al / Al 3 Ti nanocomposite. *Materials Today: Proceedings*, 5(3), 10118–10130. doi:View 10.1016/j.matpr.2017.11.008

158. Choi, J. W., & Shin, K. S. (2017). Effects of Zn Content and Initial Grain Size on Double Peak Basal Textures of Mg-Zn-Al Alloys, 23(4), 745–755. doi:View 10.1007/s12540-017-6841-3
159. Dryzek, E., Dryzek, J., & Metallic, I. (2016). Recrystallization in severely, 2042(10), 2031–2042. doi:View 10.1002/pssb.201600280
160. Dufrenoy, S., Chauveau, T., Brenner, R., & Bacroix, B. (2018). Comparison of 2 methodologies developed for the determination of residual stresses through X-ray diffraction: application to a textured hcp titanium alloy, 341–355. doi:View 10.1007/s12289-017-1354-7
161. Gebrekrstos, A., Sharma, M., Bahl, S., Madras, G., & Suwas, S. (2018). Process mediated polymorphism , crystallographic texture and structure-property correlation in crystalline / amorphous blends. Polymer, 138, 307–319. doi:View 10.1016/j.polymer.2018.01.075
162. Ghosh, P., Petegem, S. Van, Swygenhoven, H. Van, & Chokshi, A. H. (2017). Materials Science & Engineering A An in-situ synchrotron study on microplastic flow of electrodeposited nanocrystalline nickel. Materials Science & Engineering A, 701(February), 101–110. doi:View 10.1016/j.msea.2017.06.075
163. Gu, T., Castelnau, O., Forest, S., Hervé-luanco, E., Lecouturier, F., & Proudhon, H. (2017). International Journal of Solids and Structures Multiscale modeling of the elastic behavior of architected and nanostructured Cu – Nb composite wires, 121, 148–162. doi:View 10.1016/j.ijsolstr.2017.05.022
164. Gurao, N. P., & Suwas, S. (2017). Effect of Phase Contiguity and Morphology on the Evolution of Deformation Texture in Two-Phase Alloys. Metallurgical and Materials Transactions A, 48(2), 809–827. doi:View 10.1007/s11661-016-3856-1
165. Karjalainen, L. P., & Society, M. (n.d.). Correlation of Microstructure and Texture in a Two-Phase High-Mn Twinning-Induced Plasticity Steel During Cold Rolling. doi:View 10.1007/s11661-017-4241-4
166. Kumar, G., Lodh, A., Singh, J., Singh, R., Srivastava, D., Dey, G. K., & Samajdar, I. (2017). CIRP Journal of Manufacturing Science and Technology Experimental characterization and finite element modeling of through thickness deformation gradient in a cold rolled zirconium sheet. CIRP Journal of Manufacturing Science and Technology, 19, 176–190. doi:View 10.1016/j.cirpj.2017.09.002
167. Le, T., Caleyó, F., Hallen, J. M., Benítez, J. A. P., & Hernández, J. H. E. (2017). Materials Science & Engineering B Novel method for the accurate determination of magnetocrystalline energy from Barkhausen noise in ferromagnetic materials. Materials Science & Engineering B, 225(August), 98–107. doi:View 10.1016/j.mseb.2017.08.015
168. Le, T., Caleyó, F., Hallen, J. M., Espina-hernández, J. H., & Pérez-benitez, J. A. (2018). Journal of Magnetism and Magnetic Materials Model for the correlation between magnetocrystalline energy and Barkhausen noise in ferromagnetic materials. Journal of Magnetism and Magnetic Materials, 454, 155–164. doi:View 10.1016/j.jmmm.2018.01.066
169. Leibenguth, P., Slawik, S., Coelho, R. S., Horwat, D., Migot, S., Lechthaler, B., & Mücklich, F. (2018). Estimation of residual stresses in perovskite films for capacitor applications. Thin Solid Films, 648(October 2017), 21–25. doi:View 10.1016/j.tsf.2018.01.011
170. Loganathan, A., Sharma, A., Rudolf, C., Zhang, C., & Nautiyal, P. (2017). Materials Science & Engineering A In-situ deformation mechanism and orientation effects in

sintered 2D boron nitride nanosheets. *Materials Science & Engineering A*, 708(October), 440–450. doi:View 10.1016/j.msea.2017.10.019

171. Manh, T. Le, Hallen, J. M., & Caley, F. (2018). Materials Characterization Electron backscatter diffraction helps direct calculation of magnetocrystalline anisotropy energy in API 5L steels. *Materials Characterization*, 141(April), 86–96. doi:View 10.1016/j.matchar.2018.04.033
172. Ozaltin, K., Panigrahi, A., Chrominski, W., Bulutsuz, A. G., & Kulczyk, M. (2017). Microstructure and Texture Evolutions of Biomedical Ti-13Nb-13Zr Alloy Processed by Hydrostatic Extrusion. *Metallurgical and Materials Transactions A*, 48(11), 5747–5755. doi:View 10.1007/s11661-017-4278-4
173. Park, J. W., Park, S. J., & Shin, K. S. (2017). Effects of Tensile Twinning on the Stretch Formability of Mg, 23(3), 444–449. doi:View 10.1007/s12540-017-6399-0
174. Park, S. M., Koo, Y. M., Shim, B. Y., & Lee, D. N. (2017). Effects of Process Variables in Decarburization Annealing of Fe-3 % Si-0.3 % C Steel Sheet on Textures and Magnetic Properties, 23(1), 220–232. doi:View 10.1007/s12540-017-6042-0
175. Rao, A. S., Manda, P., Mohan, M. K., Nandy, T. K., & Singh, A. K. (2018). Microstructure, texture and mechanical properties of hot rolled and annealed Ni-Fe-W and Ni-Fe-W-Co matrix alloys. *Journal of Alloys and Compounds*, 742, 937–951. doi:View 10.1016/j.jallcom.2018.01.336
176. Schmitt, J., & Solas, D. (2018). Measurement of Texture Gradient in Heavily Cold-Drawn Pearlitic Wires, 1700279, 1–8. doi:View 10.1002/adem.201700279
177. Sharma, S., Kumar, B. R., Kashyap, B. P., & Prabhu, N. (2018). Materials Science & Engineering A Effects of concurrent strain induced martensite formation on tensile and texture properties of 304L stainless steel of varying grain size distribution. *Materials Science & Engineering A*, 725(October 2017), 215–227. doi:View 10.1016/j.msea.2018.03.099
178. Suresh, M., Sharma, A., More, A. M., Nayan, N., & Suwas, S. (2018). Effect of Scandium addition on evolution of microstructure, texture and mechanical properties of thermo-mechanically processed Al-Li alloy AA2195. *Journal of Alloys and Compounds*, 740, 364–374. doi:View 10.1016/j.jallcom.2017.12.045
179. Tekumalla, S., Bibhanshu, N., Shabadi, R., Suwas, S., Mai, T., & Ha, H. (2018). Materials Science & Engineering A Evolution of texture and asymmetry and its impact on the fatigue behaviour of an in-situ magnesium nanocomposite. *Materials Science & Engineering A*, 727(April), 61–69. doi:View 10.1016/j.msea.2018.04.101
180. Tripathi, A., Murty, S. V. S. N., & Narayanan, P. R. (2017). Microstructure and texture evolution in AZ31 magnesium alloy during caliber rolling at different temperatures. *Journal of Magnesium and Alloys*, 5(3), 340–347. doi:View 10.1016/j.jma.2017.07.001
181. Vakhitova, E., Sornin, D., Barcelo, F., & François, M. (2017). Texture evolution in Oxide Dispersion Strengthened (ODS) steel tubes during pilgering process. *Journal of Nuclear Materials*, 494, 20–28. doi:View 10.1016/j.jnucmat.2017.07.002
182. Verstraete, B. K., Azzedine, H., Helbert, A., Boumediene, H., Alia, E., & Ezzouar, B. (2017). Accumulative Roll Bonding at Room Temperature of a Bi-Metallic AA5754 / AA6061 Composite : Impact of Strain Path on Microstructure, Texture, and Mechanical Properties **, 1–8. doi:View 10.1002/adem.201700285

183. Wierzbanski, K. (2017). *Acta Materialia* Texture effects due to asymmetric rolling of polycrystalline copper, 139, 30–38. doi:View 10.1016/j.actamat.2017.07.062
184. Zuñiga, M. A. B., & Rosales, H. J. D. (2018). Effect of microstructure and crystallographic texture on the toughness anisotropy of API 5L X46 STEEL, (August 2017), 749–761. doi:View 10.1111/ffe.12782
185. Chai, L., Chen, B., Wang, S., Zhang, Z., & Murty, K. L. (2016). Microstructural, textural and hardness evolution of commercially pure Zr surface-treated by high current pulsed electron beam. *Applied Surface Science*, 390, 430–434. doi:View 10.1016/j.apsusc.2016.08.128
186. Chao, Q., Hodgson, P. D., & Beladi, H. (2017). Thermal stability of an ultra fine grained Ti-6Al-4V alloy during post- deformation annealing. *Materials Science & Engineering A*, 694(April), 13–23. doi:View 10.1016/j.msea.2017.03.082
187. Chen, X. P., Sun, H. F., Chen, D., Wang, L. X., & Liu, Q. (2016). On recrystallization texture and magnetic property of Cu-Ni alloys. *Materials Characterization*, 121, 149–156. doi:View 10.1016/j.matchar.2016.10.006
188. Cu-y, O., Maharana, H. S., Panda, S., & Basu, A. (2017). Effect of texture and microstructure on properties of electrodeposited. *Surface & Coatings Technology*, 315, 558–566. doi:View 10.1016/j.surfcoat.2017.02.035
189. Dittrich, M., Meixner, M., & Schumacher, G. (2016). Texture formation in amorphous Al₈₆Ni₆Y_{4.5}La_{1.5}Co₂ splats by thermal and mechanical treatment. *Intermetallics*, 74, 46–52. doi:View 10.1016/j.intermet.2016.04.008
190. Góral, A. (2017). Nanoscale structural defects in electrodeposited Ni/Al₂O₃ composite coatings. *Surface & Coatings Technology*. 319, 23–32. doi:View 10.1016/j.surfcoat.2017.03.061
191. Guo, F., Zhang, D., Wu, H., Jiang, L., & Pan, F. (2017). The role of Al content on deformation behavior and related texture evolution during hot rolling of Mg-Al-Zn alloys. *Journal of Alloys and Compounds*, 695, 396–403. doi:View 10.1016/j.jallcom.2016.10.222
192. Järvenpää, A., Jaskari, M., Man, J., & Karjalainen, L. P. (2017). Austenite stability in reversion-treated structures of a 301LN steel under tensile loading. *Materials Characterization*, 127, 12–26. doi:View 10.1016/j.matchar.2017.01.040
193. Korneva, A., Straumal, B., Kilmametov, A., Chulist, R., & Straumal, P. (2016). Phase transformations in a Cu-Cr alloy induced by high pressure torsion. *Materials Characterization*. 114, 151–156. doi:View 10.1016/j.matchar.2016.02.017
194. Kouadri-henni, A., Seang, C., Malard, B., & Klosek, V. (2017). Residual stresses induced by laser welding process in the case of a dual-phase steel DP600: Simulation and experimental approaches. *Materials & Design*, 123, 89–102. doi:View 10.1016/j.matdes.2017.03.022
195. Liu, S., & Gavrus, A. (2017). Numerical simulation and experimental investigation on the residual stresses in a laser beam welded dual phase DP600 steel plate, Thermo-mechanical material plasticity model. *International Journal of Mechanical Sciences*, 122(November 2016), 235–243. doi:View 10.1016/j.ijmecsci.2017.01.006
196. Miszczyk, M. M., Paul, H., Driver, J. H., & Poplewska, J. (2017). The influence of deformation texture on nucleation and growth of cube grains during primary recrystallization of AA1050 alloy. *Acta Materialia*, 129, 378–387. doi:View 10.1016/j.actamat.2017.03.004

197. Panigrahi, A., Sulkowski, B., Waitz, T., Ozaltin, K., Chrominski, W., Pukenas, A., & Horky, J. (2016). Mechanical properties , structural and texture evolution of biocompatible Ti – 45Nb alloy processed by severe plastic deformation. *Journal of the Mechanical Behavior of Biomedical Materials*, 62, 93–105. doi:View 10.1016/j.jmbbm.2016.04.042
198. Patra, A., Saxena, R., Karak, S. K., Laha, T., & Sahoo, S. K. (2017). Fabrication and characterization of nano-Y2O3 dispersed W-Ni-Mo and W-Ni-Ti-Nb alloys by mechanical alloying and spark plasma sintering. *Journal of Alloys and Compounds*, 707, 245–250. doi:View 10.1016/j.jallcom.2016.11.424
199. Ren, Y., Zhang, X., Xia, T., Sun, Q., & Liu, Q. (2017). Microstructural and textural evolution of high- purity titanium under dynamic loading. *Materials & Design*, 126 (April), 123–134. doi:View 10.1016/j.matdes.2017.04.042
200. Riedl, H., Koller, C. M., Munnik, F., Hutter, H., Martin, F. M., Rachbauer, R., Mayrhofer, P. H. (2016). Influence of oxygen impurities on growth morphology, structure and mechanical properties of Ti–Al–N thin films. *Thin Solid Films*, 603, 39–49. doi:View 10.1016/j.tsf.2016.01.039
201. Rogal, Ł. (2017). Semi-solid processing of the CoCrCuFeNi high entropy alloy. *Materials & Design*, 119, 406–416. doi:View 10.1016/j.matdes.2017.01.082
202. Sahoo, S. K., Sabat, R. K., Panda, S., Mishra, S. C., & Suwas, S. (2017). Texture and microstructure evolution of pure zinc during rolling at liquid nitrogen temperature and subsequent annealing. *Materials Characterization*, 123, 218–226. doi:View 10.1016/j.matchar.2016.11.030
203. Sahoo, S. K., Sabat, R. K., Sahni, S., & Suwas, S. (2016). Texture and microstructure evolution of commercially pure titanium during hot rolling : Role of strain-paths. *JMADE*, 91, 58–71. doi:View 10.1016/j.matdes.2015.11.073
204. Shao, Y., Tang, T., Li, D., Zhou, G., Zhang, S., & Peng, Y. (2016). Polycrystal modeling of hot extrusion texture of AZ80 magnesium alloy. *Transactions of Nonferrous Metals Society of China*, 26(4), 1063–1072. doi:View 10.1016/S1003-6326(16)64203-6
205. Sharma, A., Chhangani, S., Madhavan, R., & Suwas, S. (2017). Correlation between crystallographic texture, microstructure and magnetic properties of pulse electrodeposited nanocrystalline Nickel–Cobalt alloys. *Journal of Magnetism and Magnetic Materials*, 434, 68–77. doi:View 10.1016/j.jmmm.2016.12.146
206. Sharma, A., Mohan, S., & Suwas, S. (2016). Structural, microstructural and magnetic investigations on the epitaxially grown Ni₂MnGa (010) films on MgO (100) substrate. *Intermetallics*, 77, 6–13. doi:View 10.1016/j.intermet.2016.06.009
207. Singh, J., Mahesh, S., Roy, S., Kumar, G., Srivastava, D., Dey, G. K., Samajdar, I. (2016). A miniature physical simulator for pilgering. *Journal of Materials Processing Tech.*, 237, 126–138. doi:View 10.1016/j.jmatprotec.2016.06.009
208. Singh, J., Mahesh, S., Roy, S., Kumar, G., Srivastava, D., Dey, G. K., Samajdar, I. (2017). Temperature dependence of work hardening in sparsely twinning zirconium. *Acta Materialia*, 123, 337–349. doi:View 10.1016/j.actamat.2016.10.049
209. Srinivasan, N., Velmurugan, R., Kumar, R., & Kumar, S. (2016). Deformation behavior of commercially pure (CP) titanium under equi-biaxial tension. *Materials Science & Engineering A*, 674, 540–551. doi:View 10.1016/j.msea.2016.08.018
210. Tanaka, M., Kitaoka, S., Yoshida, M., Sakurada, O., Hasegawa, M., Nishioka, K., & Kagawa, Y. (2017). Structural stabilization of EBC with thermal energy reflection at high

- temperatures. *Journal of the European Ceramic Society*, 1, 1–7. doi:View 10.1016/j.jeurceramsoc.2017.04.055
211. Uniwersa, A., Wróbel, M., Wierzbanowski, K., Wroński, S., Wroński, M., Kalembe-Rec I., Sak T., Bacroix, B. (2016). Microstructure, texture and mechanical characteristics of asymmetrically rolled polycrystalline copper. *Materials Characterization*, 118, 575–583. doi:View 10.1016/j.matchar.2016.07.004
212. Wang, L. X., Chen, X. P., Chen, D., Sun, H. F., & Liu, Q. (2016). Effect of preferential orientation on the annealing twins during the low temperature treatment in nickel. *Materials Science & Engineering A*, 676, 48–55. doi:View 10.1016/j.msea.2016.08.092
213. Yokoi, T., Yamaguchi, N., Tanaka, M., Yokoe, D., Kato, T., Kitaoka, S., & Takata, M. (2017). Preparation of a dense ytterbium disilicate layer via dual electron beam physical vapor deposition at high temperature. *Materials Letters*, 193, 176–178. doi:View 10.1016/j.matlet.2017.01.085
214. M.H. Shaeri, M.T. Salehi, S.H. Seyyedein, M.R. Abutalebi, J.K. Park, Characterization of microstructure and deformation texture during equal channel Angular pressing of Al-Zn-Mg-Cu alloy, *J. Alloys Compd.* 576 (2013) 350–357. doi:View 10.1016/j.jallcom.2013.05.182
215. M.H. Shaeri, M. Shaeri, M.T. Salehi, S.H. Seyyedein, F. Djavanrodi, Microstructure and texture evolution of Al-7075 alloy processed by equal channel angular pressing, *Trans. Nonferrous Met. Soc. China.* 25 (2015) 1367–1375. doi:View 10.1016/S1003-6326(15)63735-9
216. R. Madhavan, R.K. Ray, S. Suwas, Texture transition in cold-rolled nickel-40 wt.% cobalt alloy, *Acta Mater.* 74 (2014) 151–164. doi:View 10.1016/j.actamat.2014.03.066
217. L. Znaidi, T. Chauveau, A. Tallaire, F. Liu, M. Rahmani, V. Bockelee, et al., Textured ZnO thin films by sol–gel process: Synthesis and characterizations, *Thin Solid Films.* (2015). doi:View 10.1016/j.tsf.2015.12.031
218. A. V. Podolskiy, C. Mangler, E. Schafler, E.D. Tabachnikova, M.J. Zehetbauer, Microstructure and mechanical properties of high purity nanostructured titanium processed by high pressure torsion at temperatures 300 and 77 K, *J. Mater. Sci.* 48 (2013) 4689–4697. doi:View
219. C. Gérard, G. Cailletaud, B. Bacroix, Modeling of latent hardening produced by complex loading paths in FCC alloys, *Int. J. Plast.* 42 (2013) 194–212. doi:View 10.1016/j.ijplas.2012.10.010
220. S.K. Hwang, H.M. Baek, J.W. Lee, I.-H. Son, Y.-T. Im, C.M. Bae, The effect of microstructure and texture evolution on mechanical properties of low carbon steel in a non-circular drawing sequence, *J. Mater. Process. Technol.* 214 (2014) 318–325. doi:View 10.1016/j.jmatprotec.2013.09.020
221. M.M. Humane, K.S. Thool, R.K. Minz, L.A.I. Kestens, Microstructures and Textures of Hot Rolled and Hot Rolled-Normalized 2.9 % Silicon Steel Sheets, *Trans. Indian Inst. Met.* 68 (2014) 371–381. doi:View 10.1007/s12666-014-0465-9
222. S.K. Hwang, H.M. Baek, Y.T. Im, I.H. Son, C.M. Bae, H.W. Lee, The effect of grain refinement by multi-pass continuous hybrid process on mechanical properties of low-carbon steel wires, *J. Mater. Process. Technol.* 214 (2014) 1398–1407. doi:View 10.1016/j.jmatprotec.2014.02.001

223. O. Renk, A. Hohenwarter, S. Wurster, R. Pippan, Direct evidence for grain boundary motion as the dominant restoration mechanism in the steady-state regime of extremely cold-rolled copper, *Acta Mater.* 77 (2014) 401–410. doi:View 10.1016/j.actamat.2014.06.010
224. K. Lukaszewicz, L.A. Dobrzański, Structure and mechanical properties of gradient coatings deposited by PVD technology onto the X40CrMoV5-1 steel substrate, *J. Mater. Sci.* 43 (2008) 3400–3407. doi:View 10.1007/s10853-008-2523-3
225. N.P. Gurao, S. Sethuraman, S. Suwas, Evolution of texture and microstructure in commercially pure titanium with change in strain path during rolling, *Metall. Mater. Trans. A Phys. Metall. Mater. Sci.* 44 (2013) 1497–1507. doi:View 10.1007/s11661-012-1484-y
226. Q.H. Bui, X.T. Pham, M. Fafard, Modelling of microstructure effects on the mechanical behavior of aluminium tubes drawn with different reduction areas, *Int. J. Plast.* 50 (2013) 127–145. doi:View 10.1016/j.ijplas.2013.04.005
227. J. Singh, S. Mahesh, G. Kumar, P. Pant, D. Srivastava, G.K. Dey, et al., Texture Development and Plastic Deformation in a Pilgered Zircaloy-4 Tube, *Metall. Mater. Trans. A Phys. Metall. Mater. Sci.* 46 (2015) 1927–1947. doi:View 10.1007/s11661-015-2807-6
228. R.K. Islamgaliev, V.D. Sitdikov, K.M. Nesterov, a. V. Ganeev, E. V. Bochkova, Microstructure and crystallographic texture of titanium subjected to combined severe plastic deformation processing, *Russ. Metall.* 2014 (2014) 234–240. doi:View 10.1134/S0036029514030136
229. W. Wang, A.L. Helbert, F. Brisset, M.H. Mathon, T. Baudin, Monte Carlo simulation of primary recrystallization and annealing twinning, *Acta Mater.* 81 (2014) 457–468. doi:View 10.1016/j.actamat.2014.08.032
230. W. Heinz, W. Robl, G. Dehm, Influence of initial microstructure on thermomechanical fatigue behavior of Cu films on substrates, *Microelectron. Eng.* 137 (2015) 5–10. doi:View 10.1016/j.mee.2014.10.024
231. C. Mondal, A.K. Singh, A.K. Mukhopadhyay, K. Chattopadhyay, Effects of different modes of hot cross-rolling in 7010 aluminum alloy: Part I. evolution of microstructure and texture, *Metall. Mater. Trans. A Phys. Metall. Mater. Sci.* 44 (2013) 2746–2763. doi:View 10.1007/s11661-013-1626-x
232. K. Yoshida, A. Ishii, Y. Tadano, Work-hardening behavior of polycrystalline aluminum alloy under multiaxial stress paths, *Int. J. Plast.* 53 (2014) 17–39. doi:View 10.1016/j.ijplas.2013.07.003
233. P. Manda, P. Ghosal, U. Chakkingal, A.K. Singh, Effect of Alloying Elements in Hot-Rolled Metastable b -Titanium Alloys : Part I . Evolution of Microstructure and Texture, (n.d.). doi:View 10.1007/s11661-015-2814-7
234. A. Kauffmann, J. Freudenberger, H. Klauss, V. Klemm, W. Schillinger, V. Subramanya Sarma, et al., Properties of cryo-drawn copper with severely twinned microstructure, *Mater. Sci. Eng. A.* 588 (2013) 132–141. doi:View 10.1016/j.msea.2013.09.022
235. T.I. Ivankina, S. Matthies, On the development of the quantitative texture analysis and its application in solving problems of the Earth sciences, *Phys. Part. Nucl.* 46 (2015) 366–423. doi:View 10.1134/S1063779615030077
236. A. Góral, M. Nowak, K. Berent, B. Kania, Influence of current density on microstructure and properties of electrodeposited nickel-alumina composite coatings, *J. Alloys Compd.* 615 (2014) S406–S410. doi:View 10.1016/j.jallcom.2014.01.025

237. H.Y. Fan, S.F. Liu, Y. Guo, C. Deng, Q. Liu, Quantifying the effects of surface quality on texture measurements of tantalum, *Appl. Surf. Sci.* 339 (2015) 15–21. doi:View 10.1016/j.apsusc.2015.01.216
238. P. Ghosh, A.H. Chokshi, Size Effects on Strength in the Transition from Single-to-Polycrystalline Behavior, *Metall. Mater. Trans. A Phys. Metall. Mater. Sci.* 46 (2015) 5671–5684. doi:View 10.1007/s11661-015-3174-z
239. N. Stanford, R.K.W. Marceau, M.R. Barnett, The effect of high yttrium solute concentration on the twinning behaviour of magnesium alloys, *Acta Mater.* 82 (2015) 447–456. doi:View 10.1016/j.actamat.2014.09.022
240. D. Rodriguez-Galan, I. Sabirov, J. Segurado, Temperature and strain rate effect on the deformation of nanostructured pure titanium, *Int. J. Plast.* 70 (2015) 191–205. doi:View 10.1016/j.ijplas.2015.04.002
241. M. Zieliński, Effects of constant magnetic field on the electrodeposition reactions and cobalt-tungsten alloy structure, *Mater. Chem. Phys.* 141 (2013) 370–377. doi:View 10.1016/j.matchemphys.2013.05.025
242. S. Roy, S. Suwas, Microstructure and texture evolution during sub-transus thermomechanical processing of Ti-6Al-4V-0.1B alloy: Part I. Hot rolling in ($\alpha+\beta$) phase field, *Metall. Mater. Trans. A Phys. Metall. Mater. Sci.* 44 (2013) 3303–3321. doi:View 10.1007/s11661-013-1672-4
243. G. Dirras, T. Chauveau, A. Abdul-Latif, S. Ramtani, Q.-H. Bui, Microstructure characterization of high-purity aluminum processed by dynamic severe plastic deformation, *Phys. Status Solidi.* 207 (2010) 2233–2237. doi:View 10.1002/pssa.201026093
244. V.D. Sitdikov, I.V. Alexandrov, Computer modeling of texture formation processes in Ti Grade 4 during continuous equal channel angular pressing, *Comput. Mater. Sci.* 76 (2013) 65–71. doi:View 10.1016/j.commatsci.2013.03.034
245. M. Palit, S. Banumathy, A.K. Singh, S. Pandian, K. Chattopadhyay, Orientation Selection and Microstructural Evolution in Directionally Solidified Tb_{0.3}Dy_{0.7}Fe_{1.95}, *Metall. Mater. Trans. A.* (2016) 0–10. doi:View 10.1007/s11661-016-3345-6
246. A. Eschke, J. Scharnweber, C.G. Oertel, W. Skrotzki, T. Marr, J. Romberg, et al., Texture development in Ti/Al filament wires produced by accumulative swaging and bundling, *Mater. Sci. Eng. A.* 607 (2014) 360–367. doi:View 10.1016/j.msea.2014.04.003
247. G. Zhou, M.K. Jain, P. Wu, Y. Shao, D. Li, Y. Peng, Experiment and crystal plasticity analysis on plastic deformation of AZ31B Mg alloy sheet under intermediate temperatures: How deformation mechanisms evolve, *Int. J. Plast.* 79 (2016) 19–47. doi:View 10.1016/j.ijplas.2015.12.006
248. K.S. Suresh, M. Geetha, C. Richard, J. Landoulsi, H. Ramasawmy, S. Suwas, et al., Effect of equal channel angular extrusion on wear and corrosion behavior of the orthopedic Ti-13Nb-13Zr alloy in simulated body fluid, *Mater. Sci. Eng. C.* 32 (2012) 763–771. doi:View 10.1016/j.msec.2012.01.022
249. M. Naderi, M. Peterlechner, E. Schafner, S. V. Divinski, G. Wilde, Kinetic, volumetric and structural effects induced by liquid Ga penetration into ultrafine grained Al, *Acta Mater.* 99 (2015) 196–205. doi:View 10.1016/j.actamat.2015.07.061
250. K.H. Oh, J.S. Jeong, Y.M. Koo, D.N. Lee, The evolution of the rolling and recrystallization textures in cold-rolled Al containing high Mn austenitic steels, *Mater. Chem. Phys.* 161 (2014) 9–18. doi:View 10.1016/j.matchemphys.2015.04.019

251. A. Polyakov, D. Gunderov, V. Sitdikov, R. Valiev, I. Semenova, I. Sabirov, Physical Simulation of Hot Rolling of Ultra-fine Grained Pure Titanium, *Metall. Mater. Trans. B.* 45 (2014) 2315–2326. doi:View 10.1007/s11663-014-0133-9
252. L. Farbaniec, A. Abdul-Latif, J. Gubicza, G. Dirras, High purity ultrafine-grained nickel processed by dynamic plastic deformation: Microstructure and mechanical properties, *Adv. Eng. Mater.* 14 (2012) 1027–1033. doi:View 10.1002/adem.201200034
253. K.S. Suresh, A.D. Rollett, S. Suwas, Evolution of microstructure and texture during deformation and recrystallization of heavily rolled Cu-Cu multilayer, *Metall. Mater. Trans. A Phys. Metall. Mater. Sci.* 44 (2013) 3866–3881. doi:View 10.1007/s11661-013-1749-0
254. A.S. Taylor, M. Weiss, T. Hilditch, N. Stanford, P.D. Hodgson, Formability of cryo-rolled aluminium in uniaxial and biaxial tension, *Mater. Sci. Eng. A.* 555 (2012) 148–153. doi:View 10.1016/j.msea.2012.06.044
255. Z. Chen, N. Prud'homme, B. Wang, P. Ribot, V. Ji, Microstructure characterization and deposition mechanism studies of zrO₂ thin films deposited by LI-MOCVD, *Surf. Coatings Technol.* 218 (2013) 7–16. doi:View 10.1016/j.surfcoat.2012.12.017
256. T. Bhattacharjee, B.C. Suh, T.T. Sasaki, T. Ohkubo, N.J. Kim, K. Hono, High strength and formable Mg-6.2Zn-0.5Zr-0.2Ca alloy sheet processed by twin roll casting, *Mater. Sci. Eng. A.* 609 (2014) 154–160. doi:View 10.1016/j.msea.2014.04.058
257. M. Andasmas, T. Chauveau, N. Fagnon, D. Vrel, Synthesis of NiAl intermetallics from cold-extruded samples, *Intermetallics.* 32 (2013) 137–144. doi:View 10.1016/j.intermet.2012.08.019
258. A. Kratzig, C. Zachaus, S. Brunken, D. Thomas, P. Bogdanoff, K. Ellmer, et al., RuS₂ thin films as oxygen-evolving electrocatalyst: Highly oriented growth on single-crystal FeS₂ substrate and their properties compared to polycrystalline layers, *Phys. Status Solidi Appl. Mater. Sci.* 211 (2014) 2020–2029. doi:View 10.1002/pssa.201431284
259. S.T. Aruna, S. Roy, A. Sharma, G. Savitha, V.K. William Grips, Cost-effective wear and oxidation resistant electrodeposited Ni-pumice coating, *Surf. Coatings Technol.* 251 (2014) 201–209. doi:View 10.1016/j.surfcoat.2014.04.026
260. A. Kouadri-Henni, L. Barrallier, Mechanical properties, microstructure and crystallographic texture of magnesium AZ91-D alloy welded by friction stir welding (FSW), *Metall. Mater. Trans. A Phys. Metall. Mater. Sci.* 45 (2014) 4983–4996. doi:View 10.1007/s11661-014-2381-3
261. N.P. Gurao, R. Kapoor, S. Suwas, Texture evolution in high strain rate deformed Cu-10Zn alloy, *Mater. Sci. Eng. A.* 558 (2012) 761–765. doi:View 10.1016/j.msea.2012.07.112
262. K. Velmanirajan, A.S.A. Thaheer, R. Narayanasamy, R. Madhavan, S. Suwas, Effect of annealing temperature in Al 1145 alloy sheets on formability, void coalescence, and texture analysis, *J. Mater. Eng. Perform.* 22 (2013) 1091–1107. doi:View 10.1007/s11665-012-0358-1
263. H.P. Lin, T.S. Ng, C.L. Chen, J.C. Kuo, S.X. Ding, Comparison of deformation texture in FePd alloy via X-ray diffraction and electron backscatter diffraction techniques, *Micron.* 44 (2013) 433–441. doi:View 10.1016/j.micron.2012.09.009
264. A. Eschke, W. Zinn, T. Marr, C.G. Oertel, W. Skrotzki, L. Schultz, et al., Local stress gradients in Ti/Al composite wires determined by two-dimensional X-ray microdiffraction, *Mater. Sci. Eng. A.* 616 (2014) 44–54. doi:View 10.1016/j.msea.2014.08.003

265. K.J. Martinschitz, R. Daniel, C. Mitterer, J. Keckes, Elastic constants of fibre-textured thin films determined by X-ray diffraction, *J. Appl. Crystallogr.* 42 (2009) 416–428. doi:View 10.1107/S0021889809011807
266. B.C. Maji, M. Krishnan, A. Verma, R. Basu, I. Samajdar, R.K. Ray, Effect of Pre-straining on the Shape Recovery of Fe-Mn-Si-Cr-Ni Shape Memory Alloys, *Metall. Mater. Trans. A Phys. Metall. Mater. Sci.* 46 (2014) 639–655. doi:View 10.1007/s11661-014-2645-y
267. N.P. Gurao, P. Kumar, A. Sarkar, H.G. Brokmeier, S. Suwas, Simulation of deformation texture evolution during multi axial forging of interstitial free steel, *J. Mater. Eng. Perform.* 22 (2013) 1004–1009. doi:View 10.1007/s11665-012-0388-8
268. A.O.F. Hayama, J.F.S.C. Lopes, M.J. Gomes da Silva, H.F.G. Abreu, R. Caram, Crystallographic texture evolution in Ti-35Nb alloy deformed by cold rolling, *Mater. Des.* 60 (2014) 653–660. doi:View 10.1016/j.matdes.2014.04.024
269. S. Bera, S. Ghosh Chowdhury, W. Lojkowsky, I. Manna, Synthesis of CuCr and CuCrAg alloys with extended solid solubility with nano-Al₂O₃ dispersion by mechanical alloying and consolidation by high pressure sintering, *Mater. Sci. Eng. A.* 558 (2012) 298–308. doi:View 10.1016/j.msea.2012.08.004
270. S. Biswas, S. Suwas, Evolution of sub-micron grain size and weak texture in magnesium alloy Mg-3Al-0.4Mn by a modified multi-axial forging process, *Scr. Mater.* 66 (2012) 89–92. doi:View 10.1016/j.scriptamat.2011.10.008
271. N. Ray, G. Jagadeesh, S. Suwas, Response of shock wave deformation in AA5086 aluminum alloy, *Mater. Sci. Eng. A.* 622 (2015) 219–227. doi:View 10.1016/j.msea.2014.10.010
272. I. Salzmann, R. Resel, STEREOPOLE: Software for the analysis of X-ray diffraction pole figures with IDL, *J. Appl. Crystallogr.* 37 (2004) 1029–1033. doi:View 10.1107/S002188980402165X
273. J.T. Bonarski, Characterization of materials structure by X-ray diffraction, personal.imim.pl/jan.bonarski/Wyklady_JB.pdf
274. K. Velmanirajan, R. Narayanasamy, K. Anuradha, Effect of chemical composition on texture using response surface methodology, *J. Mater. Eng. Perform.* 22 (2013) 3237–3257. doi:View 10.1007/s11665-013-0644-6
275. H.M. Baek, S.K. Hwang, H.S. Joo, Y.T. Im, I.H. Son, C.M. Bae, The effect of a non-circular drawing sequence on delamination characteristics of pearlitic steel wire, *Mater. Des.* 62 (2014) 137–148. doi:View 10.1016/j.matdes.2014.05.014
276. J. Gravier, V. Vignal, S. Bissey-Breton, Influence of residual stress, surface roughness and crystallographic texture induced by machining on the corrosion behaviour of copper in salt-fog atmosphere, *Corros. Sci.* 61 (2012) 162–170. doi:View 10.1016/j.corsci.2012.04.032
277. C. Mondal, A.K. Singh, Effect of change of rolling planes on orientation rotation around the ??-fiber of high-purity aluminum plate subjected to 90% cold pre-deformation, *Scr. Mater.* 66 (2012) 674–677. doi:View 10.1016/j.scriptamat.2012.01.030
278. H. Yan, X. Zhao, N. Jia, Y. Zheng, T. He, Influence of shear banding on the formation of brass-type textures in polycrystalline fcc metals with low stacking fault energy, *J. Mater. Sci. Technol.* 30 (2014) 408–416. doi:View 10.1016/j.jmst.2013.11.010

279. T. Goryczka, B. Szaraniec, Characterization of polylactide layer deposited on Ni-Ti shape memory alloy, *J. Mater. Eng. Perform.* 23 (2014) 2682–2686. doi:View 10.1007/s11665-014-1038-0
280. S. Roy, G. Kannan, S. Suwas, M.K. Surappa, Effect of extrusion ratio on the microstructure, texture and mechanical properties of (Mg/AZ91)m-SiCp composite, *Mater. Sci. Eng. A.* 624 (2015) 279–290. doi:View 10.1016/j.msea.2014.10.063
281. W. Skrotzki, A. Eschke, J. Romberg, J. Scharnweber, T. Marr, R. Petters, et al., Processing of high strength light-weight metallic composites, *Adv. Eng. Mater.* 16 (2014) 1208–1216. doi:View 10.1002/adem.201400190
282. P. Angerer, J.M. Lackner, M. Wiessner, G.A. Maier, Chromium/chromium nitride multilayers during thermal treatment: An X-ray diffraction study, *Int. J. Refract. Met. Hard Mater.* 36 (2013) 101–105. doi:View 10.1016/j.ijrmhm.2012.07.008
283. S. Panda, S.K. Sahoo, A. Dash, M. Bagwan, G. Kumar, S.C. Mishra, et al., Orientation dependent mechanical properties of commercially pure (cp) titanium, *Mater. Charact.* 98 (2014) 93–101. doi:View 10.1016/j.matchar.2014.10.011
284. B.C. De Cooman, J. Kim, S. Lee, Heterogeneous deformation in twinning-induced plasticity steel, *Scr. Mater.* 66 (2012) 986–991. doi:View 10.1016/j.scriptamat.2012.02.028
285. D. V. Gunderov, A. V. Polyakov, I.P. Semenova, G.I. Raab, A.A. Churakova, E.I. Gimaldinova, et al., Evolution of microstructure, macrotexture and mechanical properties of commercially pure Ti during ECAP-conform processing and drawing, *Mater. Sci. Eng. A.* 562 (2013) 128–136. doi:View 10.1016/j.msea.2012.11.007
286. V. Anil Kumar, R.K. Gupta, G. Sudarsana Rao, Solution Treatment and Aging (STA) Study of Ti Alloy Ti5Al3Mo1.5V, *J. Mater. Eng. Perform.* 24 (2015) 24–31. doi:View 10.1007/s11665-014-1294-z
287. E. Matykina, R. Arrabal, R.Z. Valiev, J.M. Molina-Aldareguia, P. Belov, I. Sabirov, Electrochemical Anisotropy of Nanostructured Titanium for Biomedical Implants, *Electrochim. Acta.* 176 (2015) 1221–1232. doi:View 10.1016/j.electacta.2015.07.128
288. Z. Chen, J. Li, A. Borbely, G. Ji, S.Y. Zhong, Y. Wu, et al., The effects of nanosized particles on microstructural evolution of an in-situ TiB₂/6063Al composite produced by friction stir processing, *Mater. Des.* 88 (2015) 999–1007. doi:View 10.1016/j.matdes.2015.09.127
289. A. Kauffmann, J. Freudenberger, H. Klauß, W. Schillinger, V. Subramanya Sarma, L. Schultz, Efficiency of the refinement by deformation twinning in wire drawn single phase copper alloys, *Mater. Sci. Eng. A.* 624 (2015) 71–78. doi:View 10.1016/j.msea.2014.11.052
290. A. Wauthier-Monnin, T. Chauveau, O. Castelnau, H. Réglé, B. Bacroix, The evolution with strain of the stored energy in different texture components of cold-rolled if steel revealed by high resolution X-ray diffraction, *Mater. Charact.* 104 (2015) 31–41. doi:View 10.1016/j.matchar.2015.04.005
291. S.V.S. Narayana Murty, N. Nayan, R. Madhavan, S.C. Sharma, K.M. George, S. Suwas, Analysis of Microstructure and Texture Evolution in Mg-3Al-1Zn Alloy Processed Through Groove Rolling, *J. Mater. Eng. Perform.* 24 (2015) 2091–2098. doi:View 10.1007/s11665-015-1459-4

292. E. Shinada, T. Nagoshi, T.F.M. Chang, M. Sone, Crystallographic study on self-annealing of electroplated copper at room temperature, *Mater. Sci. Semicond. Process.* 16 (2013) 633–639. doi:View 10.1016/j.mssp.2012.11.011
293. H. Qin, X. Zhang, Q. Dong, Microstructure and texture evolution for dynamic plastic deformed pure magnesium during isothermal annealing, *Mater. Sci. Eng. A.* 626 (2015) 94–101. doi:View 10.1016/j.msea.2014.12.037
294. P. Chekhonin, B. Beausir, J. Scharnweber, C.G. Oertel, T. Hausöl, H.W. Höppel, et al., Confined recrystallization of high-purity aluminium during accumulative roll bonding of aluminium laminates, *Acta Mater.* 60 (2012) 4661–4671. doi:View 10.1016/j.actamat.2012.04.004
295. A.P. Baumann, J.M. Deuerling, D.J. Rudy, G.L. Niebur, R.K. Roeder, The relative influence of apatite crystal orientations and intracortical porosity on the elastic anisotropy of human cortical bone, *J. Biomech.* 45 (2012) 2743–2749. doi:View 10.1016/j.jbiomech.2012.09.011
296. T. Sadat, G. Dirras, D. Tingaud, M. Ota, T. Chauveau, D. Faurie, et al., Bulk Ni-W alloys with a composite-like microstructure processed by spark plasma sintering: Microstructure and mechanical properties, *Mater. Des.* 89 (2016) 1181–1190. doi:View 10.1016/j.matdes.2015.10.083
297. E. Bonnot, A.L. Helbert, F. Brisset, T. Baudin, Microstructure and texture evolution during the ultra grain refinement of the Armco iron deformed by accumulative roll bonding (ARB), *Mater. Sci. Eng. A.* 561 (2013) 60–66. doi:View 10.1016/j.msea.2012.11.017
298. S.K. Sahoo, R.K. Sabat, S. Panda, S.C. Mishra, S. Suwas, Mechanical Property of Pure Magnesium: From Orientation Perspective Pertaining to Deviation from Basal Orientation, *J. Mater. Eng. Perform.* 24 (2015) 2346–2353. doi:View 10.1007/s11665-015-1522-1
299. G. Anand, K. Barai, R. Madhavan, P.P. Chattopadhyay, Evolution of annealing texture in cryo-rolled copper, *Mater. Sci. Eng. A.* 638 (2015) 114–120. doi:View 10.1016/j.msea.2015.04.034
300. C. Delle Piane, B.S.G. Almqvist, C.M. MacRae, A. Torpy, A.J. Mory, D.N. Dewhurst, Texture and diagenesis of Ordovician shale from the Canning Basin, Western Australia: Implications for elastic anisotropy and geomechanical properties, *Mar. Pet. Geol.* 59 (2015) 56–71. doi:View 10.1016/j.marpetgeo.2014.07.017
301. F. Xu, X. Zhang, H. Ni, Y. Cheng, Y. Zhu, Q. Liu, Effect of twinning on microstructure and texture evolutions of pure Ti during dynamic plastic deformation, *Mater. Sci. Eng. A.* 564 (2013) 22–33. doi:View 10.1016/j.msea.2012.11.097
302. A.B. Rodriguez-Navarro, A. Checa, M.G. Willinger, R. Bolmaro, J. Bonarski, Crystallographic relationships in the crossed lamellar microstructure of the shell of the gastropod *Conus marmoreus*, *Acta Biomater.* 8 (2012) 830–835. doi:View 10.1016/j.actbio.2011.11.001
303. M.Z. Bian, K.S. Shin, {1012} Twinning Behavior in Magnesium Single Crystal, *Met. Mater. Int.* 19 (2013) 999–1004. doi:View 10.1007/s12540-013-5012-4
304. H.F.G. Abreu, J.J. Silva, M.R. Silva, M.J. Gomes Da Silva, Influence of reverted austenite on the texture and magnetic properties of 350 maraging steel, *J. Magn. Magn. Mater.* 393 (2015) 99–104. doi:View 10.1016/j.jmmm.2015.05.037
305. K. Verstraete, A.L. Helbert, F. Brisset, A. Benoit, P. Poniard, T. Baudin, Microstructure, mechanical properties and texture of an AA6061/AA5754 composite fabricated by cross

accumulative roll bonding, *Mater. Sci. Eng. a-Structural Mater. Prop. Microstruct. Process.* 640 (2015) 235–242. doi:View 10.1016/j.msea.2015.05.106

306. S. Brahma, P. Jaiswal, K.S. Suresh, K.Y. Lo, S. Suwas, S.A. Shivashankar, Effect of substrates and surfactants over the evolution of crystallographic texture of nanostructured ZnO thin films deposited through microwave irradiation, *Thin Solid Films.* 593 (2015) 81–90. doi:View 10.1016/j.tsf.2015.09.005
307. S. Bissey-Breton, V. Vignal, Influence of post-machining thermal treatment on the corrosion behaviour of copper, *Procedia CIRP.* 13 (2014) 120–124. doi:View 10.1016/j.procir.2014.04.021
308. B. Nabi, A.L. Helbert, F. Brisset, G. André, T. Waeckerlé, T. Baudin, Effect of recrystallization and degree of order on the magnetic and mechanical properties of soft magnetic FeCo-2V alloy, *Mater. Sci. Eng. A.* 578 (2013) 215–221. doi:View 10.1016/j.msea.2013.04.066
309. S.K. Hwang, H.M. Baek, H.S. Joo, Y.T. Im, Effect of processing routes in a multi-pass continuous hybrid process on mechanical properties, microstructure, and texture evolutions of low-carbon steel wires, *Met. Mater. Int.* 21 (2015) 391–401. doi:View 10.1007/s12540-015-4382-1
310. Jia, N.; Roters, F.; Eisenlohr, P.; Kords, C.; Raabe, D."Non-crystallographic shear banding in crystal plasticity FEM simulations: Example of texture evolution in α -brass", *Acta Materialia*, 60,3 (2012) pp. 1099-1115.
311. Suresh, K.S.; Geetha, M.; Richard, C.; Landoulsi, J.; Ramasawmy, H.; Suwas, S.; Asokamani, R., "Effect of equal channel angular extrusion on wear and corrosion behavior of the orthopedic Ti–13Nb–13Zr alloy in simulated body fluid "Materials Science & Engineering C, 32, 4, 1, (2012) pp. 763-771.
312. Roy, Shibayan; D., Satyaveer Singh; Suwas, Satyam; Kumar, S.; Chattopadhyay, K., "Microstructure and texture evolution during accumulative roll bonding of aluminium alloy AA5086", *Materials Science & Engineering A*, 528, 29-30,15 (2011) pp. 8469-8478.
313. Gurao, N.P.; Sethuraman, S.; Suwas, Satyam, "Effect of strain path change on the evolution of texture and microstructure during rolling of copper and nickel", *Materials Science & Engineering A*, 528, 25-26, 25 (2011) pp. 7739-7750.
314. Rodriguez-Navarro, Alejandro B.; Checa, Antonio; Willinger, Marc-Georg; Bolmaro, Raúl; et. al., "Crystallographic relationships in the crossed lamellar microstructure of the shell of the gastropod *Conus marmoreus*", *Acta Biomaterialia*, 8,2 (2012) pp. 830-835.
315. K.Lukaszkwicz, A.Czyzniewski, W.Kwasny, M.Pancielejko, "Structure and mechanical properties of PVD coatings deposited onto the X40CrMoV5-1 hot work tool steel substrate", *Vacuum*, 86, 8,29 (2012) pp. 1186-1194.
316. Li Jizhong, Xu Wei, Wu Xiaolin, Ding Hua, Xia Kenong, "Effects of grain size on compressive behaviour in ultrafine grained pure Mg processed by equal channel angular pressing at room temperature", *Materials Science & Engineering A*, 528, 18, 15, (2011), pp. 5993-5998.
317. B.C.De Cooman, Kim Jinkyung, Lee Seil, "Heterogeneous deformation in twinning-induced plasticity steel", *Scripta Materialia*, 66,12,(2012) pp. 986-991.
318. W.J.Kim, S.J.Yoo, H.T.Jeong, D.M.Kim, B.H.Choe, J.B.Lee, "Effect of the speed ratio on grain refinement and texture development in pure Ti during differential speed rolling", *Scripta Materialia*, 64,1,(2011) pp. 49-52.

319. Q.H.Bui, X.T.Pham, "Modeling of microstructure effects on the mechanical behavior of ultrafine-grained nickels processed by hot isostatic pressing", *International Journal of Mechanical Sciences*, 53, 10, (2011), pp. 812-826.
320. L.Li, "Deformation band and texture of a cast Mg-RE alloy under uniaxial hot compression", *Materials Science & Engineering A*, 528, 24, 15, (2011), pp. 7178-7185.
321. Biswas, Somjeet; Suwas, Satyam, "Evolution of sub-micron grain size and weak texture in magnesium alloy Mg-3Al-0.4Mn by a modified multi-axial forging process ", *Scripta Materialia*, 66, 2, (2012), pp. 89-92 .
322. C.Mondal, A.K.Singh, "Effect of change of rolling planes on orientation rotation around the β -fiber of high-purity aluminum plate subjected to 90% cold pre-deformation", *Scripta Materialia*, 66, 9, (2012) pp. 674-677.
323. Yu.Ivanisenko, W.Skrotzki, R.Chulist, T.Lippmann, L.Kurmanaeva, „Texture development in a nanocrystalline Pd-Au alloy studied by synchrotron radiation", *Scripta Materialia*, 66, 3-4, (2012), pp. 131-134
324. CG.Oertel, R.Schaarschuch, G.H.Cao, H.N.Tian, J.Freudenberger, H.G.Brokmeier, et. al, "Effect of martensitic phase transformation on the ductility of polycrystalline YCu", *Scripta Materialia*, 65, 9, (2011), pp. 779-782.
325. M.J.N.V.Prasad, A.H.Chokshi, Microstructural stability and superplasticity in an electrodeposited nanocrystalline Ni-P alloy, *Acta Materialia* Volume: 59, Issue: 10, June, 2011, pp. 4055-4067
326. Jia, N.; Peng, R. Lin; Wang, Y.D.; Zhao, X., Self-consistent modeling of rolling textures in an austenitic-ferritic duplex steel, *Materials Science & Engineering A*, 528, 10-11, 25 (2011), pp. 3615-3624
327. Biswas, Somjeet; Suwas, Satyam; Sikand, R.; Gupta, Anil K., Analysis of texture evolution in pure magnesium and the magnesium alloy AM30 during rod and tube extrusion, *Materials Science & Engineering A* Volume: 528, Issue: 10-11, April 25, 2011, pp. 3722-3729
328. Vignal, V.; Zhang, H.; Delrue, O.; Heintz, O.; Popa, I.; Peultier, J., Influence of long-term ageing in solution containing chloride ions on the passivity and the corrosion resistance of duplex stainless steels, *Corrosion Science* Volume: 53, Issue: 3, March, 2011, pp. 894-903
329. Khatirkar, Rajesh K.; Kumar, Sunil, Comparison of recrystallization textures in interstitial free and interstitial free high strength steels, *Materials Chemistry and Physics* Volume: 127, Issue: 1-2, May 16, 2011, pp. 128-136
330. Andasmas, M.; Langlois, P.; Fagnon, N.; Chauveau, Th.; Hendaoui, A.; Vrel, D. Phenomenological study of the densification behavior of Aluminum-Nickel powder mixtures during cold isostatic pressing and differential hydrostatic extrusion, *Powder Technology* Volume: 207, Issue: 1-3, February 15, 2011, pp. 304-310
331. Kim, W.J.; Yoo, S.J.; Jeong, H.T.; Kim, D.M.; Choe, B.H.; Lee, J.B., Effect of the speed ratio on grain refinement and texture development in pure Ti during differential speed rolling, *Scripta Materialia* Volume: 64, Issue: 1, January, 2011, pp. 49-52
332. V.D.Hiwarkar; S.K.Sahoo; I. Samajdar; A.Satpathy; K.V.Krishna Mani; G.K.Dey; D.Srivastav; et. al., Defining recrystallization in pilgered Zircaloy-4: From preferred nucleation to growth inhibition, *Journal of Nuclear Materials* Volume: 412, Issue: 3, May 31, 2011, pp. 287-293 2005 - 2010

333. L. Tarkowski a, J. Bonarski, I. Alexandrov, Planar irregularities of texture and stress field in Ti detected by X-ray diffraction technique, *Nuclear Instruments and Methods in Physics Research B* 268 (2010) 352–355.
334. G. Dirras, H. Couque, J. Gubicza, A. Ouarem, T. Chauveau, P. Jenei, Fine-grained nickel deformed by direct impact at different velocities, *Microstructure and mechanical properties, Materials Science and Engineering A* 527 (2010) 4128–4135.
335. S.K. Sahoo, V.D. Hiwarkar, L. Jain, I. Samajdar, P. Pant, G.K. Dey, D. Srivastav R. Tewari, S. Banerjee, Deformed microstructures of two-phase Zr–2.5Nb alloy: Effects of the second phase hardness, *Journal of Nuclear Materials* 404 (2010) 222-230.
336. R. Chulist, W. Skrotzki, C.-G. Oertel, A. Bohm, T. Lippmann, E. Rybacki, Microstructure and texture in Ni₅₀Mn₂₉Ga₂₁ deformed by high-pressure torsion, *Scripta Materialia* 62 (2010) 650–653. J. Arout Chelvane, S. Banumathy, Mithun Palit, Himalay Basumatary, A.K. Singh, S. Pandian, Texture and magnetostriction studies in Bridgman solidified Ho_{0.85}Tb_{0.15}Fe_{1.95} alloys, *Journal of Alloys and Compounds* 507 (2010) 162–166.
337. Li Li, Xinming Zhang, Changping Tang, Yunlai Deng, Nan Zhou, Mechanical properties and deep drawability of Mg–Gd–Y–Zr alloy rolling sheet at elevated temperatures, *Materials Science and Engineering A* 527 (2010) 1266–1274.
338. R. Chulist, W. Skrotzki, C.-G. Oertel, A. Bohmb, M. Potschke, Change in microstructure during training of a Ni₅₀Mn₂₉Ga₂₁ bicrystal, *Scripta Materialia* 63 (2010) 548–551.
339. R. Dakhlaoui, V. Klosek, M.H. Mathon, B. Marini, Orientation stress field analysis in polycrystalline bcc steel using neutron diffraction, *Acta Materialia* 58 (2010) 499–509.
340. Akinobu Shibata, Homuro Noda, Masato Sone, Yakichi Higo, *Thin Solid Films* 518 (2010) 5153–5158.
341. W.J. Kim, S.J. Yoo, H.T. Jeong, D.M. Kim, B.H. Choe and J.B. Lee, Effect of the speed ratio on grain refinement and texture development in pure Ti during differential speed rolling, *Scripta Materialia* 64 (2011) 49–52.

6.4 ODF Transformation references

342. Adam Morawiec, *Orientations and Rotations* (2003), Springer, ISBN 3-540-40734-0.

6.5 Calculation of the Volume Fraction of Texture Component and the ODF Modeling references

343. Determination of Volume Fraction of Texture Components Using LaboTex - Integration Method (manual) - www.labotex.com
344. Determination of Volume Fraction of Texture Components Using LaboTex - Model Functions Method (manual) - www.labotex.com
345. Determination of Volume Fraction of Texture Components Using LaboTex - Modelling of ODF, pole figures and inverse pole figures (manual) - www.labotex.com
346. J.W. Flowers, "Volume Fractions of Texture Components of Cubic Materials", *Textures and Microstructures*, 1983, Vol.5, pp. 205-218, "A method for obtaining volume fractions in regions about ideal texture components of cubic materials by integration of the orientation distribution function is described".
347. J.H. CHO, A.D. ROLLETT, K.H. OH, "Determination of Volume Fractions of Texture Components with Standard Distributions in Euler Space", *METALLURGICAL AND MATERIALS TRANSACTIONS A*, VOLUME 35A, MARCH 2004—1075.

348. J. Kozaczek, D. S. Kurtz, P.R. Moran, R. Martin, M. E. Gross, K. Evans-Lutterodt, "Methodology of Quantitative Texture Analysis in Thin Films and Interconnects", <http://www.hypernex.com/news/pdfs/2000AdvMetfinal.PDF>
349. J.Jura, "Application of Model Function in Quantitative Texture Analysis of Cubic Metals", Metallurgy and Foundry Practice, Bulletin 148, No.1530,(1993).
350. S.Matthies, G.W.Vinel,K.Helming,"Standard Distribution in Texture Analysis, Akademie-Verlag Berlin (1987,1988,1991).

6.6 Measurement of Pole Figures references

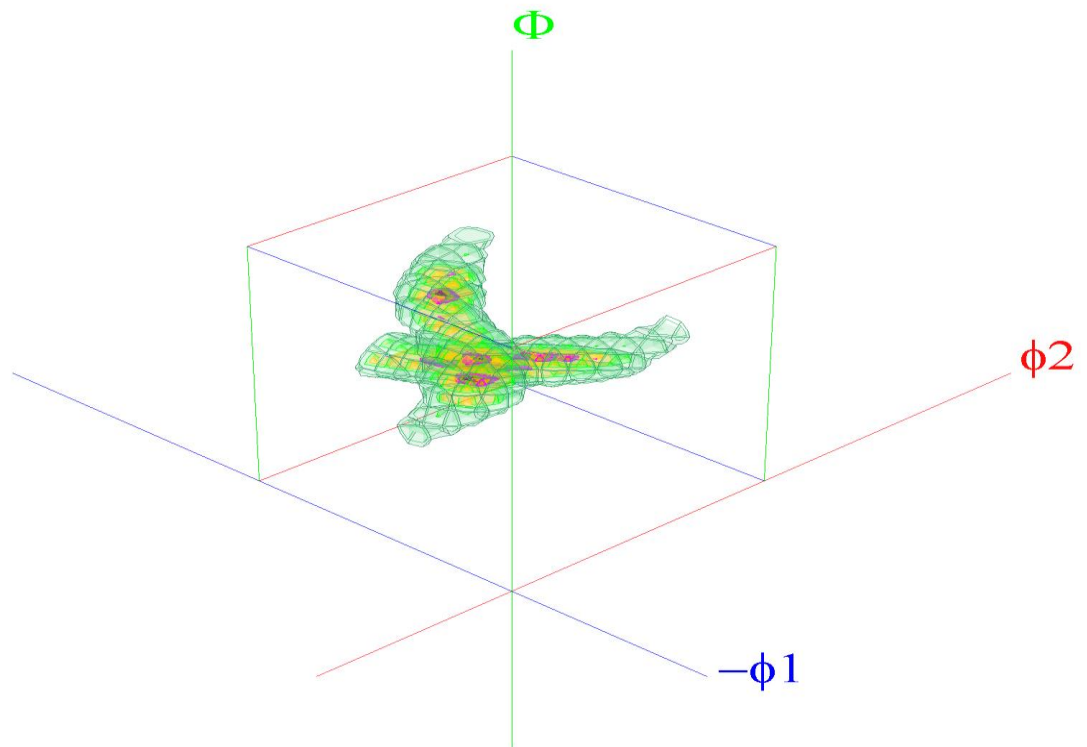
351. "Pole Figures: Registration and Plot Conventions" - www.labotex.com
352. B.D.Cullity,B. D. "Elements of X-ray Diffraction", Addison-Wesley, Reading, Mass (new edition p. 402-431 Pole Figures)
353. H.P. Klug, L.E.Alexander, "X-Ray Diffraction Procedures", John Wiley & Sons",
354. Schulz L.G.; (1949). J.Appl. Phys., 20, 1033,
355. D. Chateigner, P. Germi, M. Pernet: Texture analysis by the Schulz reflection method: defocusing corrections for thin films. J. of Applied Crystallography 25, 1992, 766-769

6.7 Texture and Quantitative Phase Analysis references

356. Bonarski J.T., Wróbel M. and Pawlik K.; (2000). Quantitative phase analysis of duplex stainless steel using incomplete pole figures, Materials Science and Technology Vol. 16 No 6, p. 657-662.

6.8 Texture and ODF references

357. H.J. Bunge, "Texture analysis in materials science". Cuvillier Verlag, Göttingen;
358. U.F.Kocks, C.N.Tome,H.R.Wenk, "Texture and Anisotropy", Cambridge University Press. (2000),



7. LaboTex: Technical specifications

Version 3.0.54

Specification / Feature	3.0.22	Comments
Windows OS compatible application (from version 2.0.)	Yes	Windows 7/8/10
Management of data and results.	Yes	Simple access to data and results. Collecting them per: users, symmetries, projects, samples and jobs.
ODF calculation (direct - ADC Method).	Yes	The best ODF calculation method.
Texture analysis of all types of sample symmetry.	Yes	
Texture analysis for materials of all types of crystal lattice symmetry.	Yes	
Fiber texture analysis.	Yes	
High resolution ODF option.	Yes	
Calculation of a fit error (RP).	Yes	
Calculation of texture index.	Yes	
ODF calculation report.	Yes	Any available.
Ghost correction.	Yes	
Truncation errors of the series.	No	
ODF calculation using pole figures.	Yes	Data from X-Ray or Neutrons measurements.
Input data in non-LaboTex data format.	Yes	LaboTex accepts data in 31 formats. For more details see www.labosoft.com.pl
Adjusting the customer data format for LaboTex	Yes	Free of charge
Correction of the pole figure for the background of pole figure.	Yes	
Indicating when background values are greater than pole figure data values.	Yes	LaboTex displays the percentage for the data
Choice of the correction method for the background.	Yes	When the background data of the pole figure is greater than the pole figure data for some values LaboTex makes: a) negative values of pole figure after the correction for background is set to zero; b) adds to all the pole figure data an absolute value of the lowest values of the pole figure after the correction for background (LaboTex makes all data positive). Option "a" is the default one.
Correction for defocusing using powder pole figures.	Yes	Correction of the powder pole figure for the background is also available
Correction for defocusing from correction coefficients.	Yes	
Correction for defocusing from Schulz equation.	Yes	
Input data in any grid.	No	Only for radial angle: 1., 1.2 ,2. ,1.25 ,1.5, 2. ,2.5 ,3. ,3.75 ,5. ,6. ,7.5 ,10. degrees and extra: 1.8 ,2.25 ,3.6 ,4.5 but with exception of the trigonal and hexagonal crystal lattice symmetry. If the azimuthal angle step is different from the radial step, the azimuthal step is adjusted to the radial step by linear interpolation. Azimuthal step has to be in the range of 1-10 deg.

Choice of the pole figures plot convention.	Yes	Users can choose to start to plot pole figures from "N", "E", "S" or "W". Users can also adjust the description of pole figure axis (e.g. denotation 'RD') to the new plot convention. ODF calculations are independent of the choice of plot convention.
Adjusting the pole figures registration convention to the LaboTex convention.	Yes	Users can choose: <ul style="list-style-type: none"> • counter-clockwise; • none rotate; • +90 deg pole figure rotate; • +180 deg pole figure rotate. Users can set up the default for the registration convention for each available format of the pole figures. ODF calculations are dependent on the choice of the registration convention (ODF may be shifted).
Maximal/minimal value of Miller indices H,K,L for input PF	9/-9	
ODF calculation from the incomplete pole figure(s).	Yes	
Indication of too small number of data for the ODF calculation.	Yes	During the ODF calculation.
ODF calculation for different parameters for the same sample.	Yes	Up to 9 jobs per sample.
Choice of the symmetrization of pole figures before the ODF calculation.	Yes	Viewing of symmetrized PF.
Choice of the sample symmetry for ODF (ODF symmetrization).	Yes	Available after the ODF calculation.
A number of the symmetrization possibilities.	8	None, triclinic to monoclinic, triclinic to orthorhombic, triclinic to axial, monoclinic to orthorhombic, monoclinic to axial, orthorhombic to axial, custom to axial.
Rotation of pole figure(s) before the ODF calculation.	Yes	For all pole figures or separately for each PF in range -90 to 90 degrees.
Cutting off the pole figure(s) in the center before the ODF calculation.	Yes	For all pole figures or separately for each PF. Users can choose the angle ranges.
Cutting off the pole figure(s) in the edge before ODF calculation.	Yes	For all pole figures or separately for each PF. Users can choose angle ranges.
Changing the parameters finishing calculation in ODF calculation.	Yes	A number of iterations (1-70), RP and dRP finishing calculation (0.1-10%).
Creation of complete pole figures.	Yes	Complete pole figures (RPF) are created during ODF calculations.
Creation of complete inverse pole figures.	Yes	
ODF calculation from sets of individual orientations (SOR).	Yes	Data from EBSD, the model calculation and other.
Roe/Bunge notation of the angles in SOR.	Yes/Yes	Notation chosen by users.
Weights of orientations in SOR.	Yes	
Choice of ODF grid (ODF from SOR).	Yes	1x1, 1.2x1.2, 1.25x1.25, 1.5x1.5, 2x2, 2.5x2.5, 3x3, 3.75x3.75, 5x5, 6x6, 7.5x7.5, 10x10.
Choice of sample symmetry (ODF from SOR).	No	Choice of the sample symmetry after the ODF calculation (ODF symmetrization).

Modelling of ODF, pole figures and inverse pole figures.	Yes	<p>Users can choose:</p> <ul style="list-style-type: none"> • Crystal Symmetry; • Sample Symmetry; • Grid cells for output ODF; • Up to 10 components. <p>For each texture component users can choose:</p> <ul style="list-style-type: none"> • volume fraction; • FWHM for each Euler angle (ϕ_1, ϕ_2 and ϕ); • distribution (Gauss or Lorentz). <p>Users can create any model pole figures or/and any model inverse pole figures from model ODF using appropriate dialog for creating APF (additional pole figures) or IPF (inverse pole figures). Model ODF is created as a new job or as a new sample.</p>
Choice of methods for the determination of volume fraction of texture components.	Yes	Users can use 2 methods: Integration and/or Model Function.
Calculation of the volume fraction of texture components by Integration Methods.	Yes	Up to 10 components simultaneously.
Choice of integration ranges.	Yes	For each Euler angle separately, with the viewing.
Evaluation of parameters of the component peak (Integration Methods).	Yes	
Choice of the components (Integration Methods).	Yes	From files or from a database.
Choice of the method of the calculation of volume fraction in Integration Methods.	Yes	3 methods.
Display of orientation overlapping (Integration Methods).	Yes	
Correction of overlapping (Integration Methods).	Yes	Dividing ODF among overlapping orientation.
Reporting from the calculation of the volume fraction of texture components by Integration Methods.	Yes	Ready to print or copy to clipboard.
Calculation of volume fraction of texture components by Model Function Methods.	Yes	Up to 10 components simultaneously. For each texture component users can choose initial parameters for fitting calculation from: volume fraction, FWHM for each Euler angle (ϕ_1 , ϕ_2 and ϕ), distribution (Gauss or Lorentz).
Choice of the components (Model Function Methods).	Yes	From files or from a database.
Choice of the mode of work during calculation of volume fraction in Model Function Methods.	Yes	Automatic and Manual ('Once' step). In the manual mode LaboTex calculates relative error between the experimental ODF and the model ODF made by the user. In the automatic mode LaboTex adjusts the model parameters (angles and volume fraction) to the optimal values.
Comparison of the 'experimental' ODF with the best fit model.	Yes	<p>LaboTex shows the calculated and 'experimental' ODF in two modes:</p> <ul style="list-style-type: none"> • common area - in blue color, different area - in red color; • 'experimental' ODF - in blue color, model ODF - red line. <p>Users can also save calculated ODF as a new job (Option: "Save and Show"). Then they can continue with the ODF comparison in LaboTex 'Compare Mode'.</p>

Reporting the calculation of the volume fraction of texture components by Model Function Method.	Yes	The report is available after saving the fitted model. It is ready to print, copy to clipboard or view.
Components (orientations) database.	Yes	100 positions for each crystal system. The orientation introduced to the database is also the denotation of the component. In texture analysis LaboTex shows all sym. equivalent positions (orientations) for orientation from the database.
Introduce orientations (components) to database in Miller indices ($\{HKL\}\langle UVW \rangle$).	Yes	Equivalent Euler angles for $\{HKL\}\langle UVW \rangle$ depend on the cell parameters when the crystal symmetry is lower than cubic. When users introduce an orientation (component) in the Miller indices, LaboTex automatically calculates Euler angles on the basis of the cell parameters. Hence for the samples with different cell parameters LaboTex shows the same orientation in the Miller indices on the different places in the Euler space.
Maximal/minimal value for the Miller indices H,K,L,U,V,W for orientation $\{HKL\}\langle UVW \rangle$	15/-15	Users can set up the maximal value for the Miller indices in the conversion from Euler angles (in the range 5 to 15).
Introduce orientations (texture components) to the database in the Euler angles.	Yes	
Introduce fiber orientations (components) to the database.	Yes	
Displaying the orientation from a database on the ODF and PF(s).	Yes	Selecting via a combo-box, Automatic mode, Next and Previous.
Displaying the symmetrically equivalent position on the ODF and PF(s).	Yes	Selecting via a combo-box or from list-box.
Presentation of the symmetrically equivalent position.	Yes	In the basic region for ODF and the full Euler space for PFs, in the Miller indices and Euler angles.
On-line identification of the orientations (components).	Yes	In Euler angles and Miller indices, ODF and pole figures (except from IPFs). In the cursor position.
Help in finding near orientations.	Yes	Near orientations sorted by: PF/ODF, Miller indices and distance.
Comparing the orientation analysis. Very useful educational purposes!	Yes	LaboTex shows simultaneously the orientation on: ODF and ODF (the same and different projection), an ODF section and ODF, pole figure(s) and ODF, pole figure(s) and an ODF section.
Showing ODF/PF values using a mouse.	Yes	For PF LaboTex shows the sum of PF values under poles of the orientation and separately for the option SORT.
Qualitative orientations analysis for PF/ODF.	Yes/Yes	Sorted orientations from database.
Report from qualitative analysis.	Yes	Only for ODF. Ready to print and copy into the clipboard.
Creation of additional, complete pole figures (APF) from ODF.	Yes	User input only HKL. Available after ODF calculation.
Creation of additional, complete inverse pole figures from ODF.	Yes	User input only XYZ. Available after ODF calculation.
Exporting ODF to ASCII format.	Yes	
Exporting Pole Figures as ASCII format.	Yes	
Exporting Inverse Pole Figures to ASCII format.	Yes	
Choice of the convention for the hexagonal system.	Yes	
2D and 3D pole figures presentation.	Yes	

Choice of the pole figures plot convention.	Yes	Users can choose to start to plot pole figures from "N", "E", "S" or "W". Users can also adjust the description of the pole figure axis (for example denotation 'RD') to a new plot convention. ODF calculations are independent of the choice of the plot convention.
Adjust of pole figures registration convention to LaboTex convention	Yes	User can choose: <ul style="list-style-type: none"> • counter-clockwise; • none rotate; • +90 deg pole figure rotate; • +180 deg pole figure rotate. User can set up default for registration convention for each available format of pole figures. ODF calculation are dependent on the choice of registration convention (ODF may be shift).
The maximal number of pole figures/inverse pole figures in one window.	100	
Pole figures descriptions.	Yes	HKL, the sample name, directions (3 characters, edited by user) and the type of a figure (CPF,RPF,NPF,APF).
Switching off pole figures descriptions.	Yes	Separately for each kind of description.
Fill-in option in 2D/3D presentation.	Yes/Yes	4 modes of the fill-in option: normal/black/white and continuous.
User defined sets of colors.	Yes	15 sets.
Isoline mode.	Yes	3 modes: automatic, manual and from user defined sets.
Changing the parameter of the pole figures presentation.	Yes	Number of isolines (maximum of 14), color, color set, value and fill-in.
2D ODF presentation for Phi1, Phi and Phi2 projections.	Yes	
2D ODF presentation for a section of a projection.	Yes	
Bunge definition of the Euler angles.	Yes	ODF presentation and export.
3D ODF presentation.	Yes	
The possibility changes of parameters of 3D ODF presentation.	Yes	Rotate, distance, shift, color, axis(on,off,length),parallel/perspective projection, top/bottom contour, animation (cycle rotation).
The possibility of the choice of isolines.	Yes	14
Arrangements mode.	3	Automatic /optimal arrangements/, automatic /vertical close horizontal and custom.
Drawing basic region of PF/INV.	Yes	IPF in a standard stereographic triangle (only for: cubic, hexagonal, trigonal and tetragonal systems)
Saving the set of isolines.	Yes	Saved features: color, value and activity.
Exporting 2D and 3D images to the bitmap format (bmp).	Yes	BMP or TIF format available.
Exporting (copying) 2D and 3D images to the clipboard.	Yes	In the bitmap format (bmp).
Choosing the resolution of the exported image.	Yes	
Online help.	Yes	
ODF section (cuts) defined by users	Yes	Users can define two points in the Euler Space. LaboTex shows ODF intensity along the section defined by these points. Users can also choose initial points from an orientations database (to access the database select 'Start Point' or 'End Point'). Comparisons up to 12 ODFs are available. Users can save current parameters and/or samples.

Skeleton lines	Yes	<p>Users can create diagrams such as: alpha-fiber, beta-fiber, gamma fiber etc. Users can choose skeleton lines on the basis of the Euler angle (Φ_1, Φ or Φ_2) and :</p> <ul style="list-style-type: none"> • maximal intensity ; • integral intensity. <p>Users can also change ranges in which LaboTex looks for the maximum odf value or makes integration (from +/-2 to +/-20 deg). Users can compare up to 12 skeleton lines. The current parameters and/or samples can be saved.</p>
Misorientation histograms	Yes	<p>Users define the starting point in the Euler Space from which LaboTex shows misorientation diagrams. The misorientations diagrams are calculated on the basis of ODFs in a range from 0 to 80 deg from the starting point (the starting orientation). LaboTex shows a relative intensity i.e. this intensity is relative to the intensity of the random sample ($I=I(\text{sample})/I(\text{random sample})$) for the same range of the misorientation angle. Users can make comparison of up to 12 misorientations histograms. Histogram steps can be changed within the range from 1 to 10 degrees. Current parameters and/or samples can be saved.</p>
Optimization of diagrams : ODF section, Skeleton lines, Misorientation histograms, PF section (arc, radial, radial-full)	Yes	<ul style="list-style-type: none"> • Scale (within the percentage of the maximum intensity value: from 0.1% to 100%); • colors (defined by the user); • types of lines (14 types with different dots + solid pattern) ; • line options (all solid, all black or black contours); • width of lines (0 to 10 pixels); • diagram fill.
ODFs - logical operations	Yes	<p>In order to activate this option switch LaboTex to Compare Mode, then choose two ODFs for comparison: one in the left window and the other one in the right window (<i>LaboTex Compare Mode</i>). On the basis these two ODFs (A - from the left window and B from the right window) LaboTex creates a new ODF which can be:</p> <ul style="list-style-type: none"> • an intersection of the ODF A and the ODF B, • a difference between the ODF A and the ODF B (or B-A), • a union of the ODF A and the ODF B, • a sum of the ODF A and the ODF B, • a ODF difference: A or B minus the intersection of A&B, • an inverted ODF (only for the ODF A). <p>The new ODF is created within the new job for the sample of ODF A. These diagrams can be copied to other applications or exported as images in 'BMP' or 'TIF' format (menu '<i>Edit</i>').</p>

Transformations of ODF	Yes	<p>There are two kinds transformations:</p> <ul style="list-style-type: none"> • Frame rotations - users can rotate a sample frame along any Euler angles. This option gives the opportunity to see the ODF for other (different) sample position. For example, to see the ODF for the perpendicular surface with relation to the surface which was measured, transform the initial ODF by $\Phi=90\text{deg}$. Users can create changes of the sample symmetry for a new ODF. • Model builder rotations - (crystalites/planes rotations). Firstly, build a rotation model and save it. Secondly, in the rotation model you can choose up to 10 orientations for which you set: <ul style="list-style-type: none"> ○ the ranges of the Euler angle around center of orientation (and for symmetrically equivalent positions); ○ the vector "hkl" around which crystalites/planes will be rotated (only these which are included in chosen ranges); ○ the rotation angle; ○ the percentage of the rotated crystalites/planes (from 0 to 100%). <p>Now choose the rotation model and make the ODF transformation. LaboTex calculates the new ODF which is a result of the transformation of the initial ODF. The new ODF is created in a new job for sample of the initial ODF.</p>
Generation of single orientations	Yes	<p>LaboTex creates a set of single orientations on the basis of the current ODF. Users can choose a number of single orientations from 10000 to 9999999. This option is very useful for example for users who model deformation (VCS users). A random set of single orientation can be also generated using this option. *.SOR files created by LaboTex can be then used as a new sample for the ODF calculation.</p>
Pole figures sections (cuts)	Yes	<p>Users define the starting and ending points on the pole figure and LaboTex shows the intensity along this section. The following cuts are available:</p> <ul style="list-style-type: none"> • 'Arc' (in the range of 0 to 360 degrees) ; • 'Radial' (in the range of 0 to 90 degrees); • 'Radial (full)' (in the range of 90 - 0 - 90 degrees). <p>To see the position of the section line on the pole figure, select the 'View' button. Up to 12 pole figures can be compared. The information about compared PFs is displayed in the <i>information window</i> on the left hand. Users must choose all pole figures for which the sections are displayed before pressing the '2D' button. If more than 12 pole figures are chosen, LaboTex shows only the first 12 pole figures sections. There is a number of options to optimize the quality of diagrams :</p> <ul style="list-style-type: none"> • scale (the percentage of the maximum intensity value: from 0.1% to 100%) ; • colors (defined by the user); • types of lines (14 types – dots and solid); • line options (all solid, all black or black contours) ; • lines width (from 0 to 10 pixels) ; • diagram ill. <p>Users can save the current parameters. These diagrams can be copied over to other applications or saved as images in *.BMP or *.TIF formats (menu 'Edit').</p>
On-line view of alpha (radial angle), beta (azimuthal angle) and pole figure value using the mouse cursor.	Yes	<p>LaboTex displays this data in the format: (alpha,beta) PF='value of PF'.</p>

User defined grid for pole figures.	Yes	Users can define a grid for the alpha angle and/or a grid for the beta angle of PF.
User Manuals and Technical Reports.	Yes	<ul style="list-style-type: none"> • <i>Short Introduction to LaboTex</i> • <i>Menu and Toolbars Commands Description</i> • <i>Determination of the Volume Fraction of Texture Components Using LaboTex - Integration Methods</i> • <i>Determination of the Volume Fraction of Texture Components Using LaboTex - Model Functions Method</i> • <i>Pole Figures: Registration and Plot Conventions</i> • <i>Nomenclature of the Inverse Pole Figures in LaboTex</i> • <i>LaboTex: Modelling of ODF, Pole Figures and Inverse Pole Figures</i>
Usage examples.	Yes	<p>The following examples are available:</p> <ul style="list-style-type: none"> • Examples for all crystal symmetry. • Examples for all sample symmetry. • Example for high resolution pole figures and ODFs (1x1 deg). • Examples for the fibre texture (in the demo version). • Additional examples (available on our website www.labosoft.com.pl)
Demo version.	Yes	The demo version is based on the version 2.1.012
Support.	Yes	Free full e-mail support and updates for 24 months
Protection.	Yes	HASP Key: Parallel Port or USB socket.
Minimal system configuration.		<ul style="list-style-type: none"> • Processor PENTIUM IV 2 GHz or higher; • 1 GB HD space; • graphic card resolution 1024x768; • CD-ROM drive; • OpenGL Graphic Card is required for 3D View in "Continuous" fill mode; • USB port.
Recommended system configuration.		<ul style="list-style-type: none"> • Processor Intel Core I5 or I7; • 20-50 GB HD space; • 4 GB RAM; • graphic card resolution 1920x1200 + OpenGL • USB port; • color laser jet or inkjet printer, • if data are measured in the grid less than 5x5 degrees, double free disk space is recommended.

